Western University Scholarship@Western

Electronic Thesis and Dissertation Repository

7-25-2016 12:00 AM

Passive Acoustic Emissions in a V-blender

Allison Crouter The University of Western Ontario

Supervisor

Dr. Lauren Briens

The University of Western Ontario

Graduate Program in Chemical and Biochemical Engineering A thesis submitted in partial fulfillment of the requirements for the degree in Doctor of Philosophy

© Allison Crouter 2016

Follow this and additional works at: https://ir.lib.uwo.ca/etd



Part of the Other Chemical Engineering Commons

Recommended Citation

Crouter, Allison, "Passive Acoustic Emissions in a V-blender" (2016). Electronic Thesis and Dissertation Repository. 3858.

https://ir.lib.uwo.ca/etd/3858

This Dissertation/Thesis is brought to you for free and open access by Scholarship@Western. It has been accepted for inclusion in Electronic Thesis and Dissertation Repository by an authorized administrator of Scholarship@Western. For more information, please contact wlswadmin@uwo.ca.

Abstract

The pharmaceutical manufacturing process consists of a number of batch steps; each step must be monitored and controlled to ensure quality standards are met. The development of process analytical technologies (PAT) can improve product monitoring with the aim of increasing efficiency, product quality and consistency and creating a better understanding of the manufacturing process.

This work investigates the feasibility of using passive acoustic emissions (PAE) to monitor particulates in a V-blender. An accelerometer was attached to the lid of a V-blender to measure vibrations from the tumbling solids. A wavelet filter removed the oscillations in the signals from the motion of the shell, focusing on the emissions from the particle interactions. The particle size, fill level and scale affected the acoustic emissions through changes in the particle momentum. Changes in particle cohesiveness and flowability were also reflected in the measured emissions.

Powder properties and behavior are critical to efficient and successful manufacturing of pharmaceutical tablets. As the powders must be transferred between the different manufacturing stages, the flowability of powders is critical. Trials were conducted to investigate the effect of moisture content of a powder on its flowability. Through avalanche behavior, it was found that the flowability and the dynamic density of a powder change with moisture content.

PAEs were used to detect changes in solids moisture content as solids tumbled within the V-blender. It was found that particle mass, coefficient of restitution (COR) and flowability impacted the amplitude of the acoustic emissions. To further investigate the effects of particle flowability, PAEs were used to monitor lubricant addition. The amplitudes of the acoustic emissions were sensitive to the lubricant addition due to changes in the flowability. A trend in the emission amplitude allowed for the progression of the lubricant mixing to be followed. Overall, the research supports the feasibility of PAEs as a PAT for mixing in a tumbling blender to increase process knowledge and improve product quality.

Keywords

Pharmaceuticals, mixing, acoustic emissions, sound, vibrations, monitoring, powder handling, moisture content, flowability, process analytical technologies

Co-Authorship Statement

Chapter 2 is a review article and chapters 3, 4, 5 and 6 are research studies that have either

been published or are accepted by peer-reviewed journals. The individual contributions of the

authors of each journal article are stated.

Chapter 3

Passive acoustic emissions from particulates in a V-blender

Authors: A. Crouter, L. Briens

Status: Published in Drug Development and Industrial Pharmacy, 41, 1809-1818, 2015.

A. Crouter conducted all experimental work and performed all data analysis. The manuscript

was jointly written and revised by A. Crouter and L. Briens. Guidance for the work was

provided by L. Briens.

Chapter 4

The effect of moisture on the flowability of pharmaceutical excipients

Authors: A. Crouter, L. Briens

Status: Published in AAPS PharmSciTech, 15, 65-74, 2014.

A. Crouter conducted all experimental work and performed all data analysis. The manuscript

was jointly written and revised by A. Crouter and L. Briens. Guidance for the work was

provided by L. Briens.

iii

Chapter 5

The effect of moisture on passive acoustic emissions in a V-blender

Authors: A. Crouter, L. Briens

Status: Published in *Powder Technology*, 299, 226-234, 2016.

A. Crouter conducted all experimental work and performed all data analysis. The manuscript

was jointly written and revised by A. Crouter and L. Briens. Guidance for the work was

provided by L. Briens.

Chapter 6

Monitoring lubricant addition using passive acoustic emissions in a V-blender

Authors: A. Crouter, L. Briens

Status: Accepted by *Powder Technology*, available online July 22, 2016.

A. Crouter conducted all experimental work and performed all data analysis. The manuscript

was jointly written and revised by A. Crouter and L. Briens. Guidance for the work was

provided by L. Briens.

iv

Acknowledgments

I would like to acknowledge the assistance provided to me by several people. I would first and foremost like to thank my thesis advisor Dr. Lauren Briens for her guidance, encouragement and friendship throughout the duration of my studies. Without her contributions and support, the completion of my thesis would not have been possible. I would also like to thank my advisory committee Dr. Madhumita Ray and Dr. Shahzad Barghi.

I would like to acknowledge the Natural Sciences and Engineering Research Council of Canada (NSERC) and the Ontario Graduate Scholarship Program (OGS) for their financial support.

I would like to thank the Chemical and Biochemical Engineering faculty and staff for providing education and support during my studies. I would like to thank Heather Bloomfield of Surface Science Western for her assistance examining my powders. I would also like to thank Brian Dennis and Souheil Afara for their assistance and expertise.

I would like to thank my friends and lab members for their constant encouragement and support. Finally I would like to thank my family; Mom, Dad, and my brother Nick, for their love and support during this journey.

Table of Contents

Abstra	act		i
Co-Aı	uthorshi	p Statement	iii
Ackno	wledgn	nents	v
Table	of Cont	ents	vi
List of	f Tables		xi
List of	f Figure:	S	xii
List of	f Appen	dices	xvi
Chapt	er 1		1
1 Int	roductio	n	1
1.1	Blendi	ng	2
	1.1.1	Tumbling blenders	2
1.2	Proces	s Monitoring	3
1.3	Passiv	e Acoustic Emissions	4
	1.3.1	Sensors	5
	1.3.2	Sampling	5
1.4	Thesis	Objectives and Overview	6
1.5	Refere	nces	7
Chapt	er 2		9
2 A 1	eview o	f monitoring methods for mixing pharmaceutical powders	9
2.1	Introdu	uction	9
2.2	Near-i	nfrared (NIR) Spectroscopy	10
	2.2.1	Introduction	10
	2.2.2	Analysis of NIR spectra	10
	2.2.3	Advantages and disadvantages of NIR spectroscopy	15

2.3	Raman	Spectroscopy	16
	2.3.1	Introduction	16
	2.3.2	Analysis of Raman spectra	16
	2.3.3	Applications of Raman spectroscopy	17
	2.3.4	Advantages and disadvantages of Raman spectroscopy	17
2.4	Magne	tic Resonance Imaging (MRI)	18
	2.4.1	Introduction	18
	2.4.2	Applications of MRI	19
	2.4.3	Advantages and disadvantages of MRI	19
2.5	Radioa	active Tracers	19
	2.5.1	Introduction	19
	2.5.2	Tracer selection	20
	2.5.3	Applications of radioactive tracers	21
	2.5.4	Advantages and disadvantages of radioactive tracers	22
2.6	Therm	al Techniques	22
	2.6.1	Thermal tracers	22
	2.6.2	Thermal effusivity	22
	2.6.3	Advantages and disadvantages of thermal techniques	23
2.7	Image	Analysis	24
	2.7.1	Introduction	24
	2.7.2	Analysis of images	24
	2.7.3	Advantages and disadvantages of image analysis	25
2.8	Laser-i	induced Fluorescence (LIF)	25
	2.8.1	Introduction	25
	2.8.2	Applications of LIF	25
	2.8.3	Advantages and disadvantages of LIF	26

	2.9	Optic 1	Probe Measurements	27
	2.10)Comp	uted Tomography	28
	2.11	l Acous	tic Emission Monitoring	28
		2.11.1	Introduction	28
		2.11.2	Applications of acoustic emission monitoring	29
		2.11.3	Advantages and disadvantages of acoustic emission monitoring	30
	2.12	2Concl	usions	30
	2.13	3Refere	nces	32
C	hapte	er 3		40
3	Pass	sive acc	oustic emissions from particulates in a V-blender	40
	3.1	Introd	uction	40
	3.2	Materi	als and Methods	43
		3.2.1	Particles	43
		3.2.2	V-blender	43
		3.2.3	Sensors and data acquisition system	44
	3.3	Result	s and Discussion	44
		3.3.1	Signal capturing and filtering.	44
		3.3.2	Sensor location	47
		3.3.3	Effect of particle size	52
		3.3.4	Effect of fill level	53
		3.3.5	Effect of scale	56
		3.3.6	Effect of particle type	58
	3.4	Conclu	usions	60
	3.5	Refere	ences	61
C	hapte	er 4		65
4	The	effect	of moisture on the flowability pharmaceutical excipients	65

	4.1	Introdu	action	65
	4.2	Materi	als and Methods	69
		4.2.1	Materials	69
		4.2.2	Moisture adsorption isotherms	70
		4.2.3	Flowability measurements	71
		4.2.4	Dynamic density	72
	4.3	Result	S	72
		4.3.1	Powder size, shape and morphology	72
		4.3.2	Moisture adsorption isotherms	74
		4.3.3	Flowability	76
		4.3.4	Dynamic density	77
	4.4	Discus	sion	78
	4.5	Conclu	isions	82
	4.6	Refere	nces	83
Cl	napte	er 5		86
5	The	effect	of granule moisture on passive acoustic emissions in a V-blender	86
	5.1	Introdu	action	86
	5.2	Materi	als and Methods	89
		5.2.1	Solids	89
		5.2.2	Equipment and acoustic measurements	90
		5.2.3	Flowability measurements	91
		5.2.4	Drying experiments	92
		5.2.5	Supplemental experiments	92
	5.3	Result	S	92
		5.3.1	Wooden beads	92
		5.3.2	Formulation 1	95

		5.3.3	Formulation 2	98
		5.3.4	Supplemental experiments	100
	5.4	Discus	sion	102
	5.5	Conclu	usions	108
	5.6	Refere	nces	109
Cl	napte	er 6		113
6	Moi	nitoring	Lubricant Addition using Passive Acoustic Emissions in a V-blende	er 113
	6.1	Introdu	action	113
	6.2	Materi	als and Methods	116
		6.2.1	Solids	116
		6.2.2	Equipment and acoustic measurements	118
		6.2.3	Flowability measurements	119
		6.2.4	Supplemental experiments	119
	6.3	Result	s	120
		6.3.1	Sugar spheres	120
		6.3.2	Formulation A	126
		6.3.3	Formulation B	131
	6.4	Discus	sion	135
	6.5	Conclu	ısions	141
	6.6	Refere	nces	142
Cl	napte	er 7		145
7	Gen	eral Di	scussion and Conclusion	145
	7.1	Refere	nces	150
A _j	ppen	dices		151
C.	ırricı	ılıım V	itaa	150

List of Tables

Table 2.1: NIR spectroscopy applications for monitoring mixing	11
Table 2.2: Summary of monitoring techniques	31
Table 3.1: Applications of acoustic emission monitoring	42
Table 3.2: Particle properties	43
Table 3.3: V-blender shell properties	43
Table 4.1: Summary of previous studies	68
Table 4.2: Summary of parameters from the fitted GAB equation	76
Table 5.1: Applications of acoustic emission monitoring	88
Table 5.2: Formulation composition	90
Table 5.3: Solids properties	90
Table 5.4: Coefficient of restitution	92
Table 6.1: Formulation composition	117
Table 6.2: Solids properties	117
Table 6.3: Coefficient of restitution of sugar spheres	119

List of Figures

Figure 1.1: Schematic of pharmaceutical tablet manufacturing pathway	1
Figure 3.1: Sensor locations	44
Figure 3.2: (a) Signal of empty V-blender, (b) Windowed sinc filter of signal, and (c)	
Wavelet filter of signal captured from top sensor	46
Figure 3.3: Photographs showing motion of sugar spheres during rotation of V-shell	48
Figure 3.4: Filtered signals of 14-18 mesh spheres captured by (a) top sensor, (b) bottom sensor, and (c) side sensor	
Figure 3.5: Filtered signal of 14-18 mesh spheres captured by top sensor related to particular motion	
Figure 3.6: Sugar sphere particle sizes; (a) 60-80 mesh, (b) 20-25 mesh, (c) 16-20 mesh, (d) 14-18 mesh	
Figure 3.7: Effect of particle size on vibration amplitudes for sugar spheres	53
Figure 3.8: V-blender filled at (a) 40%, (b) 60%, and (c) 75% of capacity with sugar sph	
Figure 3.9: Effect of scale on acoustic emissions using an equal of mass of sugar sphere (a) 4 QT, (b) 8 QT, and (c) 16 QT shell	
Figure 3.10: Effect of particle type on measured acoustic emissions in the 8 QT V-shell	using
(a) MCC, (b) lactose, and (c) 60-80 mesh sugar spheres	59
Figure 4.1: Schematic diagram of the humidity chamber	70
Figure 4.2: Particle size distributions of the powders	73
Figure 4.3: Scanning electron micrographs of the powders	74
Figure 4.4: Moisture adsorption isotherms of the tested powders	75

Figure 4.5: Avalanche times and standard deviations for (a) MCC, (b) CMC, (c) HPMC, (d)
PVP, (e) Corn starch and (f) Potato starch	77
Figure 4.6: Dynamic density measurements of (a) the celluloses and PVP and (b) the starc	
Figure 5.1: Sensor location	91
Figure 5.2: Filtered signal of wooden beads for one rotation of the V-blender	93
Figure 5.3: Maximum vibration amplitude for feature 1, feature 2, and feature 3 for the wooden beads at measured solids moisture contents	94
Figure 5.4: Difference in maximum vibration amplitude between feature 1 & 2 and feature & 3 for the wooden beads at measured solids moisture contents	
Figure 5.5: Avalanche time for the wooden beads at measured solids moisture contents	95
Figure 5.6: Filtered signal of formulation 1 granules for one rotation of the V-blender	96
Figure 5.7: Maximum vibration amplitude for feature 1 for the formulation 1 granules at measured solids moisture contents	96
Figure 5.8: Difference in maximum vibration amplitude between feature 1 & 2 and feature & 3 for the formulation 1 granules at measured solids moisture contents	
Figure 5.9: Avalanche time for the formulation 1 granules at measured solids moisture contents	97
Figure 5.10: Filtered signal of formulation 2 granules for one rotation of the V-blender	98
Figure 5.11: Maximum vibration amplitude for feature 1 for the formulation 2 granules at measured solids moisture contents	
Figure 5.12: Difference in maximum vibration amplitude between feature 1 & 2 and featu	re 1
& 3 for the formulation 2 granules at measured solids moisture contents	99

Figure 5.13: Avalanche time for the formulation 2 granules at measured solids moisture
contents
Figure 5.14: Filtered signal of sugar spheres at (a) dry and (b) wet states for one rotation of the V-blender
TOT
Figure 5.15: Avalanche time for the sugar spheres at measured solids moisture contents 102
Figure 6.1: Sensor location
Figure 6.2: Filtered signal of sugar spheres (a) prior to and (b) immediately after lubricant addition, and (c) after dispersal for one rotation of the V-blender
Figure 6.3: Maximum vibration amplitude for feature 1 of the sugar spheres for lubricant addition of (a) 1wt%, (b) 2.5wt%, and (c) 5wt% over the entire dispersal
Figure 6.4: Avalanche angle for the sugar spheres before lubricant addition and after the addition of 1wt%, 2.5wt%, and 5wt%
Figure 6.5: Photographs of sugar sphere samples removed at (a) 1, (b) 10, and (c) 30 revolutions after lubricant addition
Figure 6.6: Scanning electron micrographs of (a) sugar spheres, (b) formulation A granules, and (c) formation B granules; (i) plain solids, (ii) 1wt%, (iii) 2.5wt%, and (iv) 5wt%
lubricant dispersed
Figure 6.7: Filtered signal of formulation A granules (a) prior to and (b) immediately after lubricant addition, and (c) after dispersal for one rotation of the V-blender
Figure 6.8: Maximum vibration amplitude for feature 1 of the formulation A granules for lubricant addition of (a) 1wt%, (b) 2.5wt%, and (c) 5wt% over the entire dispersal 130
Figure 6.9: Avalanche angle for the formulation A granules before lubricant addition and after the addition of 1wt%, 2.5wt%, and 5wt%
Figure 6.10: Filtered signal of formulation B granules (a) prior to and (b) immediately after lubricant addition, and (c) after dispersal for one rotation of the V-blender
, , , , , , , , , , , , , , , , , , ,

Figure 6.11: Maximum vibration amplitude for feature 1 of the formulation B g	ranules for
lubricant addition of (a) 1wt%, (b) 2.5wt%, and (c) 5wt% over the entire disper-	sal 134
Figure 6.12: Avalanche angle for the formulation B granules before lubricant ac	ldition and
after the addition of 1wt%, 2.5wt%, and 5wt%	135

List of Appendices

Appendix A: Sample matlab code for wavelet filter	5	1
---	---	---

Chapter 1

1 Introduction

The pharmaceutical manufacturing process is a number of batch steps; Figure 1.1 is a schematic of the most common pharmaceutical tablet manufacturing pathway. After each step, the process is stopped for testing to ensure the product complies with quality standards. The process continues only after the product at each stage successfully meets standards, otherwise the product is discarded and the process must begin again.



Figure 1.1: Schematic of pharmaceutical tablet manufacturing pathway

During the final blending stage, granules are mixed with additional excipients, such as lubricants and/or glidants, in preparation for tabletting. This final blending stage is critical as this is the last step before tabletting and uniformity is necessary to produce a tablet that has a reproducible dissolution profile, uniform taste and colour, and to guarantee the appropriate amount of active ingredient in every dosage unit (1, 2). The following sections will introduce blending, process monitoring, and passive acoustic emissions.

1.1 Blending

It can be difficult to achieve homogeneity in a mixture when there are differing particle sizes, shapes, and densities. To reduce these issues, the active ingredient is usually granulated with various excipients to form a more stable unit as a granule. A granule is a combination of the initial powders that have been adhered together using a binder. The granules are larger than the individual components and help to reduce segregation and improve content uniformity of the final product (3).

In the final blending stage, the dried granules are mixed with additional excipients in preparation for tabletting. Usually the blending is performed in a tumbling blender as this type of blender provides gentle mixing so that the added excipients are not over-mixed with the granules. While excipients, such as glidants and lubricants, are necessary to ensure good flow of the granules into the tablet press and ensure that the tablet is cleanly ejected from the tablet die, the level of blending is critical. For example, while reducing friction, lubricant addition may also cause undesirable changes in the properties of the tablet. The effect of lubricant concentration on the tensile strength of tablets was investigated and, for plastic materials, the tensile strength decreased as the lubricant concentration increased (4). The effect of mixing time has also been investigated; the hardness and ejection force of the tablets decreased with mixing time and the disintegration time increased; the trends were similar with an increase in lubricant concentration (5).

1.1.1 Tumbling blenders

A thorough review of solid mixtures, mixing mechanisms and mixing equipment can found from Fan et al. (6). Mixers can generally be divided into two categories: convective blenders and tumbling blenders (7). Convective blenders use an impeller to stir the powder within a fixed vessel while tumbling blenders rely on the action of gravity to cause the powder to cascade within a rotating vessel. The research presented in this thesis was conducted in a V-blender, a tumbling blender that is widely studied and used in industry.

Several flow regimes are possible within a rotating cylinder including slipping, slumping, rolling, cascading, cataracting and centrifuging. The speed of the vessel relative to the critical speed required for centrifugation to occur is an indication of which flow regime will dominate. This can be represented by the Froude number:

$$Fr = \frac{V^2}{gL} \tag{eq. 1}$$

where V is the characteristic speed, usually the tip speed, and L is the characteristic length, usually the diameter of the vessel (7). Large scale tumbling blenders usually operate at a Froude number less than 0.2 and studies have shown that within that range the tumbling regime dominates with particles cascading from one end of the shell to the other (7, 8).

In the tumbling regime the flow within a V-blender can be divided into two phases: from 0-180° the powder bed separates into two streams, one in each arm, and then from 180-360° the material in each arm recombines in the bottom of the V-blender (8). The repetition of these phases leads to convection of the materials within each arm but dispersion between the arms tends to be slower, as materials only cross the plane of symmetry as the mixture is reassembled (7, 8).

1.2 Process Monitoring

As the level of blending has an impact on the final product quality it is important to be able to monitor blending progress. Currently, the pharmaceutical industry assesses blend uniformity through the extraction of samples using thief probes followed by analytical methods, such as spectroscopy, to determine the sample composition. This method suffers from many disadvantages: multiple samples are required from various positions within the powder bed, it is difficult to obtain representative samples as the probes disturb the bed and can promote channeling and segregation, sub-sampling may be required, and the analysis is labour intensive and time consuming (9, 10).

The development of process analytical technologies (PAT) can improve product monitoring with the aim of increasing efficiency, product quality and consistency and creating a better understanding of the manufacturing process. Ideally these are inline methods to remove issues related to extractive sampling and allow direct monitoring of the system using various sensors. For mixing processes, PAT would improve efficiency through better monitoring and control resulting in fewer rejected batches and also improve product quality.

Many technologies have been investigated, including near-infrared spectroscopy, Raman spectroscopy, magnetic resonance imaging, radioactive tracers, image analysis, tomography, and acoustic emission monitoring. Chapter 2 will provide a more detailed discussion of the application and development of these technologies.

1.3 Passive Acoustic Emissions

The focus for this thesis is the development of passive acoustic emissions as a method for monitoring solids tumbling in a V-blender. Passive acoustic emission monitoring offers many advantages over other monitoring methods under development: (i) the method is completely non-invasive, not requiring any window or ports into the process vessel, (ii) the method is non-destructive, passive emissions are generated by the process itself, (iii) the capital cost is less than other methods. Although passive acoustic emissions produce large volumes of data that must be appropriately analyzed to extract the relevant information for monitoring, this processing can be less extensive than the complex calibrations and processing required for other techniques. Therefore, the many advantages easily outweigh any possible disadvantages.

Acoustics refers to the generation, transmission and reception of energy in the form of vibration waves (11). Frequencies in the audible range, between 20 and 20,000 Hz, are known as sound waves and can be detected by the human ear. Below 20 Hz are infrasonic waves and above 20,000 Hz are ultrasonic waves (12). Frequencies in the audible range were examined in this research.

Acoustic emissions from blending processes are thought to result from particle-particle collisions and particle-equipment collisions, with the major source identified to be particle-equipment collisions (13-18). Bellamy et al. (19) compared near-infrared

spectroscopy (NIR) and acoustic emission monitoring to obtain mixing profiles and Allan et al. (20) compared acoustic emissions and NIR to investigate the effect of impeller speed, mass/density of the powder, and particle size on the mixing profile. Both of these studies showed that mixing profiles from NIR and acoustic emission monitoring were equivalent. However, signals obtained from acoustic emissions were noisier and therefore need further development for this measurement technique to realize its full potential.

1.3.1 Sensors

In this research, acoustic emissions from the tumbling solids were collected using PCB® (PicoCoulomB) Piezotronics accelerometers combined with ICP® (integrated circuit piezoelectric) signal conditioners. Piezoelectric accelerometers use the piezoelectric effect of quartz to generate an electrical output that is proportional to the applied acceleration. The piezoelectric effect produces an opposed accumulation of charged particles on the crystal; the charge is proportional to the applied force. An applied force alters the alignment of the positive and negative ions on the quartz crystal lattice structure which results in an accumulation of these charged ions on opposed surfaces. These charged ions accumulate on an electrode and are transmitted to a signal conditioner (21).

The mounting of the accelerometer is one of the most important considerations; the mounting technique has an effect on the accuracy of the usable frequency response (21). Adhesive mounting was chosen for this work as it allowed a stable attachment to provide the most accurate results and did not interfere with the equipment operation.

1.3.2 Sampling

The voltage signal acquired during tumbling is a continuous analog signal. For computer processing, the signal must be converted to a digital format by sampling at discrete time intervals. Based on Nyquist theorem, the minimum sampling frequency must be at least twice the maximum frequency of the signal being acquired. For signals in the audible range with a maximum frequency of 20,000 Hz a sampling rate of at least 40,000 Hz must be used to obtain representative data. This is done to prevent signal distortion that can occur when a continuous signal is reconstructed in a digital format. The

accelerometers had a range of 0.35-12,000 Hz and a sampling rate of 40,000 Hz was used.

1.4 Thesis Objectives and Overview

The objective of this thesis was to develop passive acoustic emissions as a method for monitoring solids tumbling in a V-blender. The objective was not only to understand how different particle parameters could affect the acoustic emissions but also to investigate the origin of such relationships and build process knowledge. In addition, it was desired to understand the robustness of the method in terms of detecting changes in critical quality attributes and process parameters. The objectives are addressed over the subsequent chapters, as follows:

Chapter 2: Provides a summary of PAT development for mixing processes.

Chapter 3: Uses PAEs to monitor various process conditions while solids are tumbling in a V-blender.

Chapter 4: Investigates the relationship between the moisture content of a powder and its effect on flowability. The avalanche behavior was chosen as indication of flowability.

Chapter 5: Applies PAEs to detect changes in solids moisture content as they tumbled in a V-blender.

Chapter 6: Expands the development of PAEs for inline use by investigating the sensitivity of PAEs to lubricant addition.

Chapter 7: Summarizes the progress made in the development of PAEs as a PAT and discusses potential applications as well as opportunities for future work.

1.5 References

- 1. Mathews L, Chandler C, Dipali S, Adusumilli P, Lech S, Daskalakus S, Mathis N. Monitoring blend uniformity with effusivity. Pharm Technol 2002; 26: 80-84.
- Leonard G, Bertrand F, Chaouki J, Gosselin PM. An experimental investigation of effusivity as an indicator of powder blend uniformity. Powder Technol 2008; 181: 149-159.
- 3. Sherrington PJ, Oliver R. Granulation. In: Goldberg AS, ed. Monographs in powder science and technology. London: Heyden, 1981.
- 4. Jarosz PJ, Parrott EL. Effect of lubricants on tensile strengths of tablets. Drug Dev Ind Pharm 1984; 10: 259-273.
- Kikuta JI, Kitamori N. Effect of mixing time on the lubricating properties of magnesium stearate and the final characteristics of the compressed tablets. Drug Dev Ind Pharm 1994; 20: 343-355.
- 6. Fan LT, Chen Y-M, Lai FS. Recent developments in solids mixing. Powder Technol 1990; 61: 255-287.
- 7. Brone D, Alexander A, Muzzio F. Quantitative characterization of mixing of dry powders in v-blenders. AIChE J 1998; 44: 271-278.
- 8. Lemieux M, Bertrand F, Chaouki J, Gosselin P. Comparative study of the mixing of free flowing particles in a V-blender and a bin-blender. Chem Eng Sci 2007; 62: 1783-1802.
- 9. Vergote GJ, De Beer TRM, Vervaet C, Remon JP, Baeyens WRG, Diericx N, Verpoort F. In-line monitoring of a pharmaceutical blending process using FT-Raman spectroscopy. Eur J Pharm Sci 2004; 21: 479-485.
- 10. Hausman DS, Cambron RJ, Sakr A. Application of Raman spectroscopy for on-line monitoring of low dose blend uniformity. Int J Pharm 2005; 298: 80-90.
- 11. Kinsler LE, Frey AR, Coppens AB, Sanders JV. Fundamentals of acoustics. United States of America: John Wiley & Sons Inc., 2000.
- 12. Boyd J, Varley J. The uses of passive measurement of acoustic emissions from chemical engineering processes. Chem Eng Sci 2001; 56: 1749-1767.
- 13. Leach M, Rubin G, Williams J. Particle size determination from acoustic emissions. Powder Technol 1977; 16: 153-158.

- 14. Leach M, Rubin G, Williams J. Particle size distribution characterization from acoustic emissions. Powder Technol 1978; 19: 157-167.
- 15. Leach M, Rubin G, Williams J. Analysis of polydisperse systems of rigid particles from acoustic emissions. Powder Technol 1978; 19: 169-176.
- 16. Leach M, Rubin G, Williams J. Analysis of a Gaussian size distribution of rigid particles from their acoustic emissions. Powder Technol 1978; 19: 189-195.
- 17. Leach M, Rubin G. Size analysis of particles of irregular shape from their acoustic emissions. Powder Technol 1978; 21: 263-267.
- 18. Tily P, Porada S, Scruby C, Lidington S. Monitoring of mixing processes using acoustic emission. In: Harnby N, Benkreira H, Carpenter K, Mann R, eds. Fluid Mixing III. Rugby: The Institute of Chemical Engineers, 1988: 75-94.
- 19. Bellamy L, Nordon A, Littlejohn D. Non-invasive monitoring of powder mixing with near infrared spectroscopy and acoustics. Spectrosc Eur 2004: 25-27.
- 20. Allan P, Bellamy L, Nordon A, Littlejohn D. Non-invasive monitoring of the mixing of pharmaceutical powders by broadband acoustic emission. Anal 2010; 135: 518-524.
- 21. PCB Goup Inc., 2016. Introduction to piezoelectric accelerometers. [Online]

 Available at: http://www.pcb.com/techsupport/tech_accel [Accessed 31 May 2016].

Chapter 2

2 A review of monitoring methods for mixing pharmaceutical powders

2.1 Introduction

The pharmaceutical industry has a critical interest in powder mixing processes as approximately 80% of marketed products are in solid dosage forms. Powder blend uniformity is not only necessary to produce a tablet or capsule that has reproducible dissolution profile, uniform taste, and colour, but homogeneity is essential to guarantee the appropriate amount of active ingredient in every dosage unit (1, 2). New formulations can contain actives that are very targeted and potent and therefore only required in small quantities. Blend uniformity is critical for these low concentration actives, but it is also more difficult to achieve. Therefore, there is an increasing need for methods that provide accurate and reliable information about the mixture homogeneity and can identify the optimal process end-point.

Currently, the pharmaceutical industry assesses blend uniformity through extraction of samples using thief probes followed by analytical methods, such as spectroscopy, to determine the sample composition. This assessment suffers from many disadvantages: multiple samples are required from various positions within the beds, it is difficult to obtain representative samples as the probes disturb the beds and can also promote channelling and segregation, sub-sampling may be required, segregation or other changes in the sample could occur between extraction and analysis, and the analysis is labour intensive and time consuming (3, 4). The Barr Laboratories trial in 1993 highlighted the difficulties in sampling and the need for better methods to monitor and control mixing processes (5). The ICH (International Council for Harmonization of Technical Requirements for Pharmaceuticals for Human Use) Q8 guideline for pharmaceutical development defines a process analytical technology (PAT) as "a system for designing, analyzing, and controlling manufacturing through timely measurements (i.e., during processing) of critical quality and performance attributes of raw and in-process materials and processes with the goal of ensuring final product quality" (6). For mixing processes,

PAT would improve efficiency through better monitoring and control resulting in fewer rejected batches and also improve product quality. These PAT methods are inline methods so the issues related to sampling are removed as these methods directly monitor the process using sensors.

Many technologies have been investigated to evaluate the uniformity of the mixture and to monitor and identify the optimal mixing time. These technologies include near-infrared spectroscopy, Raman spectroscopy, magnetic resonance imaging, radioactive tracers, image analysis, tomography, and acoustic emission monitoring.

2.2 Near-infrared (NIR) Spectroscopy

2.2.1 Introduction

Near-infrared spectroscopy identifies components in the probe measurement volume based on bond vibrations following irradiation. The NIR probe irradiates the powder within its measurement volume and then measures the absorption of energy within the near-infrared region of 800 to 2,500 nm. Each powder absorbs energy differently as each has a unique combination of bonds, particularly C-H, N-H and O-H bonds (7, 8). The obtained NIR spectra will therefore have a complex pattern that depends on the composition within the measurement volume.

2.2.2 Analysis of NIR spectra

The NIR spectra obtained from measurements are complex: the absorption bands are weak with broad and overlapping energy peaks. As shown in Table 2.1, the NIR spectra may be pre-treated and then analyzed in many ways to determine mixture homogeneity.

Table 2.1: NIR spectroscopy applications for monitoring mixing

Reference	Active(s)	Excipients	Mixer	Pre-treatment method	Spectral analysis
Sekulic et al. (9)	sodium	lactose, avicel,	V blender	second derivative	visual analysis,
	benzoate	magnesium stearate			moving block of
II.'1 (1 (10)	· · · · · · · · · · · · · · · · · · ·	1	N/	SNV with DT	standard deviation
Hailey et al. (10)	active from Pfizer	lactose, maize starch	Y cone blender	SNV with D1	moving block of standard deviation
Wargo and	hydrocholor	Fast-flo lactose,	twin shell	second derivative	PCA, BEST, modified
Drennen (11)	thiazide	croscarmellose sodium, magnesium	blender		BEST
Berntsson et al. (7)		stearate	Nauta-mixer	MSC, SNV	
Moes et al. (12)			14auta-IIIIXCI	second derivative,	moving block of
111005 et al. (12)				SNV	standard deviation
De Maesschalck et	active	lactose, maize	tumbling	second derivative,	mean standard
al. (13)		starch, aerosil	blender	SNV, DT	deviation, dissimilarity, PCA
Sekulic et al. (14)	active	Avicel, DCP,	flo-bin	DT, SNV, SNV with	moving block of
		sodium glycolate	blender	DT, second derivative	standard deviation,
		starch, magnesium			dissimilarity, PCA,
DI (17)	G 61 11	stearate		1'	SIMCA
Blanco et al. (15)	Gemfibrozil	maize starch,	rotary agitator	normalization,	PLSR
		magnesium stearate, colloid silica		derivatives, MSC, SNV, DT	
Blanco et al. (16)	otilonium	corn starch,	bladed mixer	SNV	dissimilarity, moving
	bromide	carboxymethyl			block of standard
		starch,			deviation, mean
		microcrystalline cellulose			square of differences
Cuesta Sanchez et				DT, SNV, second	Visual analysis, mean
al. (17)				derivative, SNV with	standard deviation,
				DT	dissimilarity, PCA, SIMPLISMA
Ciurzack et al. (18)	Aspirin	lactose, talc		SNV, second	Visual analysis,
	Vitamin B12			derivative	spectral match value, PCA
El-Hagrasy et al.	salicylic	Fast-flo lactose	V blender	SNV, MSC, second	PCA, SIMCA,
(19)	acid			derivative	moving block of
					standard deviation
El-Hagrasy et al. (20)	salicylic acid	Fast-flo lactose	V blender	SNV, MSC, second derivative	PCA
El-Hagrasy et al.	salicylic acid	Fast-flo lactose	V blender	second derivative	SIMCA, PC-MBEST
(21) El-Hagrasy and	salicylic	Fast-flo lactose	V blender	second derivative	PLS, PCR, MLR
Drennen (22)	acid	rast-no lactuse	v Dielidel	SCORU UCIIVALIVE	1 LS, I CK, WILK
Bellamy et al. (23)	aspirin	Avicel, citric acid,	convective	first derivative	visual observations
		aspartame, povidone	mixer		
Koller et al. (8)	salicylic	lactose	bladed mixer	SNV with DT	PLSR and PCR
	acid	monohydrate			
Shi et al. (24)	acetaminop	Avicel, lactose	Bin blender	Savitzky-Golay	PLS, RMS, relative
	hen			smoothing with	standard deviation,
				second derivative and	moving block
T 1 /05			B: 11 :	normalization, SNV	standard deviation
Liew et al. (25)	chlorphenira mine	Avicel, lactose, magnesium stearate	Bin blender	smoothing with SNV and first derivative	PLSR
#PECE!	maleate				

^{*}BEST bootstrap error-adjusted single-sample technique, DCP dibasic calcium phosphate, SIMCA soft idependent modeling class analogy, PLSR partial-least squares regression, SIMPLISMA simple-to-use interactive self-modeling

mixture analysis, PC-MBEST principal-component modified BEST, PCR principal component regression, MLR multi-term linear regression, RMS root mean square

2.2.2.1 NIR spectra pre-treatment

NIR spectra pre-treatment corrects or minimizes spectral contributions that are due to the physical properties of the powders such as particle size or bulk density as well as measurement volume (8, 16). Pre-treatment methods include normalization, smoothing, derivatives, multiplicative scatter correction (MSC), standard normal variate (SNV), and detrending (DT). Normalization involves dividing the spectra by the mean value of each individual spectrum. Smoothing reduces the noise in the spectra caused by random high frequency perturbations: the simple filter coefficient vector uses a moving average method, calculating the arithmetic mean of the values within a spectral window, while the Savitzky-Golay filter fits a low-degree polynomial through the points within the spectral window. Derivatives are used to remove or minimize constant background signals while enhancing the resolution of the absorbance peaks of the spectra. The second derivative is a popular pre-treatment method as it helps identify weak peaks that are not visible in the original spectrum. Derivative pre-treatment, however, results in the loss of the original shape of the spectral curve and also a reduction of the signal to noise ratio. Multiplicative scatter correction shifts and scales each spectrum to fit a specified target spectrum, usually the spectrum corresponding to the uniform final mixture. A linear regression based on the sum of the squared differences between the transformed and target spectra is used to estimate the parameters for shifting and scaling. The standard normal variate centers each spectrum around zero by subtracting the mean and dividing by the standard deviation of the entire spectrum. Detrending fits a low degree polynomial through all data points of the spectrum and then subtracts the fitted polynomial curve from the spectrum. Detrending is often used together with standard normal variate pre-treatment (26).

Blanco et al. (15) examined the effect of pre-treatment methods in NIR spectroscopy to determine the amount of active Gemfibrozil in formulation samples. Normalization, first and second derivatives, MSC, SNV and DT were examined with the effectiveness of each method assessed using the V/M ratio, a measure of the scatter due to particle size relative to the spectral features. The second derivative was identified as the most effective for

reducing scatter in the NIR spectra. El-Hagrasy et al. (20) also found the second derivative to be more effective than SNV or MSC pre-treatment methods. Comparing SNV, DT and the second derivative of NIR spectra from mixing lactose, maize starch and aerosol in a tumbling blender, de Maesschalck et al. (13) concluded that SNV was the best pre-treatment method, as replicate spectra of the individual components showed the least variation with this method. This different conclusion could be due to the pre-treatment methods using individual compounds rather than mixtures as performed by Blanco et al. (15) and El-Hagrasy et al. (20).

2.2.2.2 NIR spectra comparison

After pre-treatment, the NIR spectra are compared to show changes with time, with homogeneity assumed at the point at which significant changes no longer occur or compared to a spectrum of an independently prepared homogeneous sample.

2.2.2.2.1 Visual analysis

The NIR spectra obtained at various processing times can be visually compared to a spectrum of an independently prepared homogenous sample. This allows assessment of changes in the mixture uniformity with time. Visual analysis, however, is subjective and therefore usually mathematical evaluations are used to compare the spectra (16).

2.2.2.2. Dissimilarity

Dissimilarity monitors changes in the mixture uniformity in real-time by comparing spectra measured at different times during the process to a spectrum from a homogeneous sample. The measured spectra are normalized and projected onto the normalized homogeneous sample spectrum. Dissimilarity is then calculated by:

$$D_i = z_i - \left(z_i z_{mix}^T\right) z_{mix}$$
 (eq. 1)

where z_i are the normalized spectra and z_{mix} is the homogeneous sample spectrum with T indicating the transpose of the variable z_{mix} . Dissimilarity ranges from zero indicating large differences between the spectra to 1 indicating minimal differences. Dissimilarity is then plotted against time to monitor the process.

2.2.2.2.3 Standard deviation

The moving block of standard deviation calculates the standard deviation at each wavelength i for a set of n consecutively recorded spectra:

$$S_{i} = \sqrt{\frac{\sum_{j=1}^{n} (A_{ij} - \overline{A}_{i})^{2}}{n-1}}$$
 (eq.2)

where A_{ij} is the absorbance at wavelength i in spectrum j and \overline{A}_i is the mean absorbance for the n spectra at the same wavelength. The mean standard deviation is then calculated:

$$S = \frac{\sum_{i=1}^{m} S_i}{m}$$
 (eq. 3)

where S_i is the standard deviation of each window and m is the number of windows. This mean standard deviation is then plotted against time to monitor the process; homogeneity is indicated at the point at which this profile reaches a plateau.

2.2.2.4 Mean square of differences

Blanco et al. (16) proposed an analysis method that relies on the difference between two spectra recorded at two consecutive times. The mean square of differences between these spectra is calculated:

$$S^{2} = \frac{\sum_{i=1}^{m} (A_{i}^{t_{1}} - A_{i}^{t_{0}})^{2}}{m}$$
 (eq. 4)

where $A_i^{t_1}$ is the absorbance at each wavelength i for the spectrum at time t_1 and $A_i^{t_0}$ is the absorbance at the same wavelength at the immediately preceding time t_0 . The mean square of differences is plotted against time and the process end-point is identified as the time at which this parameter becomes low and constant. An advantage of the mean square of differences analysis over many other analysis techniques is that a spectrum corresponding to a homogeneous sample is not required (16).

2.2.2.5 Principal component analysis (PCA) and partial least squares analysis (PLS)

Principal component analysis (PCA) and partial least squares (PLS) are the two most commonly selected multivariate analysis techniques for comparing NIR spectra. PCA decomposes an X matrix, created from the collected spectra arranged in rows with each row representing one time point in the blend monitoring process, into three matrices:

$$X = USV^{T}$$
 (eq. 5)

where U represents scores, S is a diagonal matrix of the square root of the eigenvalues of X^TX and XX^T , V contains loadings, and T indicates transpose. The S matrix is ordered such that $S_1 > S_2 > ... > S_N$ or the first principal component describes the direction of the greatest variance encountered in the response space, the next principal component describes the next greatest amount of variance and so on. The score plot provides qualitative information about the similarity between the spectra and the mixture spectrum and also the similarity between the spectra themselves. The mixture is homogeneous when the scores of the measured spectra are close to the mixture spectrum and equally distributed around them, indicating that they are indistinguishable at different locations.

PLS is a bilinear regression method where many collinear spectral variables are transformed to a small number of new orthogonal variables. The method aims to determine reliable predictors $\hat{Y} = f(X)$ by projecting the many variables $X = (x_1, x_2, ... x_k)$ onto a few variables $\hat{T} = (\hat{t_1}, \hat{t_2}, ... \hat{t_a})$ and using these compressed variables \hat{T} as repressors for y. Common structures in the X variables are compressed into a stabilized more easily interpretable model leaving out any noise such as residuals. It is important to define the most relevant factors \hat{T} both from an interpretation and prediction point of view. A plot of the \hat{Y} vector scores versus the scores for the X matrix is prepared and the best polynomial fit is determined.

2.2.3 Advantages and disadvantages of NIR spectroscopy

NIR spectroscopy is the most widely studied technique for monitoring pharmaceutical mixing processes. It can identify components in a mixture with appropriate calibrations.

This technique, however, requires a measurement window in the process equipment or a port into which the sensor can be inserted. Modifications of the process equipment are therefore required which leads to increased costs and regulatory steps. The tip of the sensor and/or the measurement window must be clear to provide accurate measurements. Therefore, measurement difficulties may occur with cohesive or moist powders (27). As shown by the number of pre-treatment and analysis techniques, interpretation of the NIR spectra can be difficult (27). The peaks in a NIR spectrum corresponding to water are very strong and can easily overlap with other peaks and therefore NIR spectroscopy is not recommended for wetted systems unless the objective is to measure the water content.

2.3 Raman Spectroscopy

2.3.1 Introduction

Raman spectroscopy involves irradiating the powder mixture with monochromatic light and then detecting the scattered light with different frequencies to the incident beam. The difference between the incident and scattered radiation results in characteristic Raman shifts (28). Each component in a mixture will scatter light differently giving a Raman spectrum that will have a complex pattern reflecting the composition of the mixture within the measurement volume. Light with wavelengths between 532 and 1064nm can be used to irradiate the mixture, with probes using 785nm light the most common.

2.3.2 Analysis of Raman spectra

The peaks in Raman spectra are generally sharper and with less overlap than those in NIR spectra. Therefore, only simple univariate techniques are usually required (3). Rantanen et al. (29) compared univariate and multivariate analysis of Raman spectra for binary mixtures of four model systems. A variety of univariate analyses, using different normalization basis, were compared to partial least squares multivariate analysis. Differences between these two analyses were minimal. This is in contrast to NIR spectra where multivariate analysis provides better interpretation than univariate methods. Similar conclusions were obtained by Sasic et al. (30), but with ordinary least squares regression as the univariate method and partial least squares regression as the multivariate method. At high levels of noise in the spectra, however, multivariate analysis was

recommended. Hausman et al. (4) compared univariate and multivariate methods to characterize uniformity of blends containing azimilide, dihydrochloride, spray dried lactose, crospovidone and magnesium stearate mixed using a V-blender. Normalization was used as the univariate method and SNV pre-processing with Mahalanobis distance, comparing the distance of a measured point to points obtained from the calibration using a uniform sample, as the multivariate method. There were no significant differences between the results from the univariate and multivariate methods.

2.3.3 Applications of Raman spectroscopy

Breintenbach et al. (31) investigated Raman spectroscopy through mixing a drug and polymer in a Bohle mixer. The mixture was extruded through a twin-screw configuration, melting the components together. Raman spectroscopy and high performance liquid chromatography (HPLC) analysis was applied to the extruded matrix; the drug with the measured amount was homogeneously distributed within the extruded matrix in agreement between both HPLC and the Raman technique (31). Vergote et al. (3) examined mixing of binary mixtures consisting of diltiazem hydrochloride pellets and paraffinic wax beads in a planetary mixer with a K-shaped mixing arm using Raman spectroscopy. The probe was positioned outside the mixing vessel at a measurement glass window and the spectra were analyzed using the mean square of differences between two consecutive spectra to identify the end-point. This study showed the potential of Raman spectroscopy for inline monitoring of blend homogeneity. De Beer et al. (32) used Raman spectroscopy to examine the effect of mixing speed and loading order on the required mixing time for a multi-component mixture in a high shear mixer. The spectra were normalized and then compared using multivariate analysis to determine the effect of the process parameters.

2.3.4 Advantages and disadvantages of Raman spectroscopy

Raman spectroscopy has some of the same disadvantages as NIR spectroscopy: requirement of a measurement window or port into the mixing vessel, fouling of the probe tip or measurement window, requirement of multiple measurements to ensure accurate representation of the blend and extensive analysis of the measurements.

Raman spectroscopy provides some advantages over NIR spectroscopy. The peaks in a NIR spectrum corresponding to water are very strong and can easily mask the peaks from other components. In contrast, water does not give strong Raman scattering. Therefore, to determine the composition of moist powders, Raman spectroscopy should be used over NIR spectroscopy. As Raman spectra provide sharper and more distinct peaks compared to NIR spectra, only simpler univariate analysis are usually required. Also, Raman spectroscopy is not sensitive to variations in bulk density and particle size within the measurement volume. Therefore, minimal pre-processing of the spectra to minimize these effects is needed.

A disadvantage of Raman spectroscopy is that fluorescence can occur and mask the Raman signal. In Raman scattering the incident photon of light is not fully absorbed, but instead perturbs the molecule. In fluorescence, the photon is completely absorbed followed by the emission of a photon of less energy. A lower light wavelength can reduce fluorescence, but also results in a weaker Raman spectrum. Therefore, for fluorescing components, NIR spectroscopy should be used over Raman spectroscopy.

2.4 Magnetic Resonance Imaging (MRI)

2.4.1 Introduction

An atomic nucleus with a magnetic moment rotates around a magnetic field in the direction of gravity. For each atomic nucleus within a specified magnetic field, there is a unique rotation frequency, known as the Larmor frequency. A known spatial variation of the magnetic field will cause the nucleus at each point to rotate at a different Larmor frequency. MRI measures the distribution of signals as a function of the frequency and relates it to the spatial distribution of nuclear spins (33). MRI provides details about mixing through information about the spatial distribution of certain components in the mixture.

2.4.2 Applications of MRI

Hardy et al. (34) used MRI to evaluate the homogeneity of a binary system mixed in a modified tumbling blender. The binary system consisted of microcapsules filled with oil and solid polymer spheres. The oil filled microcapsules were visible in the images allowing their spatial distribution to be obtained. Hill et al. (35) used MRI to examine axial and radial segregation of granular materials rotated in a drum. The binary mixture consisted of MRI visible 1 mm diameter pharmaceutical spherical pills and 3 mm diameter plastic spheres. The MRI images showed that the structure within the bulk mixture was more complicated than visible surface measurements indicated and that segregation depended on rotational velocity. Sommier et al. (36) studied mixing and segregation of binary mixtures of sugar beads in a Turbula mixer. Some of the beads were doped with organic oil to create MRI visible beads. The results showed that segregation occurred after only a few rotations for beads of different sizes. Porion et al. (37) also studied mixing and segregation in a Turbula mixer with sugar beads. Kawaguchi et al. (38) used MRI to measure segregation in rotating horizontal drums; small polystyrene particles and MRI visible larger vitamin E filled gelatin spheres were used. The MRI images allowed comparison of segregation in a straight and tapered drum and determined the effect of operational parameters on the segregation.

2.4.3 Advantages and disadvantages of MRI

Magnetic resonance imaging (MRI) can provide non-invasive spatial information about a mixture and is therefore valuable for indicating uniformity of a mixture. The mixture, however, must have a MRI sensitive or "visible" particle whose distribution within the mixture is representative of the uniformity. A significant disadvantage is the extensive and expensive equipment required to obtain the images.

2.5 Radioactive Tracers

2.5.1 Introduction

Positron emission particle tracking (PEPT) is a radioactive technique that can provide information about mixing dynamics by tracking the location of a single positron labeled

tracer particle within a powder mixture. The PEPT technique was developed from the radioactive decay process which is related to isotopes with proton-rich nuclei undergoing β^+ decay, a proton decaying to a neutron while emitting a positron (e⁺) and a neutrino (v). When the emitted positron annihilates with an electron, two co-linear gamma-ray photons are produced. A series of positron detectors allows the location of the tracer to be estimated and followed with time (39).

2.5.2 Tracer selection

Radioactive materials or particles coated with radioactive materials are injected into the mixture to act as tracers. The ideal tracer should have similar physical and surface properties to materials in the mixture and also not induce changes in the mixture that could lead to segregation. Fan et al. (40) described a technique to create tracers by irradiating the tracer particles with a neutron flux. They used their technique successfully to study motionless mixers. Doucet et al. (41) studied the flow dynamics of 3 mm glass beads in a V blender using a glass tracer particle containing 5 mg of Scandium 46 isotope activated in a nuclear reactor.

Since not every mixture contains components that can be easily used as a tracer particle, sometimes it is necessary to use an independent tracer which can vary considerably from the particulates being used in size, shape, and/or density. There are then concerns that the motion of the tracer particle does not reflect the motion of the bulk mixture. Broadbent et al. (42) investigated the effect of tracer size on the mixing of rice in a ploughshare mixer. The rice grains were approximately 5 mm long and 2 mm in diameter with a density of 1.5 g/cm³. Silica cylindrical tracers 2mm, 4mm and 8 mm diameter with an equal length to diameter ratio were created by irradiating with a ³He beam or, for the 8mm diameter tracer, by sealing a tracer within the cylinder. In general, the three different size tracers behaved similarly and therefore reflected the average bulk flow of the rice. The relative size of the tracer particle did however affect measurements of the axial mixing time and therefore, for mixing time measurements, it was concluded that tracer size may be critical. Jones et al. (43) also investigated tracer size while mixing rice in a ploughshare mixer. They found that the largest tracer, an irradiated silica glass cylinder with a diameter of 4 mm, segregated at a low 2 Hz rotor frequency. The smaller tracer, closer in

size to the rice, did not segregate and reflected the bulk motion of the rice. Laurent and Cleary (44) also investigated rice mixing in a ploughshare mixer, but used a glass sphere with a diameter of 2 mm and a density of 2500 kg/m³. This tracer was therefore very different in size, shape and density from the rice. The tracer did show some differences in flow behaviour from the bulk rice: the smaller tracer was predisposed to be closer to the mixer blades and therefore was lifted out of the bed more frequently and also showed some segregation in the avalanching flow back into the bed. The errors from these differences in motion, however, were assumed to be small as the analysis used time averaged data.

For specific applications, tracers that are significantly different from the bulk properties can be advantageous. Broadbent et al. (39) used a cylindrical steel capsule 6 mm in diameter and 8 mm in length containing ²²Na as a tracer with significantly smaller 100 µm granular sodium phosphate as the bulk material. The objectives of the research, however, included the study of the behaviour of a lump of material as it passed through the ploughshare mixer. A larger tracer was therefore ideal for representing the large lump.

2.5.3 Applications of radioactive tracers

Radioactive tracers have been used to examine mixing dynamics and the effect of parameters on the mixing. Lai and Fan (45) studied radial mixing of flour in a Sulzer (Koch) motionless mixer by measuring the radial dispersion of a radioactive tracer, irradiated flour, to convert the manganese within the flour to ⁵⁶Mn. Radial dispersion was found to increase with the number of passes through the mixer and a mechanistic model was developed and verified by the results. Portillo et al. (46) used a radioactive tracer to examine many factors (impeller rotation rate, powder flow rate, powder cohesion and residence time) for mixing lactose in a continuous powder mixer. Perrault et al. (47) examined the mixing of magnesium stearate with microcrystalline cellulose and lactose pre-blend in a V blender. The magnesium stearate was activated in a nuclear reactor to become the radioactive tracer. The goals of this study were, first, to validate radioactive tracers as an inline method and, second, to study the effect of rotational speed and pre-blend composition on the mixing dynamics.

2.5.4 Advantages and disadvantages of radioactive tracers

Radioactive tracers allow mixing dynamics to be effectively studied. The requirement of a radioactive tracer and appropriate sensors to follow the tracer trajectories limits this technique to small scale development phases; commercial monitoring and control of mixing is not possible.

2.6 Thermal Techniques

2.6.1 Thermal tracers

Saberian et al. (48) developed a thermal tracer technique to examine the mixing of polyvinyl chloride resin in high speed vertical mixers. Most of the solids were introduced into the mixer at room temperature. A small amount, which had been cooled to -12° in a freezer, was then added. The temperatures at various locations in the mixer were measured throughout the procedure. The dimensionless standard deviation of the temperatures was calculated as a function of time to monitor the progress of mixing and the end-point. The thermocouples did not significantly interfere with the flow patterns in the mixer and the technique was easily implemented. An issue not addressed in this study was potential problems due to temperature changes due to equilibration with room temperature rather than changes due to mixing.

2.6.2 Thermal effusivity

Thermal effusivity is defined as $\sqrt{k\rho C_p}$ where k is the thermal conductivity, ρ is the density, and C_p is the heat capacity of a component or mixture (2). As each component in a mixture has a different thermal effusivity, a probe measuring the change in effusivity with time allows monitoring of the mixing and identification of an end-point. The probe detects the rate of heat transfer from its heating element to the powder in contact with the probe (1).

Dipali et al. (49) retrofitted existing blenders with real time testing of effusivity to detect convergence of a commercially available product to a uniform blend. Mathews et al. (1) measured the effusivity of eight pharmaceutical powders, showing that their values were significantly different. They then showed that the blend uniformity of formulations

containing these powders could be monitored through effusivity as it changed with mixing and increasing homogeneity, reaching a plateau at the end-point. Closs (50) used thermal effusivity to measure the dry mixing of a two component placebo formulation in a high shear granulator, finding that a high impeller speed and the chopper were required to obtain a homogeneous mixture. Closs et al. (51) used a retrofitted bin blender to test the ability of the effusivity sensors on monitoring a blend before and after the addition of a lubricant. The average effusivity and the relative standard deviation (RSD) values were used to identify the optimum blend parameters required to achieve uniformity. Fariss et al. (52) used thermal effusivity for monitoring granulation including the dry mixing period. The relative standard deviation values of effusivity were measured at multiple locations with a low RSD value at the end of the dry mix period indicating homogeneity and then a high RSD value at the onset of wet granulation. Leonard et al. (2) examined thermal effusivity for indicating blend uniformity of binary mixtures of acetaminophen and lactose in a V blender. Thermal effusivity effectively indicated the process end-point, but only for mixture containing more than 10 wt% acetaminophen.

2.6.3 Advantages and disadvantages of thermal techniques

There are three main disadvantages in applying thermal tracers to mixing of pharmaceuticals: thermocouples must be inserted into the process vessel and are therefore in contact with the product which then requires additional compliance measures, many mixers are tumbling making it difficult to insert thermocouples at multiple locations into the vessel, and many pharmaceuticals are temperature sensitive such that a large enough difference in temperature for the tracer could not be achieved without degrading the powder.

Effusivity is affected by the bulk density of the powder. Locations of the effusivity probes are then critical to ensure that measurement differences are due to mixture content rather than local variations in the bulk density.

2.7 Image Analysis

2.7.1 Introduction

Image processing provides a non-invasive technique that can be used to monitor mixing homogeneity; by observing and monitoring the changes in the mixture colour over time the end-point can be determined (53). A simple image processing system would include a charge coupled device (CCD) camera or complementary metal oxide semiconductor (CMOS) camera and image processing software or a computer program (53).

2.7.2 Analysis of images

Realpe and Velazquez (54) developed a technique for image processing using univariate and multivariate gray image analysis. Binary systems of different colours were used with lactose, microcrystalline cellulose, chocolate and a colour additive to create blue lactose. Chen and Yu (55) examined dry and wet mixing methods of two powder systems, Ti/SiO₂ and C/SiO₂. The images were compared to a perfect powder mixture, a chessboard like distribution of the two particles, and a two dimensional mixing efficiency was calculated. Le Coent et al. (56) found that analysis of images by calculating the fractal dimension from the box-counting procedure was not appropriate for determining mixture homogeneity. They developed a technique to examine variations in the fractal dimension as the images are modified by an erosion process. The time profile of this fractal dimension versus the erosion number indicated mixture homogeneity. In 2007, Bulent Koc et al. (53) performed a study to develop and evaluate a PC-based continuous image processing technique to monitor binary dry powder mixing homogeneity in real time. A vessel type batch mixer was used with white plaster and black and red dyes were used as colour tracers for the system; a CMOS camera was used for the image processing system (53). The PC-based continuous image processing technique successfully monitored and evaluated the change in homogeneity during the binary mixing of powders; the method allowed monitoring of a large powder surface area providing a more accurate determination of homogeneity than analysis of a small and localized image (53).

2.7.3 Advantages and disadvantages of image analysis

For image analysis, one component of the mixture must be a different colour. Most pharmaceutical powders are white and therefore this limits the applications of imaging. A measurement window into the mixing vessel is required to obtain the images and the measurement window must remain clear to allow provide accurate images. Cohesive powders are therefore difficult to measure as they would foul the window leading to poor images. The images only provide an indicator of mixture homogeneity at the measurement window. These local indicators may not be representative of the entire mixture (56). As equipment must be modified to allow the images, multiple measurement locations that would provide a more representative indicator of the mixture are not possible.

2.8 Laser-induced Fluorescence (LIF)

2.8.1 Introduction

Laser-induced fluorescence (LIF) involves irradiating samples at a suitable wavelength for excitation and evaluating the emission at another wavelength. Many active pharmaceutical ingredients can fluoresce when excited at the proper wavelength. The measured signal represents the number of fluorescent particles within the measurement volume. Blend homogeneity is established when the LIF signal reaches a plateau (57).

2.8.2 Applications of LIF

Lai et al. (57) examined the mixing of the active triamterene with anhydrous lactose in a glass microblender using triamterene excited at 488 nm as the laser induced fluorescent particles. As the blender was glass, the LIF sensor was placed outside the vessel with measurements either one-third from the top or the bottom of the powder bed. The technique identified the mixing end-point even for a triamterene concentration as low as 0.1% demonstrating the potential for using the technique for monitoring mixing of highly potent actives which are usually required in only very small quantities. Further studies with triamterene using a battery operated portable LIF sensor and a tumbling mixer

showed that blend homogeneity could be identified for the active concentration as low as 0.02 wt% (58).

Karumanchi et al. (59) used LIF to examine the mixing of two commercial formulations in a 124 litre tote blender. Two separate granulations were mixed in a ratio of 25:75 with the nonfluoresecent granulation added first and the fluorescent granulation on top. The trials were mixed at 16 rpm and samples collected at defined intervals and LIF measurements made on each sample. The LIF measurements identified the mixing endpoint and also two sampling locations as dead-spots.

2.8.3 Advantages and disadvantages of LIF

The primary disadvantage of laser-induced fluorescence is that one of the components of the formulation must have fluorescence properties and, in the case of multiple fluorescent components, the corresponding LIF signals must be different. A second disadvantage is that the LIF sensor requires a measurement window into the mixing vessel. This limits the applications as cohesive materials will foul the window leading to inaccurate measurements (58).

Lai and Cooney (58) examined the penetration depth of LIF into powders. The LIF signal was measured as layers of non-fluorescent powders were added on top. The signal decreased exponentially with an increase in the powder thickness. From these measurements it was estimated that the LIF penetration depth would not be more than 1 mm. Karumanchi et al. (59) estimated a penetration depth of 1.5 mm for their study. Penetration depth is dependent on the selected wavelengths and particles sizes and bulk density of the powder bed (58, 59). This means that any LIF measurements are very local and limited to those near the measurement window at the perimeter of the mixing vessel.

Lai et al. (57) reported that voidage and bulk density affected the LIF signal. They recommended measurements close to the bottom of a vessel where changes in the bulk density are minimal. It was reported that only one measurement location was required as the constant motion of the powder ensured that the powder within the measurement volume was representative of the bulk mixture.

2.9 Optic Probe Measurements

Light reflected from a powder surface is dependent upon its composition. Optic probes therefore measure mixing by emitting light and then measuring the scatter (60, 61). Ashton et al. (60) were able to determine the frequency distribution of the composition of binary mixtures of witherite and pyrites or white and red sand in a Nauta mixer with reproducible results. Kaye et al. (62) compacted 1% carbon black in TiO₂ powder in a conventional blender. Probe sensitivity was investigated and was able to distinguish between 1 and 2% of carbon black in the white powder. Harwood et al. (61) studied the mixing of a red powder into a white base with an optic probe inserted into the side of a Hobart mixer. The measurements were compared to a calibration curve of the reflectance versus percent composition of the white base powder to monitor the progress of mixing and determine and end-point. Oki et al. (63) used an optic probe to measure the diameter of particles by inserting the probe into the bulk flow of a mixture of powders. An optic probe has also been used to investigate the performance of a rocking motion mixer (64). Alonso et al. (65) performed a subsequent study investigating mixer operating conditions, mixtures containing cohesive powders, particles of differing size or density, the coating of particles and the electrostatic effect; the performance of two types of mixers was investigated all using an optic probe. Concentration curves were obtained and the degree of mixing was plotted. Poux et al. (66) used an optical sensor to determine the concentration of powders mixed in a fluidized bed. Dead zones within the bed were identified as well as the mixing time. Gratton-Liimatainen (67) developed an optical system to provide information about the mixture concentration of cohesive powders.

One disadvantage of optic probe measurements is the requirement of components with different light reflection properties. Other disadvantages are similar to previous techniques with probes that require a measurement window into the mixing vessel or unobstructed probe tip and limited penetration depth limiting measurements to very localized locations usually near the vessel perimeter.

2.10 Computed Tomography

X-ray computed tomography is an imaging technique using X-rays passed through the material to generate the images. Yang and Fu (68) used X-ray computed tomography to study the mixing of microcrystalline cellulose in a model V-blender. Lead (II) acetate trihydrdate was used to label the microcrystalline cellulose particles to allow these particles to be traceable on the images. The study showed that the initial fill configuration affected mixing with a layer-filled configuration providing better mixing within a specified number of rotations than a column-filled configuration. Chester et al. (69) studied mixing in a double-cone blender with pellets and spherical beads, some of which were labeled with molybdenum through impregnation with ammonium heptamolybdate. The tomographic images showed that radial mixing was almost complete within 10 to 20 rotations, radial mixing was poor, and an 80% fill level promoted segregation and therefore very poor mixing.

Major disadvantages of X-ray computed tomography include required labeling of a component of the mixture to be visually traceable in the images and then the extensive and expensive equipment and analysis required to obtain the images. These requirements limit the technique to development at small scales; commercial monitoring and control of mixing is not possible.

2.11 Acoustic Emission Monitoring

2.11.1 Introduction

Acoustic emissions are the release of transient elastic waves caused by sudden localized changes in stress (70). The waves generated, transmitted and received from acoustic emissions are related to vibrations and can be parallel or perpendicular, longitudinal or transverse, from the source of emissions (71). Longitudinal waves can exist in any phase, while transverse waves can only propagate through solids. The following relationship can be used to describe both types of waves:

$$c = \lambda f$$
 (eq.6)

where c is the speed, λ is the wavelength and f is the frequency. The speed is dependent on the elasticity and density of the matter that the wave propagates though and the frequency is the reciprocal of the time required to complete one cycle of a sinusoidal tone. Frequencies can be below 20 Hz in the form of infrasonic waves, between 20 to 20,000 Hz in the form of audible sound waves, or above 20,000 Hz as ultrasonic waves (72). There is a third type of wave, Rayleigh waves, which exist in semi-infinite media.

When a sound wave is moving through a fluid and strikes the interface of a different material, a portion of the acoustic energy is transmitted into the second material and a portion is reflected (73). Acoustic energy is attenuated or dissipated as the wave moves through a medium due to three mechanisms. The viscous effects or dissipation due to fluid friction results in a thermodynamically irreversible propagation of sound (73). The heat conduction effects or heat transfer in the wave results in non-adiabatic propagation of sound (73). And, the internal molecular energy interchanges or molecular energy relaxation effects which result in a time lag between changes in translation kinetic energy and energy associated with rotation and vibration of molecules (73).

Passive acoustic emissions refer to sound made by the process itself. For particulate processes, such as mixing, the sound may be due to particle-particle and particle-equipment collisions as well as friction generated by contact and flow. Passive acoustic emissions for monitoring mixing are based on differences in the emissions from the heterogeneous to the homogeneous states.

2.11.2 Applications of acoustic emission monitoring

Acoustic emissions monitoring has been applied to a variety of particulate operations including fluidization (74), rotary drying (75), pneumatic transport (76) and granulation (77). However, only a few studies on passive acoustic emission monitoring of powder mixing have been presented in the literature (27, 70, 78). Allan et al. (27) investigated passive acoustic emission monitoring of mixing aspirin or citric acid with Avicel in a bench-top convective mixer. Mixing profiles were obtained by determining the change in average acoustic emission signal area between selected frequency ranges (approximately 18 and 300 kHz) with time. The mixture was uniform and an end-point identified when

the profiles reached a plateau. Bellamy et al. (78) examined passive acoustic emissions during the mixing of aspirin and cellulose in a high shear mixer. The emissions were processed using the same technique as Allan et al. (27) to obtain profiles with a plateau indicating the end-point. Tily et al. (70) used passive acoustic emissions to investigate mixing of various powders in a lab scale Kenwood mixer. Changes in the root mean square of the emissions with time indicated an end-point when a plateau in the profile was reached.

2.11.3 Advantages and disadvantages of acoustic emission monitoring

Passive acoustic emission monitoring offers many advantages over other monitoring methods under development: (i) the method is completely non-invasive as the sensors can be attached to the outside of the equipment, (ii) the method is non-destructive as the measurements are passive emissions generated by the process itself, (iii) the method is less expensive to set up than other methods, particularly spectroscopic or radiation techniques (79). A disadvantage of the technique is that the measurements produce large volumes of data that must be appropriately analyzed to extract the relevant information for monitoring.

2.12 Conclusions

Blend uniformity is critical, but it is also difficult to achieve. Therefore, there an increasing need for methods that provide accurate and reliable information about the mixture homogeneity and can identify the optimal process end-point. Currently, the pharmaceutical industry assesses blend uniformity through extraction of samples using thief probes followed by analytical methods; this assessment suffers from many disadvantages. For mixing processes, PAT would improve efficiency through better monitoring and control resulting in fewer rejected batches and also improve product quality.

Many technologies have been investigated to evaluate the uniformity of the mixture and to monitor and identify the optimal mixing time; Table 2.2 summarizes these monitoring techniques discussed. There are advantages of some techniques and demonstrated

potential. However, many of the tested techniques have significant disadvantages including the need for equipment modification, specific requirements of the material, expensive equipment, extensive analysis, the location of the probes may be critical and/or invasive, and lastly, the technique may only be applicable to the development phase. Both the advantages and disadvantages of the technologies should be considered in application to a specific system. Multiple technologies might also be considered to ensure accurate and reliable monitoring of a mixing process.

Table 2.2: Summary of monitoring techniques

Technique	Measured Parameter
Near Infrared Spectroscopy	Absorption energy
Raman Spectroscopy	Scattered light
Magnetic Resonance Imaging	Magnetic field
Radioactive Tracers	Positron detection
Thermal Tracers	Temperature
Thermal Effusivity	Effusivity
Image Analysis	Colour
Laser Induced Fluorescence	Fluorescence
Optic Probe	Light
Computed Tomography	X-Ray
Acoustic Emissions	Sound and vibrations

2.13 References

- 1. Mathews L, Chandler C, Dipali S, Adusumilli P, Lech S, Daskalakus S et al. Monitoring blend uniformity with effusivity. Pharm Technol 2002; 26: 80-84.
- Leonard G, Bertrand F, Chaouki J, Gosselin PM. An experimental investigation of effusivity as an indicator of powder blend uniformity. Powder Technol 2008; 181: 149-159.
- 3. Vergote GJ, De Beer TRM, Vervaet C, Remon JP, Baeyens WRG, Diericx N et al. In-line monitoring of a pharmaceutical blending process using FT-Raman spectroscopy. Eur J Pharm Sci 2004; 21: 479-485.
- 4. Hausman DS, Cambron RJ, Sakr A. Application of Raman spectroscopy for on-line monitoring of low dose blend uniformity. Int J Pharm 2005; 298 : 80-90.
- 5. Muzzio FJ, Robinson P, Wightman C, Brone D. Sampling practices in powder blending. Int J Pharm 1997; 155: 153 178.
- 6. U.S. Department of Health and Human Services, Food and Drug Administration, Center for Drug Evaluation and Research (CDER), Center for Biologics Evaluation and Research (CBER) [Internet]. Silver Spring: Division of Drug Information; c2009 [revision 2 2009 Nov]. Guidance for Industry Q8 Pharmaceutical Development; [29 pages]. Available from: http://www.fda.gov/downloads/Drugs/GuidanceComplianceRegulatoryInformation/Guidances/ucm073507.pdf
- 7. Berntsson O, Danielsson LG, Lagerholm B, Folestad S. Quantitative in-line monitoring of powder blending by near-infrared reflection spectroscopy. Powder Technol 2002; 123: 185-193.
- 8. Koeller DM, Posch A, Hori G, Voura C, Radl S, Urbanetz N et al. Continuous quantitative monitoring of powder mixing dynamics by near-infrared spectroscopy. Powder Technol 2011; 205: 87-96.
- 9. Sekulic SS, Ward HW, Brannegan DR, Stanley ED, Erans CL, Sciavolino ST et al. On-line monitoring of powder blend homogeneity by near-infrared spectroscopy. Anal Chem 1996; 68: 509-513.

- 10. Hailey PA, Doherty P, Tapell P, Oliver T, Aldridge PK. Automated system for the on-line monitoring of powder blending processes using near-infrared spectroscopy. Part 1: System development and control. J Pharm Biomed Anal 1996; 14: 551-559.
- 11. Wargo DJ, Drennen JK. Near-infrared spectroscopic characterization of pharmaceutical powder blends. J Pharm Biomed Anal 1996; 14: 1415-1423.
- 12. Moes JJ, Ruijken MM, Gout E, Frijlink HW, Ugwoke MI. Application of process analytical technology in tablet process development using NIR spectroscopy: blend uniformity, content uniformity, and coating thickness measurement. Int J Pharm 2008; 357: 108-118.
- 13. De Maesschalck R, Cuesta Sanchez F, Massart DL, Doherty P, Hailey P. On-line monitoring of powder blending with near-infrared spectroscopy. Appl Spectrosc 1998; 52: 725-731.
- 14. Sekulic SS, Wakeman J, Doherty P, Hailey PA. Automated system for the on-line monitoring of powder blending process using near-infrared spectroscopy. Part 2: Qualitative approaches to blend evaluation. J Pharm Sci 1998; 17: 1285-1309.
- 15. Blanco M, Coello J, Iturriaga H, Maspoch S, de la Pezula C. Effect of data preprocessing methods in near-infrared diffuse reflectance spectroscopy for the determination of the active compound in a pharmaceutical preparation. Appl Spectrosc 1997; 51: 240-246.
- 16. Blanco M, Gozalex Bano R, Bertran E. Monitoring powder blending in pharmaceutical processes by use of near infrared spectroscopy. Talanta 2002; 56: 203-212.
- Cuesta Sanchez F, Toft J, van den Bogaert B, Massart DI, Dive SS, Hailey P.
 Monitoring powder blending by NIR spectroscopy. Fresenius J Anal Chem 1995;
 352: 771-778.
- 18. Ciurzack EW. Following the progress of pharmaceutical mixing study via near-infrared spectroscopy. Pharm Technol 1991; 15: 140-145.
- 19. El-Hagrasy AS, Morris HR, D'Amico F, Lodder RA, Drennen JK. Near-infrared spectroscopy and imaging for the monitoring of powder blend homogeneity. J Pharm Sci 2001; 90: 1298-1307.

- 20. El-Hagrasy AS, D'Amico F, Drennen JK. A process analytical technology approach to near-infrared process control of pharmaceutical powder blending. Part 1: Doptimal design for characterization of powder mixing and preliminary spectral data evaluation. J Pharm Sci 2006; 95: 392-406.
- 21. El-Hagrasy AS, Delago-Lopez M, Drennen JK. A process analytical technology approach to near-infrared process control of pharmaceutical powder blending. Part 2: Qualitative near-infrared models for prediction of blend homogeneity. J Pharm Sci 2006; 95: 407-421.
- 22. El-Hagrasy AS, Drennen JK. A process analytical technology approach to near-infrared process control of pharmaceutical powder blending. Part 3: Quantitative near-infrared calibration for prediction of blend homogeneity and characterization of powder mixing kinetics. J Pharm Sci 2006; 95: 422-434.
- 23. Bellany LJ, Nordon A, Littlejohn D. Effects of particle size and cohesive properties on mixing studied by non-contact NIR. Int J Pharm 2008; 361: 87-91.
- 24. Shi Z, Cogdill RP, Short SM, Anderson CA. Process characterization of powder blending by near-infrared spectroscopy: blend end-points and beyond. J Pharm Biomed Anal 2008; 47: 738-745.
- 25. Liew CV, Karande AD, Heng PWS. In-line quantification of drug and excipients in cohesive powder blends by near infrared spectroscopy. Int J Pharm 2010; 386: 138-148.
- 26. Heise HM, Winzen R. Chemometrics in Near-Infrared Spectroscopy. In: Siesler HW, Ozaki Y, Kawata S, Heise HM, editors. Near-Infrared Spectroscopy. Weinheim: Wiley-VCH; 2002. p. 125-162.
- 27. Allan P, Bellamy LJ, Nordon A, Littlejohn D. Non-invasive monitoring of the mixing of pharmaceutical powders by broadband acoustic emissions. Anal 2010; 3: 518-524.
- Rantanen J. Process analytical applications of Raman spectroscopy. J Pharm Pharmacol 2007; 59: 171-177.
- 29. Rantanen J, Wikstrom H, Rhea FE, Taylor LS. Improved understanding of factors contributing to quantification of anhydrate/hydrate powder mixtures. Appl Spectrosc 2005; 59: 942-951.

- 30. Sasic S, Clark DA, Mitchell JC, Snowden MJ. A comparison of Raman chemical images produced by univariate and multivariate data processing a simulation with an example from pharmaceutical practice. Anal 2004; 129: 1001-1007.
- 31. Breintenbach J, Schrof W, Neumann J. Confocal Raman-spectroscopy: analytical approach to solid dispersions and mapping of drugs. Pharm Res 1999; 16: 1109-1113.
- 32. De Beer TRM, Bodson C, Dejaegher B, Walczak B, Vercryysse P, Burgraeve A et al. Raman spectroscopy as a process analytical technology (PAT) tool for the in-line monitoring and understanding of a powder blending process. J Pharm Biomed Anal 2008; 48: 772-779.
- 33. Nakagawa M, Altobelli SA, Caprihan A, Fukushima E, Jeong EK. Non-invasive measurements of granular flows by magnetic resonance imaging. Exp Fluids 1993; 16: 54-60.
- 34. Hardy EH, Hoferer J, Kasper G. The mixing state of fine powders measured by magnetic resonance imaging. Powder Technol 2007; 177: 12-22.
- 35. Hill KM, Caprihan A, Kakalios J. Bulk segregation in rotated granular material measured by magnetic resonance imaging. Phys Rev Lett 1997; 78: 50-53.
- 36. Sommier N, Porion P, Evesque P, Leclerc B, Tchoreloff P, Couarraze G. Magnetic resonance imaging investigation of the mixing-segregation process in a pharmaceutical blender. Int J Pharm 2001; 222: 243-258.
- 37. Porion P, Sommier N, Faugere AM, Evesque P. Dynamics of size segregation and mixing of granular materials in a 3D-blender by NMR imaging investigation. Powder Technol 2004; 141: 55-68.
- 38. Kawaguchi T, Tsutsumi K, Tsuji Y. MRI measurement of granular motion in rotating drum. Part Part Syst Charact 2006; 23: 266-271.
- 39. Broadbent CJ, Bridgewater J, Parker DJ, Keningley ST, Knight P. A phenomenological study of a batch mixer using a positron camera. Powder Technol 1993; 76: 317-329.
- 40. Fan LT, Chen SJ, Sckhoff ND, Watson CA. Evaluation of a motionless mixer using a radioactive tracer technique. Powder Technol 1971; 4: 345-350.

- 41. Doucet J, Bertrand F, Chaouki J. Experimental characterization of the chaotic dynamics of cohesionless particles: application to a V-blender. Granul Matter 2008; 10: 133-138.
- 42. Broadbent CJ, Bridgewater J, Parker DJ. The effect of fill level on powder mixer performance using a positron camera. Chem Eng J 1995; 56: 119-125.
- 43. Jones JR, Parker DJ, Bridgewater J. Axial mixing in a ploughshare mixer, Powder Technol 2007; 178: 73-86.
- 44. Laurent BFC, Cleary PW. Comparative study by PEPT and DEM for flow and mixing in a ploughshare mixer. Powder Technol 2012; 228: 171-186.
- 45. Lai FS, Fan LT. A study on the mixing of flour in a motionless Sulzer (Koch) mixer using a radioactive tracer. Powder Technol 1976; 13: 73-83.
- 46. Portillo PM, Vanarase AU, Ingram A, Seville JK, Ierapetritou MG, Muzzio FJ. Investigation of the effect if impeller rotation rate, powder flow rate, and cohesion on powder flow behaviour in a continuous blender using PEPT. Chem Eng Sci 2010; 65: 5658-5668.
- 47. Perrault M, Bertrand F, Chaouki J. An investigation of magnesium stearate mixing in a V-blender through gamma-ray detection. Powder Technol 2010; 200: 234-245.
- 48. Saberian M, Segonne Y, Briens C, Bousquet J, Chabagno JM, Denizart O. Blending of polymers in high speed, vertical mixers: development of a thermal tracer measurement procedure. Powder Technol 2002; 123: 25-32.
- 49. Dipali SR, Chandler C, Adusumilli P, Lech S, Daskalakis S, Mathis N, editors. A novel technique for determination of real time blend uniformity using thermal effusivity. Proceedings of AAPS Convention; 2001 October 20-25; Denver, US. Parsippany: GlaxoSmithKline Consumer Healthcare, New Brunswick: Mathis Instruments Ltd.; 2001.
- 50. Closs S, editor. Thermal effusivity as a means to determine the uniformity of a dry blend in a high shear granulator. Proceedings of AAPS Convention; 2004 November 7-11; Baltimore, US. Durham: Patheon Inc.; 2004.
- 51. Closs S, Mathis N, Meyer W, Roy W, editors. Thermal effusivity as a process analytical technology (PAT) to optimize blend uniformity: A case study in on-line monitoring of a pharmaceutical blend in a bin blender. Proceedings of AAPS

- Convention; 2004 November 7-11; Baltimore, US. New Brunswick: Mathis Instruments Ltd.; 2004.
- 52. Fariss G, Keintz R, Okoye P. Thermal effusivity and power consumption as PAT tools for monitoring granulation end point. Pharm Technol 2006; 6: 60-72.
- 53. Bulent Koc A, Silleli H, Koc C, Dayioglu MA. Monitoring of dry powder mixing with real-time image processing. J Appl Sci 2007; 7: 1218-1223.
- 54. Realpe A, Velazquez C. Image processing and analysis for determination of concentrations of powder mixtures. Powder Technol 2003; 134: 193-200.
- 55. Chen CC, Yu CK. Two-dimensional image characterization of powder mixing and its effects on the solid-state reactions. Mater Chem Phys 2004; 85: 227-237.
- 56. Le Coent AL, Rivoire A, Briancon S, Lieto J. An original image-processing technique for obtaining the mixing time: the box-counting with erosions method. Powder Technol 2005; 152: 62-71.
- 57. Lai CK, Holt D, Leung JC, Cooney CL, Raju GK, Hansen P. Real time and noninvasive monitoring of dry powder blend homogeneity. AIChE J 2001; 47: 2618-2622.
- 58. Lai CK, Cooney CC. Application of a fluorescence sensor for miniscale on-line monitoring of powder mixing kinetics. J Pharm Sci 2004; 93: 60-70.
- 59. Karumanchi V, Taylor MK, Ely KJ, Stagner WC. Monitoring powder blend homogeneity using light-induced fluorescence. AAPS PharmSciTech 2011; 12: 1031-1037.
- 60. Ashton MD, Schofield C, Valentin FHH. The use of a light probe for assessing the homogeneity of powder mixtures. Chem Eng Sci 1966; 21: 843-849.
- 61. Harwood CF, Davies R, Jackson M, Freeman E. An optic probe for measuring the mixture composition of powders. Powder Technol 1971/72; 5: 77-80.
- 62. Kaye BH, Brushenko A, Ohlhaber RL, Pontarelli DA. A fiber optic probe for investigating the internal structure of powder mixtures. Powder Technol 1968/69; 2: 243-245.
- 63. Oki K, Akehata T, Shirai T. A new method for evaluating the size of moving particles with a fiber optic probe. Powder Technol 1975; 11: 51-57.

- 64. Alonso M, Satoh M, Miyanami K. Influence of rocking motion on the mixing of powders. Powder Technol 1989; 59: 65-67.
- 65. Alonso M, Satoh M, Miyanami K. Recent works on powder mixing and powder coating using an optical measuring method. Kona 1989; 7: 97-105.
- 66. Poux M, Lescure M, Steinmetz D, Bertrand J. Optical sensors for the characterization of powder mixtures. Sens Actuators 1995; 46/47: 494-496.
- 67. Gratton-Liimatainen JL. Characterizing the structure of cohesive powder mixtures by optical methods [Master's Thesis]. Sudbury (ON): Laurentian University; 1995.
- 68. Yang CY, Fu XY. Development and validation of a material labeling method for powder process characterization using x-ray computed tomography. Powder Technol 2004; 146: 10-19.
- 69. Chester AW, Kowalski JA, Coles ME, Muegge EL, Muzzio FJ, Brone D. Mixing dynamics in catalyst impregnation in double-cone blenders. Powder Technol 1999; 12: 85-94.
- 70. Tily PJ, Porada S, Scruby CB, Lidingon S. Monitoring of mixing processes using acoustic emission. In: Harnby N, Benkreira H, Carpenter KJ, Mann R, editors. Fluid Mixing III. Rugby: Institute of Chemical Engineers Symposium Series NO. 108; 1988. p. 75-94.
- 71. Kinsler LE, Frey AR, Coppens AB, Sanders JV. Fundamentals of acoustics. United States of America: John Wiley & Sons Inc., 2000.
- 72. Boyd J, Varley J. The uses of passive measurement of acoustic emissions from chemical engineering processes. Chem Eng Sci 2001; 56: 1749-1767.
- 73. Barron RF. Industrial noise control and acoustics. United States of America: Marcel Dekker, Inc., 2003.
- 74. Vervloet D, Nijenhuis J, van Ommen J. Monitoring a lab-scale fluidized bed dryer: a comparison between pressure transducers, passive acoustic emissions and vibration measurements. Powder Technol 2010; 197: 36-48.
- 75. Briens L, Smith R, Briens C. Monitoring of a rotary dryer using acoustic emissions. Powder Technol 2008; 181: 115-120.

- 76. Albion K, Briens L, Briens C, Berruti F. Flow regime determination in horizontal pneumatic transport of fine powders using non-intrusive acoustic probes. Powder Technol 2007; 172: 157-166.
- 77. Hansuld E, Briens L, Sayani A, McCann J. Monitoring quality attributes for high-shear wet granulation with audible acoustic emission. Powder Technol 2011; 215-216: 117-123.
- 78. Bellamy LJ, Nordon A, Littlejohn D. Non-invasive monitoring of powder mixing with near infrared spectrometry and acoustics. Spectrosc Eur 2004: 25-27.
- 79. Crouter A, Briens L. Passive acoustic emissions from particulates in a V-blender. Drug Dev Ind Pharm 2015; 41: 1809-1818.

Chapter 3

3 Passive acoustic emissions from particulates in a Vblender

3.1 Introduction

The pharmaceutical manufacturing process consists of a number of batch steps and each step must be monitored and controlled to ensure quality standards are met. To improve pharmaceutical efficiency, flexibility, product quality and consistency, regulatory agencies are recommending the development of process analytical technologies (PAT) for monitoring product quality and improving process understanding. Ideally these are inline methods to remove issues related to extractive sampling and allow direct monitoring of the system using various sensors. Many technologies have been investigated, including near-infrared spectroscopy (1-3), Raman spectroscopy (4), magnetic resonance imaging (5), radioactive tracers (6), image analysis (7), tomography (8), and acoustic emission monitoring (9, 10).

Passive acoustic emission monitoring offers many advantages over other monitoring methods under development: (i) the method is completely non-invasive, not requiring any window or ports into the process vessel, as the sensors can be attached to the outside of the equipment, (ii) the method is non-destructive as the measurements are passive emissions generated by the process itself, (iii) the capital cost is less than other methods, particularly spectroscopic or radiation techniques. Although passive acoustic emissions produce large volumes of data that must be appropriately analyzed to extract the relevant information for monitoring, this processing can be less extensive than the complex calibrations and processing required for other techniques. Therefore, the many advantages easily outweigh any possible disadvantages.

In the 1970s acoustic emissions were used to study different sizes and types of particles in a rotary drum (11-15). In 1988, Tily et al. (16) demonstrated the potential of passive acoustic emissions for monitoring binary solid-solid mixing in an orbital mixer. A major source of the acoustic emissions was identified as particle-wall collisions with the

emissions related to particle size. The acoustic emissions changed from an initial level to a final stable level at the mixing endpoint corresponding to the mean contributions of the components of the mixture. Subsquently acoustic emission monitoring has been utilized in a variety of applications; Table 3.1 highlights some of these applications related to particulate operations. Of note there have been two studies that used acoustic emissions with pharmaceutical powders in a convective blender: Bellamy et al. (9) compared near-infrared spectroscopy (NIR) and acoustic emission monitoring to obtain mixing profiles while Allan et al. (10) compared acoustic emissions and NIR to investigate the effect of impeller speed, mass/density of the powder, and particle size on the mixing profile. Both of these studies showed that mixing profiles from NIR and acoustic emission monitoring were equivalent. However, signals obtained from acoustic emissions were noisier and therefore need further development for this measurement technique to realize its full potential (9, 10).

Many studies have been conducted on parameters affecting the mixing performance and particle motion in a V-blender (39-43). Lemieux et al. (41) described the particle motion in a V-blender as a granular flow which is induced due to the geometry of the blender. The flow is divided into separation and recombination phases with a predominant convective mixing mechanism and slower dispersive mixing mechanism (41). The study also found that while front to back and top to bottom loading was successful and accurately modelled, right to left loading had poor mixing performance due to the need for axial dispersion and there was a larger discrepancy in the model (41). This is also in agreement with the findings of Brone et al. (39) who concluded that in a symmetric blender, such as a V-blender, the rate of mixing is limited by the rate of mass transfer across the vessel's plane of symmetry orthogonal to the axis of rotation. The particle motion in a V-blender was also described by Kou et al. (43) using positron emission particle tracking. A relationship was found between the rotational speed and the axial dispersion coefficient at set fill levels (43) which is important since dispersive mixing is the rate limiting form of particle motion. Understanding particle motion within a Vblender is critical in studying powder mixing.

Table 3.1: Applications of acoustic emission monitoring

Application	Reference	Research Objective
Absorption	Hansuld et al. (17)	Monitoring column operations i.e. flooding
-		onset
Fluidization	Tsujimoto et al.(18)	Monitoring particle fluidization during
		fluidized bed granulation
	Vervloet et al. (19)	Monitoring process changes during fluidized
		bed drying
Hydro-	Albion et al. (20)	Flow regime detection
transport	Albion et al. (21)	Detection of oversized material
Mixing	Bellamy et al. (9)	Monitoring mixing and comparison to NIR
	Allan et al. (10)	Monitoring dynamics of mixing and
		comparison to NIR
	Tily et al. (16)	Monitoring dynamics of solid mixing
		processes
Rotary drying	Briens et al. (22)	End-point detection
Powder	Hakanen and Laine (23)	Monitoring
compaction	Hakanen and Laine (24)	Monitoring
	Serris et al. (25)	Monitoring phenomena i.e. fragmentation
Pneumatic	Hou et al. (26)	Monitoring of flow and related process
transport		parameters
	Albion et al. (27)	Detection of tablet breakage
	Albion et al. (28)	Flow regime detection
	Albion et al. (29)	Flow regime detection
Granulation	Whitaker et al. (30)	Monitor changes in physical properties i.e.
	, ,	particle size
	Briens et al. (31)	Monitoring
	Daniher et al. (32)	End-point detection
	Papp et al. (33)	Monitor changes in physical properties
	Gamble et al. (34)	End-point detection
	Hansuld et al. (35)	End-point detection
	Hansuld et al. (36)	Monitoring size and density
	Hansuld et al. (37)	Monitoring size
	Hansuld et al. (38)	Monitoring changes in process parameters

As the motion of particles within a V-blender is complex and the corresponding mixing dynamics can vary, it is difficult to predict and control mixing within a V-blender. As mixing within this blender is an important process for many industries, including pharmaceuticals, the control is essential. There is therefore a demand for the development of a reliable online or inline monitoring method. The aim of this study was to investigate the potential of passive acoustic emission monitoring of a tumbling V-blender.

3.2 Materials and Methods

3.2.1 Particles

The particles that were used in the experimental trials included Paulaur white sugar spheres, colored sugar spheres, lactose monohydrate from EMD Chemicals Inc., and Avicel PH-101 microcrystalline cellulose (MCC) from FMC BioPolymer. Table 3.2 lists the particles and their properties.

Particle Size (mm) Sphericity Density (g/cm³) 14-18 mesh spheres 1.00-1.40 ~1 1.58 16-20 mesh spheres 0.85 - 1.18~1 1.58 1.58 20-25 mesh spheres 0.71 - 0.85~1 60-80 mesh spheres 0.177-0.25 ~1 1.58 Purple spheres 1.18-1.68 ~1 1.58 0.075 Lactose 0.8 - 0.91.55 **MCC** 0.05 < 0.5 1.51

Table 3.2: Particle properties

3.2.2 V-blender

A Patterson-Kelley V-blender was used for all trials. Four different shells were used as listed in Table 3.3. This V-blender rotates at a fixed speed of 25 rpm. Unless otherwise stated, the V-shells were filled to 40% of their volume with the specified particles.

Shell	Size (QT)	Material
1	4	Stainless steel
2	8	Stainless steel
3	16	Stainless steel
4	16	Acrylic

Table 3.3: V-blender shell properties

3.2.3 Sensors and data acquisition system

Vibrations from the passive acoustic emissions were measured using PCB Piezotronics accelerometers (model 353B34) with a frequency range of 0.35-12,000 Hz combined with an ICP signal conditioner (model 480C02) at an acquisition frequency of 40,000 Hz. Three sensor locations, shown in Figure 3.1, were investigated: a top sensor position on the top of the left V-shell lid, a bottom sensor position on the base of the shell and a bottom right side sensor position with the sensor attached to the right side and 4 cm above the base. The sensors were securely attached to the V- shells using adhesive wax.

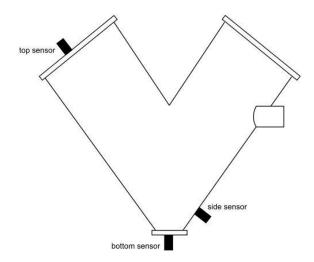


Figure 3.1: Sensor locations

The signals were recorded using Labview 8.5 with a National Instruments DAQ-6036E card. Signal analysis was performed in Matlab. Videos of the particle motion were taken using a Canon EOS-60D camera at 30 frames per second and VLC Media Player was used to extract the video stills.

3.3 Results and Discussion

3.3.1 Signal capturing and filtering

The V-blender is a tumbling blender that rotates about a horizontal axis. Figure 3.2a shows the vibrations measured from the top sensor using the empty 8 QT shell over a period of 5 rotations. The large oscillations in the signal are due to the overall movement of the sensor attached to the tumbling shell. To focus on the acoustic emissions from the

particle interactions within the shell, the oscillations in the signals from the motion of the shell must be removed. Three techniques were investigated: a manual filter, a windowed sinc filter based on code provided by Smith (44) (Figure 3.2b) and a Daubechies 6 wavelet filter based upon the description given in Daubechies (45) (Figure 3.2c). For a manual filter, the signal from the empty V-shell was subtracted from the signal of a trial containing particles. Aligning the signals to correctly subtract the oscillations was difficult and therefore a manual filter method was not selected. Both a windowed sinc filter and a wavelet filter showed similar results (Figure 3.2b and c). However, the wavelet filter was selected as the windowed sinc filter created a lag in the filtered signal which can be seen by the gap present at the beginning of the signal in Figure 3.2b.

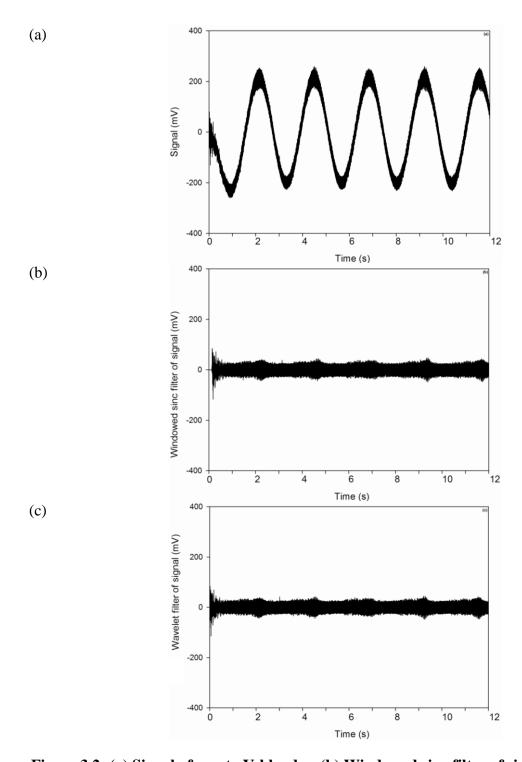


Figure 3.2: (a) Signal of empty V-blender, (b) Windowed sinc filter of signal, and (c) Wavelet filter of signal captured from top sensor

3.3.2 Sensor location

Sugar spheres were loaded into the acrylic shell to observe the motion of the particles (Figure 3.3). Initially the particles were at the bottom of the V-shell (Figure 3.3a) and then, as the rotation began, the particles slid down one side of the V-shell and impacted upon the inner portion of the top lid and slid along the lid towards the outside (Figure 3.3b). The particles continued to split and fill each arm of the V-shell (Figure 3.3c) eventually becoming fully split into the two arms (Figure 3.3d). As the rotation continued, the particles then slid down the other side of the V-shell (Figure 3.3e) and eventually accumulating at the bottom of the V-shell (Figure 3.3f). This pattern continued with each rotation.

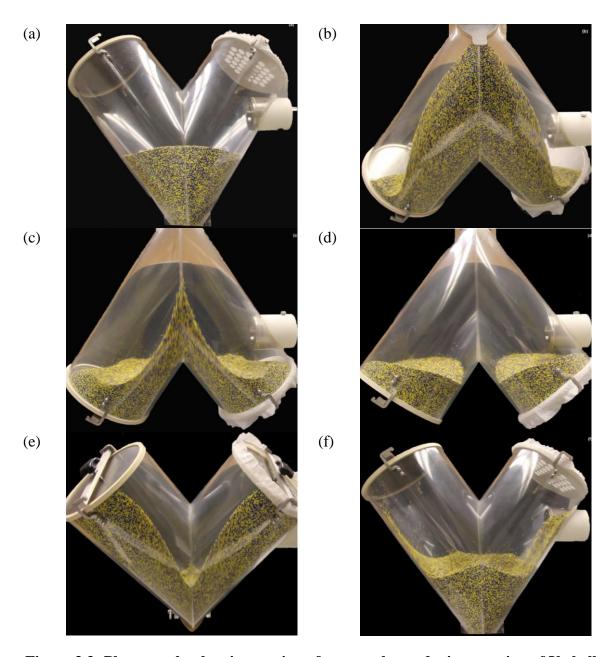


Figure 3.3: Photographs showing motion of sugar spheres during rotation of V-shell

To capture the different aspects of the particle motion and interactions, the sensors were initially located on the top of the lid, the bottom of the V-shell and the side of the V-shell as indicated in Figure 3.1. The measurements were made by three separate accelerometers of the same model with comparable response characteristics. Examples of the filtered signals are shown in Figure 3.4 using the 4 QT shell and 1.3 kg of 14-18 mesh sugar spheres. The measurements from the top lid sensor showed groupings of larger fluctuations reaching amplitudes of about +/- 100 mV (Figure 3.4a). Most of the

fluctuations from the bottom sensor (Figure 3.4b) were smaller than the groupings featured in Figure 3.4a; were less distinct and the signal was contaminated with larger, random fluctuations. The bottom of the V-shell was a plate that was attached through a rubber gasket to ensure a seal between the V-shell and the removable bottom plate. This gasket reduced the transmission of the vibrations to the sensor attached externally to this bottom plate. The measurements from the side sensor showed groups of fluctuations that reached large amplitudes of about +/- 300 mV. Vibrations from the sliding of the particles along side of the V-shell were easily transmitted to this side sensor, appearing as large fluctuations (Figure 3.4c). This transmission of the sliding motion partially masked the vibrations from particles impacting the lids and bottom plate of the V-shell.

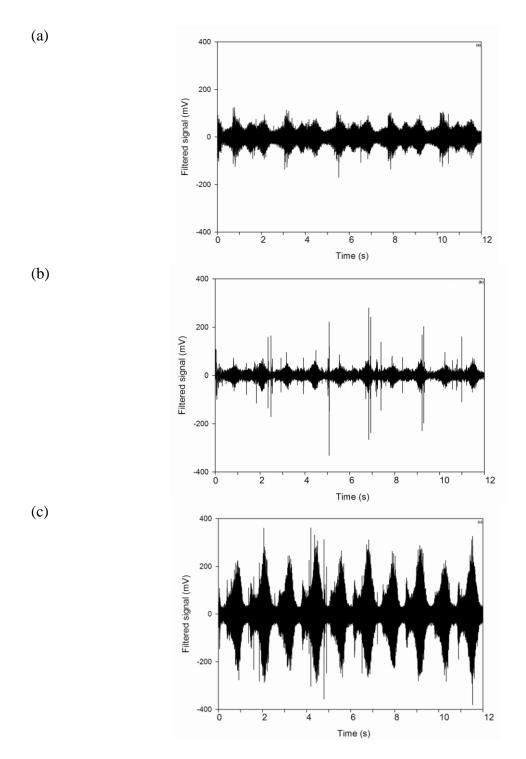


Figure 3.4: Filtered signals of 14-18 mesh spheres captured by (a) top sensor, (b) bottom sensor, and (c) side sensor

In Figure 3.5, the groupings of the larger fluctuations shown by the top lid sensor are further examined. There are three distinct groupings, each of which can be attributed to

phases of the particle motion shown in Figure 3.3. These groupings repeat every 2.4 s corresponding to the rotation of the V-blender at 25 rpm. The first grouping contains fluctuations due to the impact of the particles on the lid and the sliding down the side of the V-shell and across the lid. These particle motions overlap. The amplitude of the fluctuations within this grouping is the largest, reaching almost +/- 100 mV, as the transmission distance to the sensor is short for the vibrations from the particles impacting the lid. The second grouping of fluctuations was due to the particles sliding along the other side of the V-shell away from the sensor on the lid and back towards the bottom of the V-shell. The fluctuations in this second grouping were small as the sliding motion of the particles resulted in smaller vibrations than collisions and the transmission distance to the sensor was longer resulting in some dampening of the vibrations. The third grouping of fluctuations was due to the particles impacting the bottom of the V-shell, both the bottom plate and the adjacent sloped walls of the V-shell. Although the collisions of the particles with the bottom of the V-shell would have created large vibrations, the fluctuations measured by the top lid sensor were relatively small. The vibrations were dampened as they were transmitted a large distance along the length of the shell to the sensor. In addition, vibrations from the collisions on the bottom plate were further dampened due to reduced transmission from the plate to the V-shell through the rubber gasket.

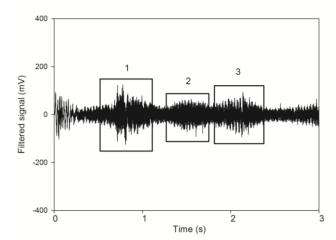


Figure 3.5: Filtered signal of 14-18 mesh spheres captured by top sensor related to particle motion

In summary, the top lid sensor location was considered to be optimal to measure the different particle motion and interactions within the V-shell. This top lid sensor location was therefore used for all subsequent trials.

3.3.3 Effect of particle size

To investigate the effect of particle size on the acoustic emissions, trials were conducted using four size cuts of white sugar spheres in the 8 QT V-shell. The filtered measurements are shown in Figure 3.6. The amplitude of the vibrations increased with average particle size. As the shape and the density of each size cut of the sugar spheres was the same, the change in the amplitude of the vibrations was attributed to size. The higher mass of the larger spheres created larger vibrations when particles collided with each other and with the V-shell (10).

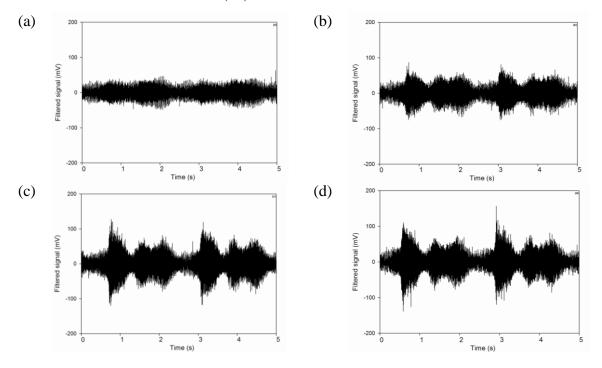


Figure 3.6: Sugar sphere particle sizes; (a) 60-80 mesh, (b) 20-25 mesh, (c) 16-20 mesh, and (d) 14-18 mesh

To compare the effect of particle size on the amplitude of fluctuations of each of the three groups discussed for Figure 3.5, an average of the largest amplitude of each grouping over three trials at every particle size was determined. Figure 3.7 shows these amplitudes at each particle size. As the particle size increased, the amplitudes increased. The

amplitude of the first grouping showed the largest increase with particle size. Vibrations in this first grouping were partially due to the impact of the particles on the lid with the sensor attached. Vibrations in the second and third groupings were either from particle sliding motion or showed dampening during transmission to the sensor and therefore these were not as sensitive to changes in the particle size.

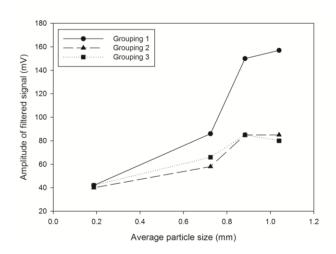


Figure 3.7: Effect of particle size on vibration amplitudes for sugar spheres

3.3.4 Effect of fill level

To investigate the effect of fill level on the acoustic emissions, the fill level of 16-20 mesh white sugar spheres was varied in the 8 QT V-shell. The filtered acoustic measurements are shown in Figure 3.8. As the fill level increased, the characteristic groupings of vibrations described and shown in Figure 3.5 began to change. The second and third groupings merged at fill levels of 60% and 75% volume capacity. The larger volumes of particles resulted in overlapping of the sliding of particles along the side of the V-shell and falling and impacting particles at the base of the V-shell. At a very high fill level of 75% of the shell volume capacity, the first grouping of vibrations also changed. The very large volume of particles significantly restricted particle movement. The distance from the top of the bed of particles resting at the bottom of the V-shell to the lid decreased from 22.9 cm to 19.0 cm to 16.5 cm as the fill level was increased from 40 to 60 to 75% volume capacity. This change reflected the decrease in distances that a particle could fall unimpeded within the V-shell before collision with another particle or

the V-shell. Shorter unimpeded distances reduced the potential of a particle reaching its maximum velocity or momentum before a collision. Hou et al. (46) showed that acoustic emissions primarily reflect the impact of particles with the equipment and the amplitude of the emissions are related to the particle momentum.

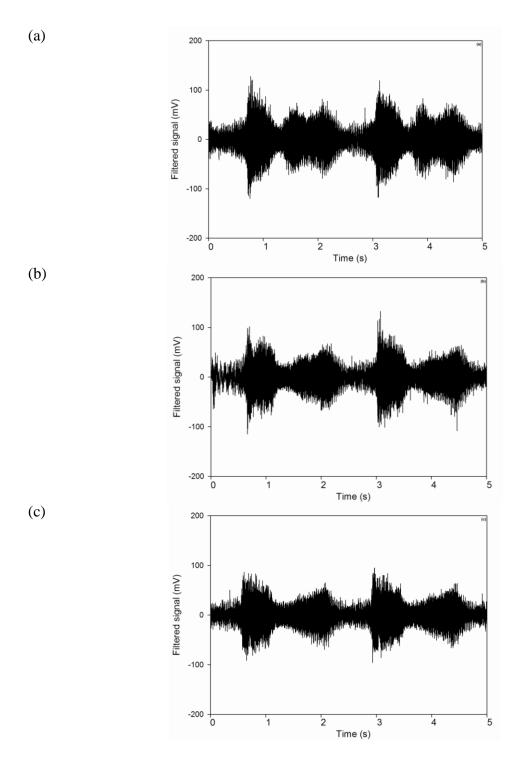


Figure 3.8: V-blender filled at (a) 40%, (b) 60%, and (c) 75% of capacity with sugar spheres

3.3.5 Effect of scale

To investigate the effect of scale on the acoustic emissions, an equal mass of 2.56 kg of 16-20 mesh sugar spheres was added to the 4, 8, and 16 QT stainless steel V-shells. The filtered measurements are shown in Figure 3.9. For the signal from the 4 QT V-shell, the characteristic three groupings described and shown in Figure 3.5 were difficult to identify. The 2.56 kg mass of particles added to this small V-shell corresponded to a fill level of approximately 80% volume capacity. This limited the movement of particles. Particles impacting upon the lid did not reach their maximum momentum before impacting upon the lid resulting in smaller acoustic emissions. In addition, all types of particle motion and interactions significantly overlapped. For the signals from the 8 QT and 16 QT V-shells, the second and third groupings of fluctuations were similar and corresponded to particles sliding along the side of the V-shell and impaction at the base. There was a significant increase in the amplitude of the vibrations in the first grouping of fluctuations as the shell size was increased to 16 QT. The 2.56 kg mass of particles in this large V-shell corresponded to a very low fill level of 20% volume capacity. Particles reached a high velocity or momentum due to the possibilities of falling long distances without collisions with other particles or the V-shell. Therefore, the particles impacting upon the lid with the sensor had high momentum and created large vibrations.

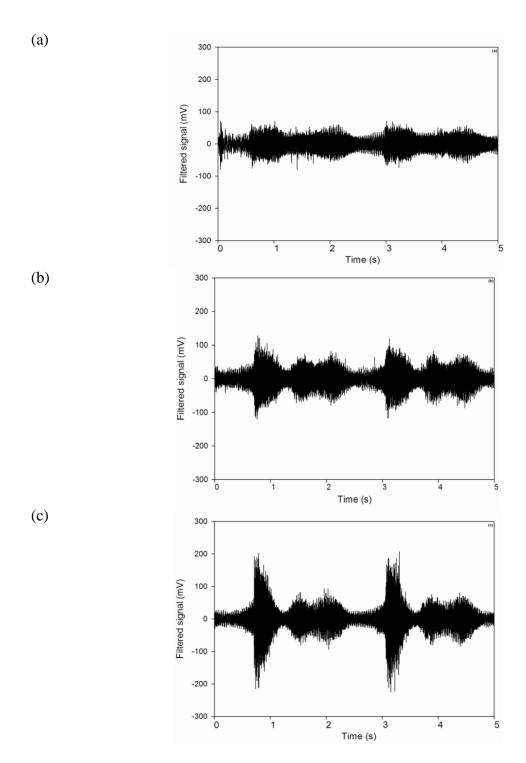


Figure 3.9: Effect of scale on acoustic emissions using an equal of mass of sugar spheres in (a) 4 QT, (b) 8 QT, and (c) 16 QT shell

3.3.6 Effect of particle type

To examine the effect of particle type on the acoustic emissions, measurements were taken with MCC, lactose and the 60-80 mesh sugar spheres in the 8 QT V-shell (Figure 3.10). Videos were also taken under the same conditions, but in the acrylic V-shell, to observe any differences in the particle motion during the tumbling of the V-shell. The particle sizes ranged from 0.05 to 0.075 to about 0.2 mm for the MCC, lactose and sugar spheres, respectively (Table 3.2). This increasing particle size was reflected in very small increases in amplitudes of the fluctuations of the acoustic emissions. The first grouping of fluctuations that was described in Figure 3.5 and attributed to particles hitting and sliding along the lid was difficult to identify as it was less pronounced as compared to the previous signals. It was almost indistinguishable for the MCC and lactose and only slightly discernible for the 60-80 mesh sugar spheres. The difference was attributed to the cohesiveness and poor flowability of the lactose and MCC. As the V-shell rotated, the sugar spheres immediately began to move and flowed easily down the side of the V-shell to impact the lid (Figure 3.10c). Due to their cohesive properties, the MCC and lactose particles did not move immediately with the rotation of the V-shell. After a delay until the V-shell was rotated almost 160° from the starting upright position, the MCC and lactose powder began to move. These powders then slowly slid down the side of the Vshell as a clump and did not impact the lid with a high momentum to create large vibrations (Figure 3.10a and b). From these observations, it was demonstrated that acoustic emissions can detect variability in particle flow through changes in the fluctuations of the acoustic emissions.

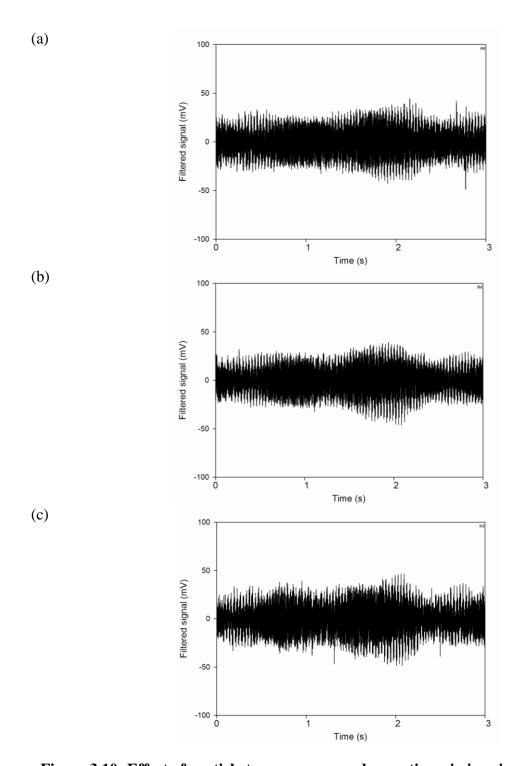


Figure 3.10: Effect of particle type on measured acoustic emissions in the 8 QT V-shell using (a) MCC, (b) lactose, and (c) 60-80 mesh sugar spheres

3.4 Conclusions

Passive acoustic emissions were measured from various particles under different process conditions during the operation of a V-blender. The ideal sensor location was found to be a lid of the V-shell, allowing the most direct transmission of vibrations from particle collisions with the V-shell. The particle size, fill level and scale affected the acoustic emissions through changes in the particle momentum upon collision with the V-shell. Similarly, changes in particle cohesiveness and flowability were also reflected in the measured acoustic emissions. This work was a feasibility study that confirmed the potential for passive acoustic emissions to be adapted as a monitoring method for V-blenders.

3.5 References

- 1. Blanco M, Gozalez B, Bertran E. Monitoring powder blending in pharmacetical processes by use of near infrared spectroscopy. Talanta 2002; 56: 203-212.
- 2. Koeller D, Posch A, Hori G, Voura C, Radl S, Urbanetz N, Fraser S, Tritthar W, Reiter F, Schlingmann M, Khinast J. Continuous quantitative monitoring of powder mixing dynamics by near-infrared spectroscopy. Powder Technol 2011; 205: 87-96.
- 3. Abe H, Otsuka M. Effects of lubricant-mixing time on prolongation of dissolution time and its prediction by measured near infrared spectra from tablets. Drug Dev Ind Pharm 2012; 38: 412-419.
- 4. Vergote G, De Beer T, Vervaet C, Remon J, Baeyens W, Diericx N, Verpoort F. Inline monitoring of a pharmaceutical blending process using FT-Raman spectroscopy. Eur J Pharm Sci 2004; 21: 479-485.
- 5. Hardy E, Hoferer J, Kasper G. The mixing state of fine powders measured by magnetic resonance imaging. Powder Technol 2007; 177: 12-22.
- 6. Perrault M, Bertrand F, Chaouki J. An investigation of magnesim stearate mixing in a V-blender through gamma-ray detection. Powder Technol 2010; 200: 234-245.
- 7. Realpe A, Velazquez C. Image processing and analysis for determination of concentrations of powder mixtures. Powder Technol 2003; 134: 193-200.
- 8. Yang C, Fu X. Development and validation of a material-labeling method for powder process characterization using X-ray computed tomography. Powder Technol 2004; 146: 10-19.
- 9. Bellamy L, Nordon A, Littlejohn D. Non-invasive monitoring of powder mixing with near infrared spectroscopy and acoustics. Spectrosc Eur 2004: 25-27.
- 10. Allan P, Bellamy L, Nordon A, Littlejohn D. Non-invasive monitoring of the mixing of pharmaceutical powders by broadband acoustic emission. Analyst 2010; 135: 518-524.
- 11. Leach M, Rubin G, Williams J. Particle size determination from acoustic emissions. Powder Technol 1977; 16: 153-158.
- 12. Leach M, Rubin G, Williams J. Particle size distribution characterization from acoustic emissions. Powder Technol 1978; 19: 157-167.

- 13. Leach M, Rubin G, Williams J. Analysis of polydisperse systems of rigid particles from acoustic emissions. Powder Technol 1978; 19: 169-176.
- 14. Leach M, Rubin G, Williams J. Analysis of a Gaussian size distribution of rigid particles from their acoustic emissions. Powder Technol 1978; 19: 189-195.
- 15. Leach M, Rubin G. Size analysis of particles of irregular shape from their acoustic emissions. Powder Technol 1978; 21: 263-267.
- 16. Tily P, Porada S, Scruby C, Lidington S. Monitoring of mixing processes using acoustic emission. In: Harnby N, Benkreira H, Carpenter K, Mann R, eds. Fluid Mixing III. Rugby: The Institute of Chemical Engineers, 1988: 75-94.
- 17. Hansuld E, Briens L, Briens C. Acoustic detection of flooding in absorption columns and trickle beds. Chem Eng Process 2008; 47: 871-878.
- 18. Tsujimoto H, Yokoyama T, Huang C, Sekiguchi I. Monitoring particle fluidization in a fluidized bed granulator with an acoustic emission sensor. Powder Technol 2000; 113: 88-96.
- 19. Vervloet D, Nijenhuis J, van Ommen J. Monitoring a lab-scale fluidized bed dryer: a comparison between pressure transducers, passive acoustic emissions and vibration measurements. Powder Technol 2010; 197: 36-48.
- 20. Albion K, Briens L, Briens C, Berruti F. Flow regime determination in horizontal hydrotransport using non-invasive acoustic probes. Can J Chem Eng 2008; 86: 989-1000.
- 21. Albion K, Briens L, Briens C, Berruti F. Modelling of oversized material flow through a horizontal hydrotransport slurry pipe to optimize its acoustic detection. Powder Technol 2009; 194: 18-32.
- 22. Briens L, Smith R, Briens C. Monitoring of a rotary dryer using acoustic emissions. Powder Technol 2008; 181: 115-120.
- 23. Hakanen A, Laine E. Acoustic emission during powder compaction and its frequency spectral analysis. Drug Dev Ind Pharm 1993; 19: 2539-2560.
- 24. Hakanen A, Laine E. Acoustic characterization of a microcrystalline cellulose powder during and after its compression. Drug Dev Ind Pharm 1995; 21: 1573-1582.
- 25. Serris E, Perier-Camby L, Thomas G, Desfontaines M, Fantozzi G. Acoustic emission of pharmaceutical powders during compaction. Powder Technol 2002; 128: 296-299.

- 26. Hou R, Hunt A, Williams R. Acoustic monitoring of pipeline flows: particulate slurries. Powder Technol 1999; 106: 30-36.
- 27. Albion K, Briens L, Briens C, Berruti F. Detection of the breakage of pharmaceutical tablets in pneumatic transport. Int J Pharm 2006; 322: 119-129.
- 28. Albion K, Briens L, Briens C, Berruti F. Flow regime determination in horizontal pneumatic transport of fine powders using non-intrusive acoustic probes. Powder Technol 2007; 172: 157-166.
- 29. Albion K, Briens L, Briens C, Berruti F, Book G. Flow regime determination in upward inclined pneumatic transport of particulates using non-invasive acoustic probes. Chem Eng Process 2007; 46: 520-531.
- 30. Whitaker M, Baker G, Westrup J Goulding P, Rudd D, Belchamber R, Collins M. Application of acoustic emission to the monitoring and end point determination of a high-shear granulation processing. Int J Pharm 2000; 205: 79-91.
- 31. Briens L, Daniher D, Tallevi A. Monitoring high-shear granulation using sound and vibration measurements. Int J Pharm 2007; 331: 54-60.
- 32. Daniher D, Briens L, Tallevi A. End-point detection in high-shear granulation using sound and vibration signal analysis. Powder Technol 2008; 181: 130-136.
- 33. Papp M, Pujara C, Pinal R. Monitoring of high-shear granulation using acoustic emission: predicting granule properties. J Pharm Innov 2008; 3: 113-122.
- 34. Gamble J, Dennis A, Tobyn M. Monitoring and end-point prediction of a small scale wet granulation process using acoutic emissions. Pharm Dev Technol 2009; 14: 299-304.
- 35. Hansuld E, Briens L, McCann J, Sayani A. Audible acoustic emission in high-shear wet granulation: application of frequency filtering. Int J Pharm 2009; 378: 37-44.
- 36. Hansuld E, Briens L, Sayani A, McCann J. Monitoring quality attributes for high-shear wet granulation with audible acoustic emission. Powder Technol 2011; 215-216: 117-123.
- 37. Hansuld E, Briens L, Sayani A, McCann J. An investigation of the relationship between acoustic emission and particle size. Powder Technol 2012; 219: 111-117.

- 38. Hansuld E, Briens L, Sayani A, McCann J. The effect of processing parameters on audible acoustic emission from high-shear granulation. Drug Dev Ind Pharm 2013; 39: 331-341.
- 39. Brone D, Alexander A, Muzzio F. Quantitative characterization of mixing of dry powders in v-blenders. AIChE J 1998; 44: 271-278.
- 40. Kuo H, Knight P, Parker D, Tsuji Y, Adams M, Seville J. The influence of DEM simulation parameters on the particle behaviour in a V-mixer. Chem Eng Sci 2002; 57: 3621-3638.
- 41. Lemieux M, Bertrand F, Chaouki J, Gosselin P. Comparative study of the mixing of free flowing particles in a V-blender and a bin-blender. Chem Eng Sci 2007; 62: 1783-1802.
- 42. Lemieux M, Leonard G, Doucet J, Leclaire L, Viens F, Chaouki J, Bertrand F. Large-scale numerical investigation of solids mixing in a V-blender using the discrete element method. Powder Technol 2008; 181: 205-216.
- 43. Kuo H, Knight P, Parker D, Seville J. Solids circulation and axial dispersion of cohesionless particles in a V-mixer. Powder Technol 2005; 152: 133-140.
- 44. Smith SW. Windowed-sinc filters. In: Smith SW, ed. The scientist and engineers guide to digital signal processing. The United States of America: California Technical Publishers, 2011: 285-296.
- 45. Daubechies I. The wavelet transform, time-frequency localization and signal analysis. IEEE Trans Inf Theory 1990; 36: 961-1005.
- 46. Hou R, Hunt A, Williams R. Acoustic monitoring of hydrocyclones. Powder Technol 2002; 124: 176-187.

Chapter 4

4 The effect of moisture on the flowability pharmaceutical excipients

4.1 Introduction

Powder properties and behaviour are critical to efficient and successful manufacturing of pharmaceutical tablets. The water or moisture content of a powder is a key property. The "hygroscopicity" is a measure of the ability of a powder to take up water vapour from the atmosphere. Callahan et al. (1) and Newman et al. (2) outlined a hygroscopicity classification scheme based on the rate and amount of water uptake from the atmosphere with changes in the air humidity. A non-hygroscopic powder shows almost no change in moisture content with exposure to air below 90% relative humidity while the moisture content of a very hygroscopic powder would increase even in air with a relative humidity as low as 40-50%.

Water in powders can be in different physical states (3): (i) adsorbed monolayer or multilayers on the surfaces of the particle, (ii) condensed water on the particle surface, (iii) physically absorbed water within the particle, or (iv) chemisorbed water. The state and distribution of the water depends on the powder and the amount of water taken up through exposure to humid air and then affects many properties of the powder.

Moisture adsorption isotherms show the relationship at equilibrium between the water content of a material and the humidity of the contacting gas. Adsorption isotherms were originally divided into five categories. These model or ideal isotherms were originally described by Brunauer, Emmett and Teller and are therefore known as the BET isotherms (4). Type I isotherm represents monolayer adsorption with strong forces between the absorbent and the absorbate. Type II isotherm has an s-shape and represents monolayer adsorption followed by multilayer adsorption with strong forces between the absorbent and the absorbate. Type III is strictly multilayer adsorption with weak forces between the absorbent and the absorbate. Type IV is s-shaped similar to Type II and Type V has a

similar shape to Type III; however, Types IV and V exhibit hysteresis due to capillary condensation (5).

For all of the isotherms there are two possible points of interest. Oksanen and Zografi (6) and Amidon and Houghton (7) suggested that the first inflection point on a Type II adsorption isotherm corresponds to a critical moisture content: above this point water begins to act as a plasticizer due to a reduction in the glass transition temperature (7). The second critical point occurs at higher moisture levels. Above the glass transition temperature, the visco-elastic properties of a solid are altered significantly and the physical properties change from an amorphous to rubbery state (8). Oksanen and Zografi (6) found that polyvinylpyrrolidone transitioned to a rubbery state at the moisture content when the isotherm began to significantly increase and this transition was due to the reduction of the glass transition temperature to the temperature of the isotherm.

Since the original categories were developed, newer models have emerged and the Guggenheim-Ander-son de Boer (GAB) model is currently considered to be the most versatile adsorption model (9). The GAB model considers a layer or layers of sorbed vapor having properties that are intermediate to those in the first layer and of those in the bulk water; the mechanism for water sorption is the sequential formation of a monolayer, an intermediate layer and then the formation of bulk water (10). The GAB model does not predict different shapes for the moisture adsorption isotherms, but does provide a better fit of experimental data due to the extra parameter corresponding to the formation of an intermediate layer.

For normal pharmaceutical handling conditions, Newman et al. (2) indicated a possible range in relative humidity from 25-75% at a temperature of 25°C. Zografi et al. (10) reported a moisture content of 5-6% for microcrystalline cellulose (MCC) during routine handling under ambient conditions of 40-50% relative humidity. Shi et al. (11) proposed a typical moisture content of 3-5% for MCC under ambient conditions and showed that there were major property changes within this range. Sun (12) also found variations in MCC properties within the small 3-5% moisture range, but concluded that this range was still ideal as more significant property changes were observed at higher moisture levels.

These literature results indicate that the moisture content of a powder can vary during pharmaceutical handling and manufacturing and that these variations could have an impact upon the process and final tablet quality.

MCC is widely studied as it is commonly used in the pharmaceutical industry. The effect of moisture content on the behaviour of MCC has been investigated in a number of studies. Amidon and Houghton (7) found a critical moisture content of 5% and proposed it was due to water acting as a plasticizer above this moisture content as a result of the reduction in the glass transition temperature. They also indicated that this critical moisture content occurs at the point of upward curvature on the isotherm (7, 9). Sun (12) reported a critical moisture content in the range of 3.3-5% which related to a humidity of 20-50%: below 3.3% there were almost no changes while above 5% the behaviour of the powder began to change significantly. This behaviour was attributed to increasing plasticity as a result of the reduction in the glass transition temperature and the critical range was related to the completion of the monolayer (12).

Powder flow is critical during tabletting. The powder must flow easily and uniformly into the tablet dies to ensure tablet weight uniformity and production of tablets with consistent and reproducible properties (11, 13-14). Powder flows from the hopper into the tablet dies when gravitational forces become higher than particle-particle interaction forces. Friction and cohesion are the major particle-particle interaction forces. Friction acts at contact points between particles to oppose the relative motion of the particles. Particle shape and surface morphology affect contact and therefore can increase friction if contact area is increased. Water on the particle surface can act as a lubricant decreasing friction. Cohesion refers to the attraction between particles and includes van der Waals' forces, capillary force, electrical force and electrostatic force. Water primarily affects cohesion by increasing capillary forces through strengthening liquid bridges between particles (11, 15).

As shown in Table 4.1, the effect of moisture content on flowability has been examined using microcrystalline cellulose, theophylline, methyl methacrylate starch copolymers, lactose, aspartame and hydroxypropyl methylcellulose (HPMC). Lactose and HPMC

both showed decreased flowability with increasing moisture content, attributed to increased cohesion from stronger liquid bridges formed from condensed water on the surfaces of the particles (16 -17). In contrast, the flowability of aspartame was found to increase with moisture content as the particles formed agglomerates that were that were larger and more spherical than the small and needle shaped individual particles (16). Both Sandler et al. (18) and Bravo-Osuna et al. (19) found that flowability of theophylline and methyl methacrylate starch copolymers, respectively, changed with the moisture content of the powder: at low moisture levels, the water acted as a lubricant between the particles and increased the flowability while, at high moisture levels, the water increased cohesion through stronger liquid bridges thereby reducing flowability.

Table 4.1: Summary of previous studies

Powder	Moisture Content	Effect on Flowability	Measurement Method	Reference
Microcrystalline	0 – 12.2%	Decreased flowability	Shear cell	Amidon and Houghton (7)
cellulose	0 – 9%	Increased flowability	GDR	Faqih et al. (17)
Theophylline	19 – 82%	Flowability varied with moisture content	FloPro flow meter, static angle of repose, Hausner ratio	Sandler et al. (18)
Methyl methacrylate starch copolymers	0 – 19.6%	Flowability varied with moisture content	Flowmeter based on flow rate through funnels	Bravo-Osuna et al. (19)
Fast-flo lactose	0 - 0.5%	Decreased flowability	GDR	Faqih et al. (17)
Aspartame	0 – 8%	Increased flowability	Hausner ratio, Carr index, static and dynamic angle of repose, and shear cell	Emery et al. (16)
Hydroxypropyl methylcellulose	0 – 10%	0 – 10% Decreased flowability		Emery et al. (16)

Changes in moisture content can affect different stages during tablet manufacturing. Shi et al. (11) studied the high shear wet granulation of microcrystalline cellulose with different initial moisture contents ranging from 0.9 to 10.5 wt%. The granule size increased with increasing initial moisture content. This increase in granule size led to improved flowability, but the granule tabletability, as measured by the tablet tensile strength, decreased significantly. The tabletting performance decreased even over a small change in initial moisture content from 2.6 to 4.9% which is within normal variation under manufacturing conditions.

Changes in moisture content can also affect final tablet properties. de Jong (20) concluded that the tablet crushing strength increased with increasing relative density and also decreased with increasing moisture content. Khan et al. (21) found that, past 3% moisture content, tablets of MCC decreased in tensile strength as the moisture disrupted the particle bonds. Similarly, Sun (12) found that, under a constant pressure, the tablet tensile strength is optimum at an intermediate water content of 3.3-5%; outside this range the tensile strength decreased. These studies confirm that a change in the moisture content of a powder has an effect on important tablet properties; from a quality control perspective, it is critical that all parameters, including moisture content, during tabletting remain the same to ensure a consistent and high quality final product.

The objectives of the current research were to examine the effect of moisture content on properties of pharmaceutical powders with an emphasis on flowability as measured dynamically through avalanching behaviour.

4.2 Materials and Methods

4.2.1 Materials

Six powders that are commonly used excipients in the pharmaceutical industry were used for the trials: microcrystalline cellulose MCC (FMC Corporation, Avicel, PH-101), carboxymethyl cellulose CMC (Alfa Aesar), hydroxypropyl methylcellulose HPMC (Shin-Etsu Chemical Co., Ltd, Pharmacoat 603), polyvinylpyrrolidone PVP (Alfa Aesar), corn starch (Alfa Aesar) and potato starch. Particle size distributions of the powders were measured using a Malvern Mastersizer 2000. Scanning electron microscope (SEM)

images of the powders were taken using a Hitachi S-4500 field emission scanning electron microscope. The powder samples were mounted on a plate and coated with gold before examination. The images allowed the shape and surface morphology of the powders to be examined.

4.2.2 Moisture adsorption isotherms

The moisture adsorption isotherms of the powders were determined over a wide range of air humidities. The powders were spread into thin layers on trays and placed in a humidity chamber shown schematically in Figure 4.1. The humidity of the air passing over the powders was adjusted by varying the flow ratio of dry air and air humidified by bubbling through water in a column. The powders remained in the humidity chamber for 48 hours as preliminary trials showed that the powders reached equilibrium with the humid air within this time. The temperature and the humidity of the air within the humidity chamber were measured using dry and wet bulb temperature sensors.

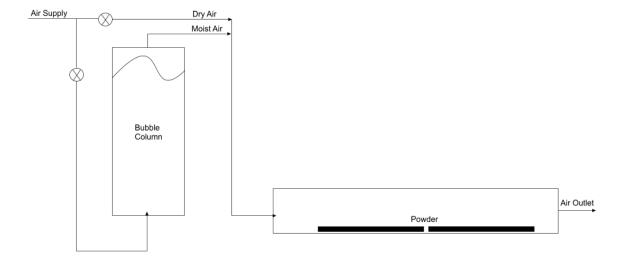


Figure 4.1: Schematic diagram of the humidity chamber

After 48 hours within the humidity chamber, the moisture content of the powders was determined using a Mettler-Toledo HG63 halogen moisture analyzer based on weight loss-on drying at 105°C. Triplicate samples of approximately 5 g were analyzed.

4.2.3 Flowability measurements

Flowability measurements were performed on the powders immediately after removal from the humidity chamber to minimize any changes in the powder moisture content during the measurements. Flowability measurements included bulk and tapped densities to obtain the Hausner ratio and the Carr index, static angle of repose, and various measurements from the Revolution Powder Analyzer (Mercury Scientific).

The bulk and tapped densities of the mixtures were measured in duplicate using 100 mL samples of the powders. For the bulk density measurements, the powder flowed down a vibrating chute into a 100 ml cylinder and the mass of the powder sample within the cylinder was then measured:

bulk density (g/mL) =
$$\frac{\text{mass of sample (g)}}{100 \text{ mL}}$$
 (eq. 1)

The sample within the cylinder was then vibrated/tapped until the volume no longer changed and then the final volume was measured to determine the tapped density:

$$tappeddensity (g/mL) = \frac{mass of sample (g)}{tappeddensity volume (mL)}$$
 (eq. 2)

The bulk and tapped density measurements then allowed the Hausner ratio and Carr index to be calculated:

Hausner Ratio =
$$\frac{\text{tappeddensity}}{\text{bulk density}}$$
 (eq. 3)

$$Carr Index = \frac{tappeddensity - bulk density}{tappeddensity} \times 100\%$$
(eq. 4)

The Hausner ratio indicates the cohesiveness of a powder. A Hausner ratio larger than 1.4 indicates a very cohesive powder that will not flow easily while a value lower than 1.25 indicates a less cohesive, more free flowing powder. Powders with Hausner ratios between 1.25 and 1.4 belong to a transitional group with some cohesive properties (22).

The Carr index also indicates flowability based on densities; values below 20-25% indicate good flowability (23).

Static angle of repose measurements were made using a Powder Research Ltd. Angle of Repose Device. Samples of about 60 mL flowed down a vibrating chute and through a funnel to form a pile below on a calibrated level platform allowing the static angle of repose to be measured. Samples were measured in triplicate.

Alternative indicators of flowability (avalanche time and avalanche time standard deviation) were measured using a Mercury Scientific Revolution Powder Analyzer. A sample size of 118 cm³ was loaded into a drum with a diameter of 11 cm and width of 3.5 cm. This drum was rotated at 0.3 rpm until 128 avalanches had occurred with an avalanche defined as a rearrangement of at least 0.65 vol% of the sample in the drum. Optical measurements with a resolution of 648 x 488 at 60 frames per second monitored the powder surface as the sample was rotated and software calculated the flowability indicators. Samples were measured in triplicate.

4.2.4 Dynamic density

The Mercury Scientific Revolution Powder Analyzer also measured the dynamic density of powders through the known sample mass and the measured volume of the powder as it moved within the drum:

$$dy namic density (g/mL) = \frac{mass of sample (g)}{volume of moving sample (mL)}$$
(eq. 5)

The dynamic density was measured in triplicate.

4.3 Results

4.3.1 Powder size, shape and morphology

Figure 4.2 shows the particle size distributions of the tested powders. CMC had the widest size distribution while PVP had the largest average size. Corn starch had the narrowest distribution and also the smallest average size of 15µm.

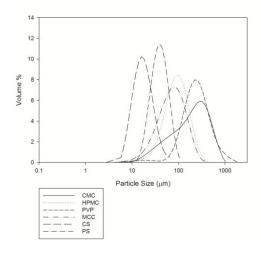


Figure 4.2: Particle size distributions of the powders

Figure 4.3 shows the scanning electron images of the powders at 250x magnification. The three cellulose based powders all had a fibrous type profile with a very irregular shape. The PVP was more spherical, but still showed a fibrous surface morphology. In contrast, the corn starch was almost spherical with a smooth surface and the potato starch was ovoid with a smooth surface.

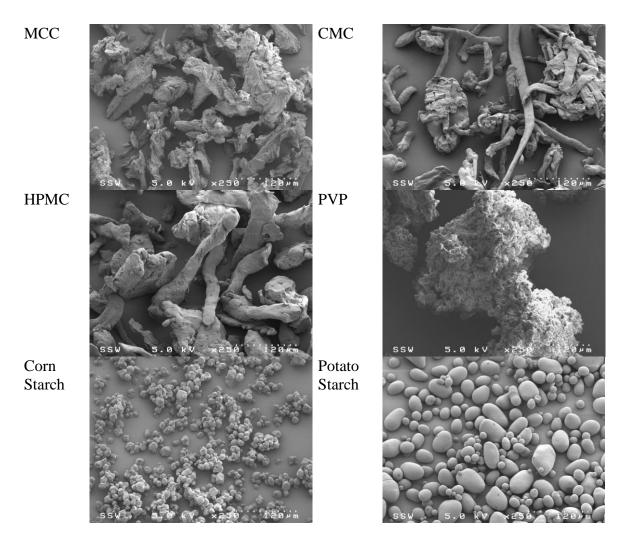


Figure 4.3: Scanning electron micrographs of the powders

4.3.2 Moisture adsorption isotherms

Figure 4.4 shows the moisture adsorption isotherms of the powders. The data was fitted using least squares regression to the GAB equation (10):

$$W = \frac{C_G K W_m(P/P_o)}{(1 - K(P/P_o))(1 - K(P/P_o) + K C_G(P/P_o))}$$
(eq. 6)

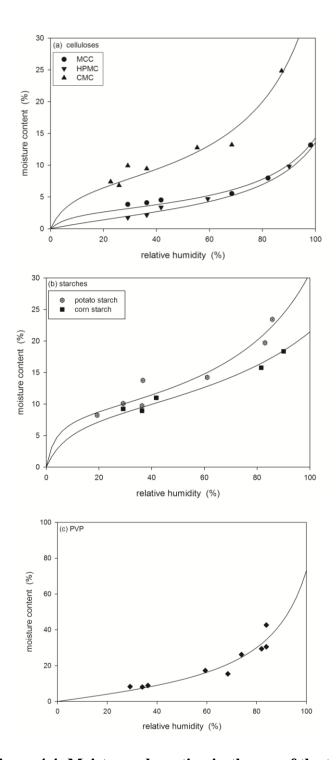


Figure 4.4: Moisture adsorption isotherms of the tested powders

where W is the mass of water taken up per gram of solid, W_m is the mass of water sorbed equivalent to monomolecular coverage, P/P_o is the relative water vapour pressure and K and C_G are constant parameters of the GAB equation. The parameters obtained from the

fitted GAB equation are summarized in Table 4.2. A second transition, W_g , can be identified on isotherms at the point at which the isotherm curves rapidly upward. The values of W_g obtained from the experimental isotherms are also listed in Table 4.2.

Table 4.2: Summary of parameters from the fitted GAB equation

Powder	W _m	C_{G}	K	W_{g}
MCC	0.029	17	0.80	0.050
CMC	0.071	16	0.82	0.100
HPMC	0.029	3.6	0.80	0.035
PVP	0.120	1.9	0.85	0.300
Corn Starch	0.089	18	0.60	0.110
Potato Starch	0.087	37	0.72	0.170

MCC microcrystalline cellulose, CMC carboxymethyl cellulose, HPMC hydroxypropyl methylcellulose, PVP polyvinylpyrrolidone,

Wm mass of water sorbed equivalent to monomolecular coverage, K and CG are constant parameters of the GAB equation, Wg point at which the isotherm curves rapidly upward

4.3.3 Flowability

Flowability was examined using the Hausner ratio, Carr index, static angle of repose and avalanche behaviour. General trends with increasing moisture content were obtained for the Hausner ratio, Carr index and static angle of repose. Figure 4.5shows the avalanche times and the standard deviations for the powders. The variation with increasing moisture content for corn starch was completely different than for the other tested powders.

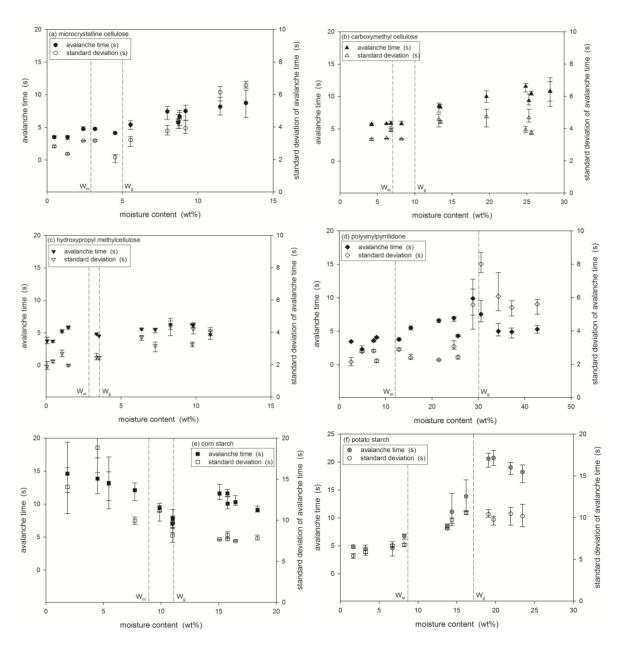


Figure 4.5: Avalanche times and standard deviations for (a) MCC, (b) CMC, (c) HPMC, (d) PVP, (e) Corn starch and (f) Potato starch

4.3.4 Dynamic density

The dynamic density of the powders was measured using the Revolution Analyzer. The dynamic density of the celluloses and the PVP decreased linearly with increasing moisture content (Figure 4.6a) while the relationship for the starches was more complex

as the dynamic density did not decrease until a critical moisture content was reached (Figure 4.6b).

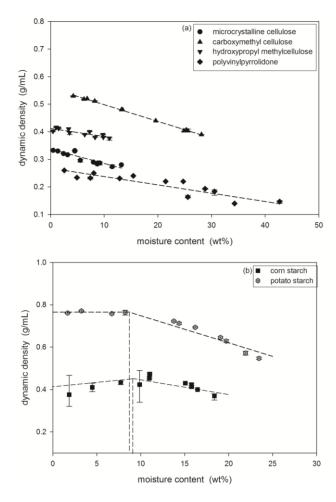


Figure 4.6: Dynamic density measurements of (a) the celluloses and PVP and (b) the starches

4.4 Discussion

The moisture adsorption isotherms shown in Figure 4.4 were fitted using least squares regression to the GAB equation. The parameters listed in Table 4.2are similar to the ranges reported in the literature (3, 6, 7, 10, 12, 24). With the exception of PVP, all of the powders showed s-shaped adsorption isotherms indicating Type II isotherms. This type of isotherm has also been reported in the literature for these powders (8, 9, 14, 25-27). PVP showed a Type III isotherm with the moisture content increasing very rapidly at high air humidities; Oksanen and Zografi (6) also reported a Type III isotherm for

PVP. Accurate isotherm measurements at very low air humidity levels were limited as it was difficult to maintain constant low levels over the 48 hour period required to ensure equilibrium conditions.

The parameter W_m of the GAB equation corresponds to the mass of water sorbed equivalent to monomolecular coverage and this transition point occurs near the first inflection point for Type II isotherms (Figure 4.4). A second transition point, W_g , was also identified on the isotherms at the point at which the isotherm curves rapidly upward. The glass transition temperature decreases with increasing moisture content as the water acts as a plasticizer (24) and this second transition point W_g then corresponds to a transition from the glassy to the rubbery state. HPMC had the smallest critical moisture range from 2.9 to 3.5 wt% moisture while PVP had the largest range of 12 to 30 wt%. Amidon and Houghton (7) reported changes in the properties of MCC in the critical moisture range between W_m and W_g . It was therefore expected that HPMC would have much smaller changes in properties with moisture than the other powders, especially PVP.

Flowability was examined using the Hausner ratio, Carr index, static angle of repose and avalanche behaviour. Only general trends with increasing moisture content were obtained for the Hausner ratio, Carr index and static angle of repose: with these techniques it is difficult to obtain consistent results and correlations to flowability have poor resolution. It was therefore not possible to draw clear conclusions about the effect of moisture content on powder flowability using these measurements.

The avalanche behaviour of a powder can indicate flowability potential. The avalanche time is the time between avalanches. For cohesive and poorly flowing powders, the powder accumulates and builds a crest at the perimeter of the rotating drum over a longer period of time before collapsing as an avalanche. Therefore, there is an inverse relationship between avalanche time and flowability. To examine avalanche behaviour, measurements were taken over 128 avalanches. The standard deviation of the avalanche time was also determined as this indicates flow uniformity: a high standard deviation

indicates non-uniform or variable flow. Previous studies (28) have found that the avalanche behaviour of powders can reliably detect small changes in flowability.

Figure 4.5 shows the avalanche times and the standard deviations with increasing powder moisture content. For MCC and CMC, the avalanche time and its standard deviation were initially constant and then increased (Figure 4.5a and b). The change corresponded to the critical range between W_m and W_g . With a monomolecular coverage of water, cohesion between particles increased as stronger liquid bridges formed. Increased cohesion then combined with a transition to the rubbery state resulted in a decrease in flowability and flow uniformity. Although still a cellulose based powder, the behaviour of HPMC differed from that of MCC and CMC. As shown in Figure 4.5c, there were only small changes in the avalanche time and its standard deviation with increasing moisture content with no clear transitions. HPMC had the smallest critical range from W_m of 2.9 wt% to W_g of 3.5 wt% and was also the least hygroscopic tested powder. Therefore, smaller changes in the avalanche time and its standard deviation were expected due to the reduced hygroscopicity of HPMC, as this means that the powder has less affinity for absorbing water and no clear transitions could be observed due to the narrow critical moisture range.

PVP was the most hygroscopic powder tested and reached a moisture content just above 40 wt% at an air humidity of about 80%. It also showed the largest critical moisture range between W_m and W_g values of 12 and 30 wt%. As shown in Figure 4.5d, the avalanche time began to increase slightly at W_m indicating increased cohesion from stronger liquid bridges between particles. The change in flowability was not large enough to lead to clear changes in flow uniformity as the standard deviation of avalanche times did not show a transition at W_m . There was a clear break, however, in both the avalanche time and its standard deviation at the transition to the rubbery state, W_g , followed by a decrease in both these parameters as the moisture content was further increased. The rubbery behaviour was observed in the avalanche drum: cohesive clumps of PVP "bounced" down the bulk powder slope making it difficult to detect distinct avalanches.

Two types of starches were tested: potato and corn starch. Differences were expected due to the different botanical origins. However, as shown in Figure 4.5e and f, the differences in flowability due to increasing moisture content followed opposite trends. Potato starch showed behaviour similar to PVP with transitions at W_m as the monolayer coverage of water increased cohesion through stronger liquid bridges and then again at W_g as the rubbery behaviour made avalanches difficult to detect by the Revolution Analyzer. Corn starch was the only tested powder that showed an increase in flowability with increasing moisture content. As shown in Figure 4.5e, both the avalanche time and its standard deviation decreased with moisture content until the critical region between W_m and W_g and then became approximately constant or increased only slightly with further increases in moisture content. At the lowest tested moisture levels, corn starch had the worst flowability potential with avalanche times near 20 s compared to the other particles that all had initial avalanche times near 5 s. Corn starch was the smallest tested particle with a mean diameter of about 15µm. For particles this small, van der Waals forces become dominant and contribute to cohesion causing poor flowability. The coverage of water around the corn starch particles acted as a lubricant and increased the distance between the particles reducing the effect of the van der Waal's forces. Once monolayer coverage was achieved at 8.9 wt%, additional water did not significantly contribute to the lubricating and spacing effect and therefore further changes in flowability were minimal.

The dynamic density of the powders was measured using the Revolution Powder Analyzer. As shown in Figure 4.6a, the dynamic density of the celluloses and PVP decreased linearly with increasing moisture content. This decrease is attributed to the swelling of the particles with the sorbed water. The potato and corn starch (Figure 4.6b); however, did not decrease in dynamic density until the moisture content reached the monolayer coverage point. For the starches, a critical amount of water was therefore required before significant swelling of the particles occurred to lead to density decreases.

A change in the density of powders can affect the final tablet through size, relative amounts of the powders and strength. Powder flows into the tablet press die for a predetermined specified time. Changes in either flowability and/or density of a powder

can therefore result in over or under-filling the tablet die. For example, over an air humidity range of just 40 to 50%, the moisture content of PVP would increase from about 7 to 11 wt% with a corresponding decrease in flowability and a decrease in dynamic density from 0.25 to 0.24 g/mL. The decrease in flowability would result in less powder flowing from the hopper into the die during the required filling period and the decreased density would result in less mass of powder filling the die volume. Combining the two effects, the resulting tablet would likely be undersized and need to be discarded. The literature (20, 21, 29) indicates that the combination of increasing moisture content and decreasing density would also yield a tablet with lower strength that may not meet product specifications.

4.5 Conclusions

For four of the tested excipients (MCC, CMC, PVP and potato starch), flowability decreased with increasing moisture content, once a critical point of monolayer water coverage was reached, due to an increase in cohesion from stronger interparticle liquid bridges. The flowability of corn starch increased with moisture content until monolayer coverage was reached as the water provided increasing interparticle lubrication as well as increasing spacing between particles thereby minimizing the relative effect of van der Waals forces. Flowability changes were not significant for HPMC, the least hygroscopic tested powder. All of the powders showed a decrease in dynamic density with increasing moisture content. For the starches, however, the decrease in density did not occur until monolayer water coverage was reached. Changes in flowability and dynamic density of excipients can significantly impact tabletability and therefore the moisture content of the excipients should be carefully monitored and controlled.

4.6 References

- 1. Callahan JC, Cleary GW, Elefant M, Kaplan G, Kensler T, Nash RA. Equilibrium moisture content of pharmaceutical powders. Drug Dev Ind Pharm 1982; 8:355-69.
- 2. Newman AW, Reutzel-Edens SM, Zografi G. Characterization of the "hygroscopic" properties of active pharmaceutical ingredients. J Pharm Sci 2008; 97: 1047-59.
- 3. Malamataris S, Goidas P, Dimitriou A. Moisture sorption and tensile strength of some tableted direct compression excipients. Int J Pharm 1991; 68: 51-60.
- 4. Brunauer S, Deming LS, Edwards Deming W, Teller E. On a theory of the van der Waals adsorption of gases. J Am Chem Soc 1940; 62: 1723-32.
- Donohue MD, Aranovich GL. Classification of Gibbs adsorption isotherms. Adv Colloid Interface Sci 1998; 76-77:137-52.
- 6. Oksanen CA, Zografi G. The relationship between the glass transition temperature and water vapor absorption by poly(vinylpyrrolidone). Pharm Res 1990; 7: 654-7.
- 7. Amidon AE, Houghton ME. The effect of moisture on the mechanical and powder flow properties of microcrystalline cellulose. Pharm Res 1995; 12: 923-9.
- 8. Kontny MJ, Zografi G. Sorption of Water by Solids. In: Brittain HG, editor. Physical characterization of pharmaceutical solids. New York: Informa healthcare; 1995. p. 387-418.
- 9. Peng G, Chen X, Wu W, Jiang X. Modeling of water sorption isotherm for corn starch. J Food Eng 2007; 80:562-7.
- 10. Zografi G, Kontny MJ, Yang AYS, Brenner GS. Surface area and water vapor sorption of microcrystalline cellulose. Int J Pharm 1984; 18: 99-116.
- 11. Shi L, Feng Y, Sun CC, Initial moisture content in raw material can profoundly influence high shear wet granulation process. Int J Pharm 2011; 416: 43-8.
- 12. Sun CC. Mechanism of moisture induced variations in true density and compaction properties of microcrystalline cellulose. Int J Pharm 2007; 346: 93-101.
- 13. Fassihi AR, Kanfer I. Effect of compressibility and powder flow properties on tablet weight variation. Drug Dev Ind Pharm 1986; 12: 1947-66.
- 14. Torres MD, Moreira R, Chenlo F, Vazquez MJ. Water adsorption isotherms of carboxymethyl cellulose, guar, locust bean, tragacanth and xanthan gums. Carbohydr Polym 2012; 89: 592-8.

- 15. Dawoodbhai S, Rhodes CT. The effect of moisture on powder flow and on compaction and physical stability of tablets. Drug Dev Ind Pharm 1989; 15: 1577-600.
- 16. Emery E, Oliver J, Pugsley T, Sharma J, Zhou J. Flowability of moist pharmaceutical powders. Powder Technol 2009; 189: 409-15.
- 17. Faqih AMN, Mehrotra A, Hammond SV, Muzzio FJ. Effect of moisture and magnesium stearate concentration on flow properties of cohesive granular materials. Int J Pharm 2007; 336: 338-45.
- 18. Sandler N, Reiche K, Heinamaki J, Yliruusi J. Effect of moisture on powder flow properties of theophylline. Pharm 2010; 2: 275-90.
- 19. Bravo-Osuna I, Ferrero C, Jimenez-Castellanos MR. Influence of moisture content on the mechanical properties of methyl methacrylate-starch co-polymers. Eur J Pharm Biopharm 2007; 66: 63-72.
- 20. de Jong JAH. Tablet properties as a function of the properties of granules made in a fluidized bed process. Powder Technol 1991; 65: 293-303.
- 21. Khan F, Pilpel N, Ingram S. The effect of moisture on the density, compaction and tensile strength of microcrystalline cellulose. Powder Technol 1988; 54:161-4.
- 22. Abdullah EC, Geldart D. The use of bulk density measurements as flowability indicators. Powder Technol 1999; 102: 151–65.
- 23. Carr R. Evaluating flow properties of solids. Chem Eng 1965; 72: 163-8.
- 24. Perfetti G, Alphazan T, Wildeboer WJ, Meesters GMH. Thermo-physical characterization of Pharmacoat® 603, Pharmacoat® 615 and Mowiol® 4-98. J Therm Anal Calorim 2012; 109: 203-15.
- 25. Nokhodchi A, Ford JL, Rubinstein MH. Studies on the interaction between water and (hydroxypropyl) methylcellulose. J Pharm Sci 1997; 86: 608-15.
- 26. Al-Muhtaseb AH, McMinn WAM, Magee TRA. Water sorption isotherms of starch powders Part 1: Mathematical description of experimental data. J Food Eng 2004; 61: 297-307.
- 27. Czepirski L, Komorowska-Czepirska E, Szymonska J. Adsorptive properties of biobased adsorbents. Adsorpt 2005; 11: 757-61.

- 28. Briens L, Logan R. The effect of the chopper on granules formed using a PMA-1 high shear granulator. AAPS PharmSciTech 2012; 12: 1358-65.
- 29. Tan SB, Newton JM. Powder flowability as an indication of capsule filling performance. Int J Pharm 1990; 61: 145-55.

Chapter 5

5 The effect of granule moisture on passive acoustic emissions in a V-blender

5.1 Introduction

The pharmaceutical tablet manufacturing process is a series of batch steps; to ensure quality control of the final product each step must be monitored and controlled. The development of process analytical technologies (PAT) can improve product monitoring with the aim of increasing efficiency, product quality and consistency and creating a better understanding of the manufacturing process. Ideally these are inline methods to remove issues related to extractive sampling and allow direct monitoring of the system using various sensors. Many PAT technologies have been investigated for pharmaceutical manufacturing; the most notable is near-infrared spectroscopy (1-4). A technology currently under investigation is passive acoustic emission monitoring (5-7) as it provides many advantages over other technologies. Passive acoustic emission monitoring is completely non-invasive as the sensors are attached to the outside of the equipment, the method is non-destructive as the measurements are passive emissions generated by the process itself, and the capital cost is less than other methods (7). One disadvantage is that large volumes of data must be analyzed to extract relevant information, but this processing can be less extensive than the complex calibrations and processing required for other techniques.

Acoustic emission technology was introduced in the 1970s to study different sizes and types of particles in a rotary drum (8-12). Subsequently, Tily et al. (13) monitored the dynamics of solid mixing processes using acoustic emissions and demonstrated that emissions from particle-wall collisions could monitor solid mixing processes. Additional applications utilizing acoustic emission monitoring for particulate operations are highlighted in Table 5.1. Crouter and Briens (7) detailed the use of acoustic emissions to monitor particle behaviour in a V-blender. It was found that particle mass and momentum influenced the acoustic signal and changes in powder flowability could be detected from the signal (7). While monitoring particle fluidization in a fluidized bed granulator,

Tsujimoto et al. (15) found that moisture absorption decreased the acoustic emission propagation capacity of particles; in regions of high moisture, when interparticle liquid levels were high, significant reduction in the intensity of the acoustics emissions generated from particle-particle and particle-wall collisions and friction caused the mean acoustic emission amplitude to decrease (15). While acoustic emissions have been used to monitor particle motion in a V-blender and moisture in a fluidized bed, the interaction between moisture and particle motion in a V-blender has not been examined.

The flowability of a powder is critical to the tabletting process; the powder must flow easily and uniformly into the tablet dies to ensure that tablets will have a uniform weight and that the tablets will be consistent with reproducible properties. Changes in the moisture content of a powder can affect its flowability and also the final tablet properties as residual moisture influences tablet breaking strength or tablet hardness, friability and disintegration time (4, 37-39). To ensure quality control it is important that critical parameters, such as moisture content, be monitored and controlled during powder processing to guarantee the quality of the final tablet product.

Many of the studies conducted on blend monitoring focus on the parameters affecting mixing performance and particle motion (1-2, 5-7). Blanco et al. (1) used near infrared spectroscopy (NIR) to monitor blend uniformity; the focus was to investigate data analysis methods. Koeller et al. (2) also used NIR to examine blend uniformity, varying the fill level and fill profile to determine the effect on mixing. While monitoring the mixing endpoint, Bellamy et al. (5) compared NIR and acoustic emission monitoring concluding that both had their own distinct advantages. More recently, Allan et al. (6) investigated factors influencing mixing dynamics including impeller speed, mass of powder, and particle size. Acoustic emission monitoring on a bench top convective mixer was used to study these parameters as well as monitor mixing profiles (6). All of these studies attempted to monitor blend uniformity and examine the influence of mixing dynamics; there are no known studies that have examined methods to obtain information about the solids properties thereby providing additional confirmation about the quality of the components that affect the success of the operation.

Table 5.1: Applications of acoustic emission monitoring

Application	Reference	Research Objective		
Absorption	Hansuld et al. (14)	Monitoring column operations i.e.		
riesorption	1141115414 01 411 (11)	flooding		
Fluidization	Tsujimoto et al. (15)	Monitoring particle fluidization during		
		fluidized bed granulation		
	Vervloet et al. (16)	Monitoring process changes during		
	, ,	fluidized bed drying		
	Aoki et al. (17)	Monitoring fluidized bed drying		
Hydro-	Albion et al. (18)	Flow regime detection		
transport	Albion et al. (19)	Detection of oversized material		
Mixing	Bellamy et al. (5)	Monitoring mixing and comparison to NIR		
	Allan et al. (6)	Monitoring dynamics of mixing and comparison to NIR		
	Crouter and Briens (7)	Monitoring dynamics of solid mixing processes		
	Tily et al. (13)	Monitoring dynamics of solid mixing processes		
Rotary drying	Briens et al. (20)	End-point detection		
Powder	Hakanen and Laine (21)	Monitoring		
compaction	Hakanen and Laine (22)	Monitoring		
_	Serris t al. (23)	Monitoring phenomena i.e.		
		fragmentation		
Pneumatic transport	Hou et al. (24)	Monitoring of flow and related process parameters		
- minport	Albion et al. (25)	Detection of tablet breakage		
	Albion et al. (26)	Flow regime detection		
	Albion et al. (27)	Flow regime detection		
Granulation	Whitaker et al. (28)	Monitor changes in physical properties		
	, ,	i.e. particle size		
	Briens et al. (29)	Monitoring		
	Daniher et al. (30)	End-point detection		
	Papp et al. (31)	Monitor changes in physical properties		
	Gamble et al. (32)	End-point detection		
	Hansuld et al. (33)	End-point detection		
	Hansuld et al. (34)	Monitoring size and density		
	Hansuld et al. (35)	Monitoring size		
	Hansuld et al. (36)	Monitoring changes in process		
		parameters		

The aim of the current research was to investigate the feasibility of passive acoustic emissions to measure and detect any change in granule moisture content as the granules tumble in a V-blender. A tumbling blender such as a V-blender is typically used in the final blending step which occurs after granulation and drying. In this final blend, the newly formed granules are mixed with additional excipients such as a lubricant and a glidant in preparation for tabletting. Prior to blending, the granules must be dried to a specified moisture content. The moisture content affects storage and handling of the granules as well as many properties of the final tablet products. Therefore, methods to confirm the moisture content of the granules during processing downstream of drying would provide important additional information to predict that the final tablet product will meet required specifications.

5.2 Materials and Methods

5.2.1 Solids

Experimental trials were first conducted with 6.35 mm diameter wooden beads (Bear Woods Supply Co. Inc). These wooden beads were selected as a model system as the beads were approximately spherical, monosize, uniform in composition and easily absorb and desorb water. Trials were then conducted with two formulations of placebo pharmaceutical granules. Both granule formulations were prepared in 1.5 kg batches in a Niro Pharma Systems PMA-1 high-shear granulator. The impeller (700 rpm) and chopper (1000 rpm) speeds were constant for 2 minutes of dry mixing, 12 minutes of water addition (~50 mL/min), and 2 – 3 minutes of wet massing. Table 5.2 lists the composition of the formulations.

Three samples from each formulation were photographed and the circularity of the granules was measured using Image Pro software. The average circularity of thirty granules from each sample was determined. The size distributions of the granules were also determined by sieving using standard sieve sizes with openings of 0.038 to 6.3 mm. Using the size distributions, an average granule size was calculated. The properties of the granules can be found in Table 5.3.

Table 5.2: Formulation composition

Particle	Formulation 1 (Wt %)	Formulation 2 (Wt %)	Manufacturer(s)
Microcrystalline cellulose	45	36	FMC BioPolymer
Lactose monohydrate	50	-	EMD Chemicals Inc., J.T. Baker
Mannitol	-	57	J.T. Baker
Hydroxypropyl methylcellulose	4	5	Alfa Aesar, Pharmacoat
Croscarmellose sodium	1	2	Alfa Aesar

The moisture content of the granules was determined using a Mettler-Toledo HG63 halogen moisture analyzer based on weight loss-on drying at 105°C. Duplicate samples of approximately 3 g were analyzed. The moisture content of the wooden beads was determined through loss on drying measurements.

Table 5.3: Solids properties

	Diameter (mm)			Mass of	
Particle	Dp_{10}	Dp ₅₀	Dp ₉₀	single particle at Dp ₅₀ (mg)	Sphericity
Wooden Beads	6.35*			93.46	~1
Formulation 1	0.09	0.17	1.30	2.79×10^{-3}	0.61
Formulation 2	0.43	1.60	4.76	2.21	0.68
Sugar Spheres		1.00*		0.65	~1

*Wooden beads and sugar spheres are approximately mono-sized particles

5.2.2 Equipment and acoustic measurements

An 8 QT stainless steel Patterson-Kelley V-blender was used for all trials. This V-blender rotates at a fixed speed of 25 rpm. The shell had an initial fill of 30% of its volume with the specified solids.

Vibrations from the passive acoustic emissions were measured at an acquisition frequency of 40,000 Hz using PCB Piezotronics accelerometers (model 353B34) with a

frequency range of 0.35-12,000 Hz combined with an ICP signal conditioner (model 480C02). As shown in Figure 5.1, the sensor position was on the top of the left V-shell lid. The sensor was securely attached to the V- shell using adhesive wax.

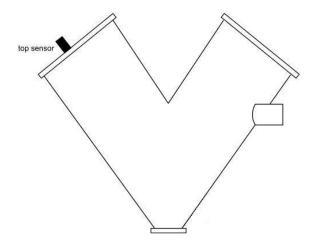


Figure 5.1: Sensor location

The signals were captured using Labview 8.5 with a National Instruments DAQ-6036E card. Signal analysis was performed in Matlab. Due to the tumbling motion of the V-blender, there were large oscillations in the signal. To focus on the acoustic emissions from the particle interactions within the shell, the oscillations in the signals from the motion of the shell were removed without interfering with the timing of the signal using a wavelet filter (7). Code for a high-pass Daubechies 6 tap wavelet decomposition filter was based on Daubechies (40).

5.2.3 Flowability measurements

The avalanche time was measured as a flowability indicator using a Mercury Scientific Revolution Powder Analyzer. A sample size of 118 cm³ was loaded into a drum with a diameter of 11 cm and width of 3.5 cm. This drum was rotated at 0.3 rpm until 128 avalanches had occurred with an avalanche defined as a rearrangement of at least 0.65 vol% of the sample in the drum. Optical measurements with a resolution of 648 x 488 at 60 frames per second monitored the powder surface as the sample was rotated and software calculated the flowability indicator. Samples were measured in triplicate.

5.2.4 Drying experiments

The drying behavior was observed for each granule formulation. Samples of each formulation were dried for 3 hours in an Armfield Tray Drier UOP-8 at an air flow rate of 0.11 kg/s and 32 °C at approximately 40 % relative humidity. Moisture content of the granules was determined using a Mettler-Toledo HG63 halogen moisture analyzer based on weight loss-on drying at 105°C.

5.2.5 Supplemental experiments

Supplemental experiments were conducted to investigate the relationship between solids mass and flowability on the passive acoustic emissions. These trials were conducted using 16-20 mesh (0.85–1.18 mm) Paulaur sugar spheres. Flowability and acoustic measurements were taken using the sugar spheres in both a dry and wet state. For the wet state, the sugar spheres were lightly sprayed with water to modify the sphere surface without significantly changing the mass.

The coefficient of restitution was measured for the wooden beads and sugar spheres at the wet and dry states. Drop tests were performed onto the lid of the V-blender with the acoustic sensor attached in a similar setup to Muller et al. (41). The coefficient of restitution (COR) was determined by comparing the peak amplitude as the solids rebounded. The COR of three drop tests was averaged and the values are summarized in Table 5.4.

Table 5.4: Coefficient of restitution

Solid	Coefficient of Restitution (COR)		
	Dry	Wet	
Wooden beads	0.69	0.55	
Sugar spheres	0.68	0.35	

5.3 Results

5.3.1 Wooden beads

For solids tumbling in a V-blender, three features have been identified in passive acoustic emissions measured using a sensor attached to the lid of the V-shell: fluctuations due to

the impact of the particles on the lid and sliding down the side of the V-shell and across the lid (feature 1), fluctuations due to sliding of particles along the other side of the V-shell away from the sensor (feature 2), and fluctuations due to the particles impacting the walls and bottom of the V-shell (feature 3) (7). These features were identified from acoustic emissions measured with wooden beads, at approximately 20 wt% moisture content, tumbling within the V-blender (Figure 5.2). The three features were distinct and observed for emissions measured from the wooden beads at various moisture levels. The maximum amplitude of each feature versus moisture content is shown in Figure 5.3. For all three features, there was an increase in amplitude with the moisture content. Feature 1 had the largest change followed by feature 2 and then feature 3.

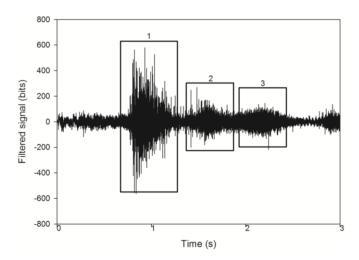


Figure 5.2: Filtered signal of wooden beads for one rotation of the V-blender

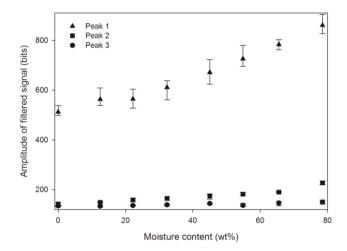


Figure 5.3: Maximum vibration amplitude for feature 1, feature 2, and feature 3 for the wooden beads at measured solids moisture contents

There was an increase in amplitude of each feature; the degree of change in amplitude with moisture content, however, varied for each of the features. To compare the relative changes of each feature, the differences in the maximum feature amplitude between features 1 & 2 and features 1 & 3 were plotted (Figure 5.4). The differences increased with solids moisture content.

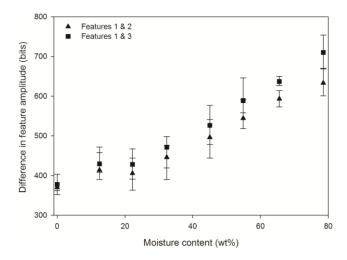


Figure 5.4: Difference in maximum vibration amplitude between feature 1 & 2 and feature 1 & 3 for the wooden beads at measured solids moisture contents

Flowability of the wooden beads at different moisture levels was measured as indicated through avalanche time (Figure 5.5). There was almost no change in these flowability measurements as the moisture content of the wooden beads was varied.

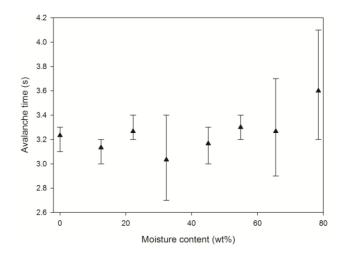


Figure 5.5: Avalanche time for the wooden beads at measured solids moisture contents

5.3.2 Formulation 1

Comparing the passive acoustic emissions measured using formulation 1 granules at approximately 20 wt% moisture content (Figure 5.6), the features were more difficult to determine and the amplitude of the emissions was much smaller than the wooden beads (Figure 5.2). Feature 1 had the greatest change with solids moisture content (Figure 5.7); in contrast to the trend observed for the wooden beads, there was a decrease in amplitude as the solids moisture content increased.

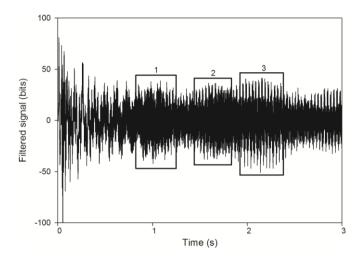


Figure 5.6: Filtered signal of formulation 1 granules for one rotation of the V-blender

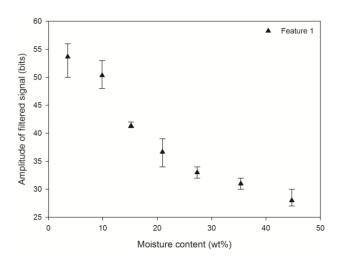


Figure 5.7: Maximum vibration amplitude for feature 1 for the formulation 1 granules at measured solids moisture contents

The maximum amplitude of each feature decreased as the solids moisture content of formulation 1 granules increased. To examine the relative changes in the amplitudes of the features, the differences in amplitude between features 1 & 2 and features 1 & 3 were calculated and are shown in Figure 5.8. There was a minimum in the differences at approximately 15 wt% solids moisture content.

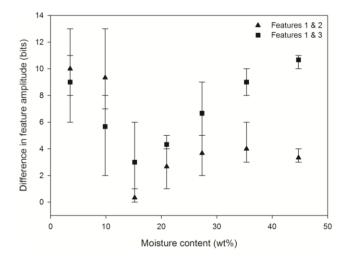


Figure 5.8: Difference in maximum vibration amplitude between feature 1 & 2 and feature 1 & 3 for the formulation 1 granules at measured solids moisture contents

The avalanche time for the granules as the moisture content varied was measured (Figure 5.9). The avalanche time was approximately constant up to a solids moisture content of about 15 wt%. There was then an increase with further increases in solids moisture content indicating decreased flowability of the solids.

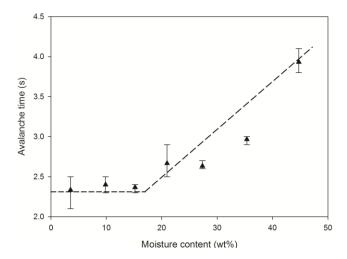


Figure 5.9: Avalanche time for the formulation 1 granules at measured solids moisture contents

5.3.3 Formulation 2

Comparing the passive acoustic emissions measured using formulation 2 granules at approximately 20 wt% moisture (Figure 5.10); the amplitude of the emissions from these granules was larger than for formulation 1 granules (Figure 5.6), but smaller than for the wooden beads (Figure 5.2). Similar to the trend observed for the formulation 1 granules, there was a decrease in the maximum amplitude of feature 1 as the solids moisture content decreased (Figure 5.11).

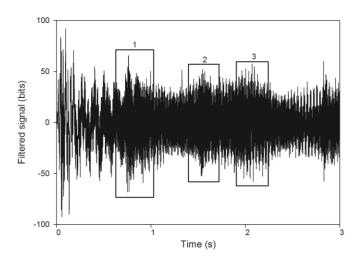


Figure 5.10: Filtered signal of formulation 2 granules for one rotation of the V-blender

The differences in amplitude between features 1 & 2 and features 1 & 3 with the moisture content of formulation 2 granules are plotted in Figure 5.12. The differences decreased with moisture content and then remained low at moisture levels higher than approximately 15-20 wt%.

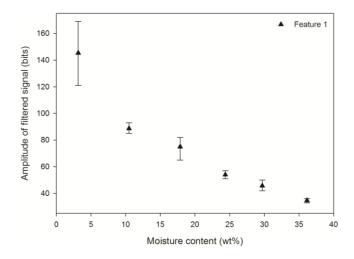


Figure 5.11: Maximum vibration amplitude for feature 1 for the formulation 2 granules at measured solids moisture contents

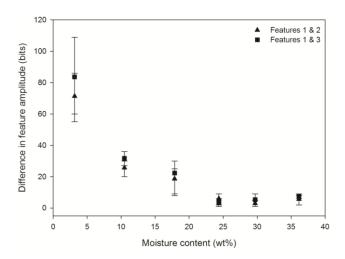


Figure 5.12: Difference in maximum vibration amplitude between feature 1 & 2 and feature 1 & 3 for the formulation 2 granules at measured solids moisture contents

Flowability of the formulation 2 granules was indicated by avalanche time. The avalanche time was almost constant until a solids moisture content of about 15 wt% and then increased with solids moisture content indicating decreased flowability of the solids (Figure 5.13).

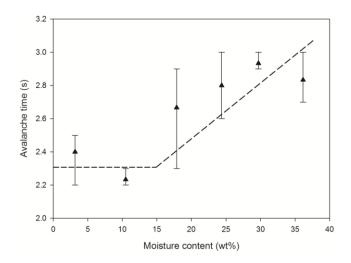


Figure 5.13: Avalanche time for the formulation 2 granules at measured solids moisture contents

5.3.4 Supplemental experiments

The acoustic emissions were measured with sugar spheres in the V-blender with the spheres in the dry (Figure 5.14a) and wet states (Figure 5.14b). The three features were again clearly visible. The amplitudes of the emissions from the wet spheres were lower than the amplitudes from the dry spheres. The amplitudes associated with feature 1 showed the largest difference between the dry and wet states.

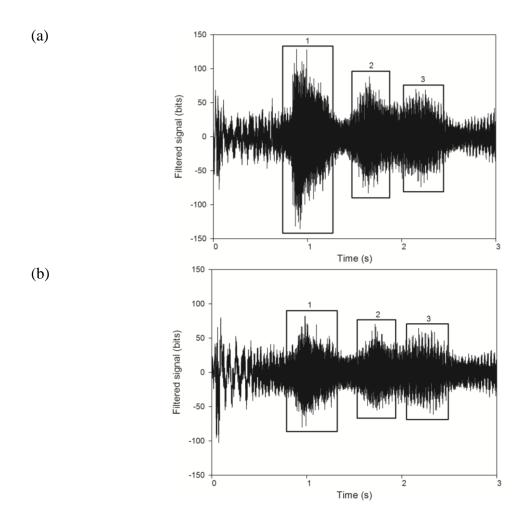


Figure 5.14: Filtered signal of sugar spheres at (a) dry and (b) wet states for one rotation of the V-blender

The avalanche times are shown in Figure 5.15. For the wet spheres, the avalanche time increased compared to the dry spheres indicating decreased flowability.

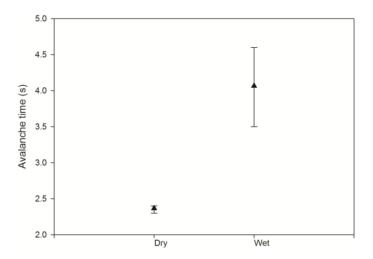


Figure 5.15: Avalanche time for the sugar spheres at measured solids moisture contents

5.4 Discussion

Wooden beads were chosen as a model system to represent an ideal granule, although the beads were larger and more spherical compared to granules. Figure 5.2 shows the filtered acoustic emissions produced from the wooden beads from one rotation of the V-blender; the emissions were loud and three features were clearly identifiable. The three features are attributed to phases of the particle motion. The features were identified for the wooden beads at various solids moisture contents and the maximum feature amplitude was measured. Figure 5.3 shows that, for all three features, as the solids moisture content increased, the acoustic emissions amplitude increased.

In general, the measured acoustic emissions are affected by both particle mass and particle flowability. The mass of the wooden beads increased with increasing moisture content as the beads absorbed water. The larger mass with moisture content increased the amplitude of the acoustic emissions as the kinetic energy of the now heavier beads was higher when they collided with each other and the V-shell imparting larger vibrations (6, 7). Measurements indicated that the flowability of the wooden beads did not significantly change with moisture content (Figure 5.5). The motion of the wooden beads within the V-shell therefore remained constant and did not contribute to changes in the amplitudes of the acoustic emissions. Another consideration is the coefficient of restitution, defined

as the ratio of resultant velocities before and after the impact of two bodies (42). The coefficient of restitution (COR) is considered a physical parameter, but it can vary for a particular material (41). Muller et al. (41) found that the COR of granular materials decreased slightly as their moisture content increased. The COR was measured and there was a slight decrease at the wet state (Table 5.4) but the decrease did not significantly impact the acoustic emissions. Collisions remained relatively elastic with minimal energy dissipated in the collision. The small change in the measured COR with moisture content of the wooden beads was supported with visual observations: the surface of the wooden beads was not found to significantly change even after soaking in water and the beads dried quickly with exposure to air. In conclusion, for the wooden beads, the COR and flowability, both of which partially depend upon surface properties, only slightly decreased over the range of tested moisture levels.

The increase in amplitude with solids moisture content of the wooden beads varied for each of the three features with feature 1 showing the largest increase (Figure 5.3). The increase was attributed to changes in the bead mass and not to changes in bead flowability or motion within the V-shell. Fluctuations of feature 1 were due to impact of the solids on the lid directly attached to the sensor. The increased mass of the beads with moisture content would significantly increase the fluctuations of feature 1 due to the higher energies of the heavier solids impacting near the sensor. Fluctuations of feature 2 were primarily due to vibration from the flow of solids along the V-shell wall. The fluctuations of this feature increased slightly with solids moisture content as the increased bead mass imparted more energy to the shell as the beads slid along its side. However, as the flow was not affected by moisture content and the interactions of the beads were not direct, full energy impact collisions, changes in the fluctuations were small. Fluctuations of feature 3 are primarily due to impact of the solids at the bottom of the V-shell. The vibrations from these collisions increased with bead mass. However, the change in the measured signal was not large as these vibrations were dampened before reaching the sensor. The difference plots shown in Figure 5.4 reflect that the largest changes were observed for fluctuations of feature 1.

To further investigate the effects of mass and flowability on the acoustic emissions, supplemental experiments were conducted with sugar spheres. The surface of the sugar spheres was wetted to change the flowability without significantly changing the solids mass. Figure 5.15 shows, through the large increase in avalanche time, that the wetted spheres exhibited poor flowability compared to the dry spheres. The wetted spheres were cohesive; solids did not move freely individually. Figure 5.14 compares the acoustic emissions of the dry and wet spheres, showing larger amplitudes for the dry spheres compared to the wet spheres. The largest change in amplitudes was observed for feature 1. Although the mass of the spheres impacting the lid near the sensor did not change, the flow of the spheres changed. Due to the cohesive surfaces, some energy from collisions was dissipated and therefore not transmitted to the sensor, decreasing the amplitude of the measured emissions. The change in the surface of the sugar spheres relates to a change in the coefficient of restitution. When the spheres were dry, the surface was strong and smooth and produced relatively elastic collisions; the COR value was found to be similar to the wooden beads (Table 5.4). The surface of wet the spheres was cohesive; energy was dissipated during the collisions with a significantly decreased COR. For the sugar spheres, both the flowability and COR are related, decreasing as the solids moisture content increased.

The amplitude of feature 2 fluctuations also decreased for the wet spheres. As the particles flow along the side of the V-shell, there are collisions between particles and with the shell that contribute to the fluctuations of feature 2. Movement of individual spheres was restricted by the cohesive wetted sphere surfaces. The energy from collisions as the particles were in motion was therefore reduced and smaller vibrations from this motion were recorded by the sensor. The amplitude of feature 3 fluctuation decreased slightly for the wetted spheres compared to the dry spheres. The fluctuations of this feature are the least sensitive to any changes as vibrations are significantly dampened by the rubber gasket attaching the bottom plate and the long distance to the sensor.

Acoustic emissions were also recorded from the V-blender using two pharmaceutical placebo wet high shear granulated formulations (Table 5.2). The acoustic emissions for these granules are shown in Figure 5.6 and Figure 5.10 for formulations 1 and 2,

respectively. The three features associated with phases of particle motion within the V-shell could be identified. The amplitudes of the acoustic emissions measured using the granules were much smaller than those of the wooden beads. As shown in Table 5.3, these granules were much smaller in size and mass than the wooden beds. As mass affects the vibrations produced form particle collisions, it was expected that the emission amplitudes of the granules would be small.

The amplitudes of the three features of the acoustic emissions of the granules varied with the moisture content of the granules. As feature 1 showed the most significant change, it is the focus for Figure 5.7 and Figure 5.11 for formulation 1 and 2, respectively. The amplitudes are affected by both particle mass and flowability. Although the granule mass increased, the emission amplitudes decreased as the granule moisture content increased. Granule flowability therefore primarily influenced the measured acoustic emissions. The flowability of the granules was estimated using the avalanche time. For a given particle type, higher avalanche times indicate a decrease in flowability. Figure 5.9 and Figure 5.13 show that the flowability of the granules was approximately constant until a critical granule moisture content of about 15-20 wt% for both formulation 1 and 2, and then flowability decreased as the granule moisture content further increased. From observing the drying behavior of the granules, it was determined that these critical granule moisture contents fell within the transition period between the constant rate and the falling rate drying periods. The moisture content of the granules was very high in the constant rate period; the surface of the granules was wet, altering the surface properties and increasing the cohesivity of the granules. The flowability of the granules at moisture content levels within the constant rate drying period was therefore poor. At low moisture content levels, within the falling rate drying period, the surface of the granules was dry and therefore the flowability improved and remained approximately constant during this period. The transition between the constant and falling rate periods did not correspond to a single critical moisture content level, but instead to a range of moisture content values. This range was attributed to the size distribution of the granules. Different sized granules of a given formulation will have slightly different critical moisture content levels, collectively as a powder creating a transition range.

The effect of moisture content of the granules on the amplitude of the acoustic emissions varied for each of the three features with the largest variation occurring for the first feature. Fluctuations of this feature were due to the impact of the solids on the lid directly attached to the sensor. When the granules were dry with relatively good flowability, individual granules impacted the lid resulting in many relatively large vibrations recorded by the sensor. The collisions produced by the dry the granules with a high COR would be relatively elastic.

Granules are agglomerates of particles held together through bonds. When the granules are wet, the bonds between particles are liquid bridges. The liquid bridges bond the particles, but also lubricate particle-particle contacts allowing deformation with collisions which is important to granulation as it allows granule nuclei to coalesce to form required larger granules. For collisions of wet granules within the V-shell, the liquid within the granules allowed the granules to deform and therefore some of the energy from the collision was dissipated and not transmitted as vibrations recorded by the sensor; the COR of wet granules was lower than that of dry granules. The lubrication of particle contacts occurs at all granule moisture content levels, but increases with moisture content. The dissipation of energy from collisions therefore increased with granule moisture content contributing to the observed decrease in recorded amplitude of fluctuations of the acoustic emissions.

The amplitude of feature 1 continuously decreased with increasing moisture content of the granules. A distinct transition at a critical moisture content that corresponded to changes in flowability was not observed. Although the fluctuations were significantly affected by granule flowability, the transfer of energy from the granule collisions, or the change in the coefficient of restitution, also affected the measured acoustic emissions.

The effect of the moisture content of the granules on the amplitude of the acoustic emission also varied for features 2 and 3. Fluctuations of feature 2 are primarily due to vibrations from the flow of solids along the V-shell wall. The fluctuations of this feature decreased with granule moisture content as increased cohesivity between the granules decreased movement and therefore energy from collisions and this energy was also

dissipated by the liquid lubricating bonds between particles. The fluctuations of feature 3 were the least affected by granule moisture content. The energy from collisions of granules at the bottom of the V-shell was not primarily affected by flow patterns, but by energy dissipation as the granules deformed by the collisions.

The differences of the effect of moisture content of the granules on the fluctuations of each feature are shown in Figure 5.8 and Figure 5.12 for formulations 1 and 2, respectively. The fluctuations from feature 1 were always very large at low granule moisture content levels as the granule surfaces were dry and granules flowed relatively well allowing high impact individual collisions with V-shell and significant energy transfer from the collision to the shell to be detected by the sensor. The differences in the fluctuations of the features showed transitions near the critical moisture content of the granules identified from flowability measurements and drying profiles. These transitions reflect the change in the movement of the granules within the V-shell as the granule surfaces become wet and cohesive, decreasing flowability and the coefficient of restitution. As the fluctuations of each feature reflect different phases of particle movement within the V-blender, the difference between the features highlight changes that affect this movement.

There were differences in the acoustic emissions recorded for the two placebo granules. The amplitude of the emissions was smaller for granules of formulation 1 compared to formulation 2 granules. This was expected as the size and mass of an average granule was smaller for formulation 1. The trend in the amplitudes of the features with granule moisture content, however, was the same for both formulations. The transition period for formulation 2 granules was larger than for formulation 1 granules due to its wider size distribution. However, for both formulations, the critical point in the flowability parameters and the minimum in differences between the features amplitudes fell within the identified transition period. Although some of the differences in the results from the two formulations were attributed to size and mass of the granules, the composition may also have had an impact. Particle-particle interactions including liquid bridge formation and contact lubrication vary with components in a granule. This would affect the coefficient of restitution of granules of a specified formation.

Granules must be dried to a specified moisture content before blending with additional excipients, commonly in a V-blender. If the granule moisture content is above a critical level then flowability will be affected and the blending will be negatively impacted. If the granule moisture content is below this critical level, the granules will appear dry and blend with the excipients. However, the moisture content may still be high enough and negatively impact tabletting and the tablet properties. As the acoustic emissions were affected by granule moisture content, monitoring these emissions could provide additional confirmation about the granules and the blend before proceeding with tabletting.

5.5 Conclusions

Passive acoustic emissions were measured from various solids over a range of solids moisture contents while tumbling in a V-blender and found to be sensitive to particle mass and surface properties which affect particle flowability within the V-shell. Three signal features related to particle motion were identified and it was found that feature 1 had the largest variation due to the impact of the solids on the lid directly attached to the sensor. Features 2 and 3 were also found to be affected by changes in solids moisture content. This work was a feasibility study that confirmed the potential for passive acoustic emissions to be adapted to provide additional information about granules before proceeding with further downstream processes.

5.6 References

- 1. Blanco M, Gozalez B, Bertran E. Monitoring powder blending in pharmaceutical processes by use of near infrared spectroscopy. Talanta 2002; 56: 203-212.
- Koeller D, Posch A, Hori G, Voura C, Radl S, Urbanetz N, Fraser S, Tritthar W, Reiter F, Schlingmann M, Khinast J. Continuous quantitative monitoring of powder mixing dynamics by near-infrared spectroscopy. Powder Technol 2011; 205: 87-96.
- 3. Abe H, Otsuka M. Effects of lubricant-mixing time on prolongation of dissolution time and its prediction by measured near infrared spectra from tablets. Drug Dev Ind Pharm 2012; 38: 412-419.
- 4. Hartung A, Knoell M, Schmidt U, Langguth P. Role of continuous moisture profile monitoring by inline NIR spectroscopy during fluid bed granulation of an Enalapril formulation. Drug Dev Ind Pharm 2011; 37: 274-280.
- 5. Bellamy L, Nordon A, Littlejohn D. Non-invasive monitoring of powder mixing with near infrared spectroscopy and acoustics. Spectrosc Eur 2004: 25-27.
- Allan P, Bellamy L, Nordon A, Littlejohn D. Non-invasive monitoring of the mixing of pharmaceutical powders by broadband acoustic emission. Anal 2010; 135: 518-524.
- 7. Crouter A, Briens L. Passive acoustic emissions from particulates in a V-blender. Drug Dev Ind Pharm 2015; 41: 1809-1818.
- 8. Leach M, Rubin G, Williams J. Particle size determination from acoustic emissions. Powder Technol 1977; 16: 153-158.
- 9. Leach M, Rubin G, Williams J. Particle size distribution characterization from acoustic emissions. Powder Technol 1978; 19: 157-167.
- 10. Leach M, Rubin G, Williams J. Analysis of polydisperse systems of rigid particles from acoustic emissions. Powder Technol 1978; 19: 169-176.
- 11. Leach M, Rubin G, Williams J. Analysis of a Gaussian size distribution of rigid particles from their acoustic emissions. Powder Technol 1978; 19: 189-195.
- 12. Leach M, Rubin G. Size analysis of particles of irregular shape from their acoustic emissions. PowderTechnol 1978; 21: 263-267.

- 13. Tily P, Porada S, Scruby C, Lidington S. Monitoring of mixing processes using acoustic emission. In: Harnby N, Benkreira H, Carpenter K, Mann R, eds. Fluid Mixing III. Rugby: The Institute of Chemical Engineers, 1988: 75-94.
- 14. Hansuld E, Briens L, Briens C. Acoustic detection of flooding in absorption columns and trickle beds. Chem Eng Process 2008; 47: 871-878.
- 15. Tsujimoto H, Yokoyama T, Huang C, Sekiguchi I. Monitoring particle fluidization in a fluidized bed granulator with an acoustic emission sensor. Powder Technol 2000; 113: 88-96.
- 16. Vervloet D, Nijenhuis J, van Ommen J. Monitoring a lab-scale fluidized bed dryer: a comparison between pressure transducers, passive acoustic emissions and vibration measurements. Powder Technol 2010; 197: 36-48.
- 17. Aoki H, Hattori Y, Otsuka M. Real-time monitoring of the drying of extruded granules in a fluid-bed dryer using audible acoustic emission chemometrics. RSC Adv 2014; 4: 50558-50565.
- 18. Albion K, Briens L, Briens C, Berruti F. Flow regime determination in horizontal hydrotransport using non-invasive acoustic probes. Can J Chem Eng 2008; 86: 989-1000.
- 19. Albion K, Briens L, Briens C, Berruti F. Modelling of oversized material flow through a horizontal hydrotransport slurry pipe to optimize its acoustic detection. Powder Technol 2009; 194: 18-32.
- 20. Briens L, Smith R, Briens C. Monitoring of a rotary dryer using acoustic emissions. Powder Technol 2008; 181: 115-120.
- 21. Hakanen A, Laine E. Acoustic emission during powder compaction and its frequency spectral analysis. Drug Dev Ind Pharm 1993; 19: 2539-2560.
- 22. Hakanen A, Laine E. Acoustic characterization of a microcrystalline cellulose powder during and after its compression. Drug Dev Ind Pharm 1995; 21: 1573-1582.
- 23. Serries E, Perier-Camby L, Thomas G, Defontaines M, Fantozzi G. Acoustic emission of pharmaceutical powders during compaction. Powder Technol 2002; 128: 296-299.
- 24. Hou R, Hunt A, Williams R. Acoustic monitoring of pipeline flows: particulate slurries. Powder Technol 1999; 106: 30-36.

- 25. Albion K, Briens L, Briens C, Berruti F. Detection of the breakage of pharmaceutical tablets in pneumatic transport. Int J Pharm 2006; 322: 119-129.
- Albion K, Briens L, Briens C, Berruti F. Flow regime determination in horizontal pneumatic transport of fine powders using non-intrusive acoustic probes. Powder Technol 2007; 172: 157-166
- 27. Albion K, Briens L, Briens C, Berruti F. Flow regime determination in upward inclined pneumatic transport of particulates using non-invasive acoustic probes. Chem Eng Process 2007; 46: 520-531.
- 28. Whitaker M, Baker G, Westrup J, Goudling P, Rudd D, Belchamber R, Collins M. Application of acoustic emission to the monitoring and end point determination of a high-shear granulation processing. Int J Pharm 2000; 205: 79-91.
- 29. Briens L, Daniher D, Tallevi A. Monitoring high-shear granulation using sound and vibration measurements. Int J Pharm 2007; 331: 54-60.
- 30. Daniher D, Briens L, Tallevi A. End-point detection in high-shear granulation using sound and vibration signal analysis. Powder Technol 2008; 181: 130-136.
- 31. Papp M, Pujara C, Pinal R. Monitoring of high-shear granulation using acoustic emission: predicting granule properties. J Pharm Innov 2008; 3: 113-122.
- 32. Gamble J, Dennis A, Tobyn M. Monitoring and end-point prediction of a small scale wet granulation process using acoutic emissions. Pharm Dev Technol 2009; 14: 299-304.
- 33. Hansuld E, Briens L, McCann J, Sayani A. Audible acoustic emission in high-shear wet granulation: application of frequency filtering. Int J Pharm 2009; 378: 37-44.
- 34. Hansuld E, Briens L, Sayani A, McCann J. Monitoring quality attributes for high-shear wet granulation with audible acoustic emission. Powder Technol 2011; 215: 117-123.
- 35. Hansuld E, Briens L, Sayani A, McCann J. An investigation of the relationship between acoustic emission and particle size. Powder Technol 2012; 219: 111-117.
- 36. Hansuld E, Briens L, Sayani A, McCann J. The effect of processing parameters on audible acoustic emission from high-shear granulation. Drug Dev Ind Pharm 2013; 39: 331-341.

- 37. Crouter A, Briens L. The effect of moisture on the flowability of pharmaceutical excipients. AAPS PharmSciTech 2014; 15: 65-74.
- 38. de Jong JAH. Tablet properties as a function of the properties of granules made in a fluidized bed process. Powder Technol 1991; 65: 293-303.
- 39. Danjo K, Kojima S, Chen CY, Sunada H, Otsuka A. Effect of water content on sticking during compression. Chem Pharm Bull 1997; 45: 706-709.
- 40. Daubechies I. The wavelet transform, time-frequency localization and signal analysis. IEEE Trans Inf Theory 1990; 36: 961-1005.
- 41. Müller P, Trüe M, Böttcher R, Tomas J. Acoustic evaluation of the impact of moist spherical granules and glass beads. Powder Technol 2015; 278: 138-149.
- 42. Li LP, Sun SQ, Li SC, Zhang QQ, Hu C, Shi SS. Coefficient of restitution and kinetic energy loss of rockfall impacts. KSCE J Civ Eng 2015: 1-11.

Chapter 6

6 Monitoring Lubricant Addition using Passive Acoustic Emissions in a V-blender

6.1 Introduction

The majority of pharmaceuticals are sold in tablet form. The tablet manufacturing process is a series of batch steps; as the powders must be transferred between the different steps, the flowability of the powders is critical. During the tabletting stage, the powder must flow easily and uniformly into the tablet dies to ensure tablet weight uniformity and production of tablets with consistent and reproducible properties (1-3).

Powder flows when gravitation forces become higher than particle-particle interaction forces such as friction and cohesion. Friction occurs at contact points between particles and opposes the relative motion of the particles. The contact is affected by particle shape and surface morphology; if the contact area is increased, the friction can increase. Cohesion is the attraction between particles and includes van der Waals' forces, capillary forces, electrical forces and electrostatic forces.

A lubricant is added to ensure that, following compression, the tablet is cleanly ejected from the tablet press die. Lubricants reduce the friction between the tablet and the die metal surface which reduces the ejection force. A lubricant can reduce friction in two ways: a liquid lubricant can form a thin continuous fluid layer between the tablet and the metal die surface or lubricant particles can form a boundary layer on the formulation particles or metal die surface. Magnesium stearate is a very commonly used lubricant; it has been extensively studied and is considered very effective. It is reported that magnesium stearate is a boundary layer lubricant with layers of magnesium stearate particles first filling any cavities of the other excipients before forming a continuous layer around the excipient particles (4-6). This mechanism improves flow by minimizing any surface irregularities, reducing contact points between excipients, which reduces friction forces.

The effect of lubricant addition on flowability has been studied by many researchers. By studying the avalanching behavior using a gravitational displacement rheometer (GDR), Faqih et al. (7) found that the presence of a lubricant did not significantly impact free flowing powders, but as powder cohesion increased, lubricants improved flowability. The study also claimed that the homogeneity of magnesium stearate plays a critical role in minimizing intra-batch variability, as a lack of homogeneity would lead to different flow properties within a batch (7). Liu et al. (8) added magnesium stearate to ibuprofen and found that, not only did the flow of the powder increase, but the internal friction angle was reduced. Lubricated samples were also able to maintain constant volume flow (8). To improve the flow properties of three active ingredients, Pingali et al. (9) added lubricants, glidants and other additives. The avalanche behaviour was studied in a GDR and the presence of colloidal silica, magnesium stearate and talc led to substantial decreases in the cohesiveness and therefore to a major improvement in flow (9). Morin and Briens (6) compared four lubricants at varying concentrations mixed with spray dried lactose and investigated magnesium stearate mixed with placebo granules. It was found that, even at low concentrations, magnesium stearate showed the highest improvement in flowability, but after a critical amount of 2wt%, there were no further increases in flow (6).

While reducing friction, lubricant addition may also cause undesirable changes in the properties of a tablet. The effect of lubricant concentration on the tensile strength of tablets was investigated and, for plastic materials, the tensile strength decreased as the lubricant concentration increased (10). The tensile strength of brittle materials was not significantly affected by an increase in lubricant concentration (10). Johansson (11) investigated lubricant properties and tablet properties on magnesium stearate lubricated granules. While the ejection force decreased with lubricant concentration, until a plateau above 2%, the tensile strength and friability of the tablets were negatively affected (11). The effect of mixing time has also been investigated; the impact of mixing time of magnesium stearate and lactose granules on the hardness, disintegration time and ejection force of the resultant tablets was investigated (12). The hardness and ejection force of the tablets decreased with mixing time and the disintegration time increased; the trends were similar with an increase in lubricant concentration (12). More recently, Abe and Otsuka (13) investigated the relationship between mixing time and dissolution time. After

mixing, magnesium stearate widely covered the surface of each particle of the bulk powder; the authors stated that the coating of the lubricant may decrease wetability and cause the prolongation of the dissolution time (13). The disintegration time was found to increase rapidly until 20 minutes of mixing and then stayed relatively constant; the dissolution time was prolonged with longer mixing times (13). The delay in disintegration time may have led to the prolongation of the dissolution time of tablets in the 20 minute mixing range (13). These studies highlight the need to optimize both lubricant concentration and the lubricant mixing time.

To ensure quality control of the final product, each step of the manufacturing process must be monitored and controlled. The development of process analytical technologies (PAT) can improve product monitoring with the aim of increasing efficiency, product quality and consistency and creating a better understanding of the manufacturing process. Ideally these are inline methods to remove issues related to extractive sampling and allow direct monitoring of the system using various sensors. Many PAT technologies have been investigated for pharmaceutical manufacturing; currently under investigation is passive acoustic emission monitoring (14-17) as it provides many advantages over other technologies. Passive acoustic emission monitoring is completely non-invasive, non-destructive, and the capital cost can be lower than other methods (16, 17). One disadvantage is that large volumes of data must be analyzed to extract relevant information, but this processing can be less extensive than the complex calibrations and processing required for other techniques.

Acoustic emission technology was introduced in the 1970s to study different sizes and types of particles in a rotary drum (18-22). Subsequently, Tily et al. (23) monitored the dynamics of solids mixing processes using acoustic emissions and demonstrated that emissions from particle-wall collisions could monitor these processes. Crouter and Briens (16) detailed the use of acoustic emissions to monitor particle behaviour in a V-blender. It was found that particle mass and momentum influenced the acoustic signals and changes in powder flowability could be detected (16). Crouter and Briens (17) also used acoustic emissions to monitor any changes in moisture content of granules while tumbling in a V-blender. Trends in the acoustic signals were identified. Surface

properties of the granules led to the changes in the signals which was then related to changes in particle motion.

It has been established that lubricant addition alters the flowability of powders and it has also been noted that the addition of a lubricant should be controlled. The aim of this paper is to investigate the feasibility of passive acoustic emissions to monitor lubricant addition and, if changes are detected, follow the progression of lubricant dispersal.

6.2 Materials and Methods

6.2.1 Solids

Experimental trials were first conducted with 14-20 mesh (0.85–1.4 mm) sugar spheres (Vanilla Food Company). The sugar spheres were selected as a model system as they were approximately spherical, uniform in composition and approximated common granule sizes. Trials were then conducted with two formulations of placebo pharmaceutical granules. Both granule formulations were prepared in 1.5 kg batches in a Niro Pharma Systems PMA-1 high-shear granulator. The impeller (700 rpm) and chopper (1000 rpm) speeds were constant for 2 minutes of dry mixing, 12 minutes of water addition (~50 mL/min), and 2 – 3 minutes of wet massing. Table 6.1 lists the composition of the formulations. For all trials, the solids were mixed with 1, 2.5 or 5 wt% magnesium stearate, MgSt (Alfa Aesar); the average particle size of MgSt was 10.2 μm.

Table 6.1: Formulation composition

Particle	Formulation A (Wt %)	Formulation B (Wt %)	Manufacturer(s)
Microcrystalline cellulose	36	45	FMC BioPolymer
Lactose monohydrate	-	50	EMD Chemicals Inc., J.T. Baker
Mannitol	57	-	J.T. Baker
Hydroxypropyl methylcellulose	5	4	Alfa Aesar, Pharmacoat
Croscarmellose sodium	2	1	Alfa Aesar

Three samples from each formulation were photographed and the circularity of the granules was measured using Image Pro software. The average circularity of thirty granules from each sample was determined. The size distributions of the granules were also determined by sieving using standard sieve sizes with openings of 0.038 to 6.3 mm. Using the size distributions, an average particle size was calculated. The properties of the solids can be found in Table 6.2. Scanning electron microscope (SEM) images of the solids were taken using a Hitachi S-4500 field emission scanning electron microscope. The solid samples were mounted on a plate and coated with gold before examination. The images allowed the surface morphology of the solids to be examined and compared before and after the addition of the lubricant.

Table 6.2: Solids properties

Solid Diameter (mm)		Mass of single	Sphericity		
Solid	Dp_{10}	Dp_{50}	Dp_{90}	particle at Dp ₅₀ (μg)	Sphericity
Sugar Spheres		1.13*		879	~1
Formulation A	0.36	1.14	3.30	799	0.68
Formulation B	0.09	0.17	1.00	2.79	0.61

*Sugar spheres are approximately mono-sized particles

6.2.2 Equipment and acoustic measurements

An 8 QT stainless steel Patterson-Kelley V-blender was used for all trials. This V-blender rotates at a fixed speed of 25 rpm. The V-blender had a fill of 25% of its volume with the specified solids.

Vibrations from the passive acoustic emissions were measured at an acquisition frequency of 40,000 Hz using PCB Piezotronics accelerometers (model 353B34) with a frequency range of 0.35-12,000 Hz combined with an ICP signal conditioner (model 480C02). As shown in Figure 6.1, the sensor position was on the top of the left V-blender lid. The sensor was securely attached to the V-blender using adhesive wax.

The signals were captured using Labview 8.5 with a National Instruments DAQ-6036E card. Signal analysis was performed in Matlab. Due to the tumbling motion of the V-blender, there were large oscillations in the signal. To focus on the acoustic emissions from the particle interactions within the V-blender, the oscillations in the signals from the motion of the V-blender were removed without interfering with the timing of the signal using a wavelet filter (17). Code for a high-pass Daubechies 6 tap wavelet decomposition filter was based on Daubechies (24). All acoustic trials were captured in triplicate; however, as replicates were similar, only one trial is shown for each condition.

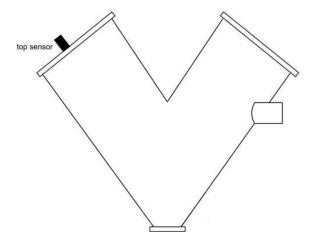


Figure 6.1: Sensor location

6.2.3 Flowability measurements

The dynamic avalanche angle was selected as a flowability indicator; it was measured using a Mercury Scientific Revolution Powder Analyzer. The dynamic avalanche angle was measured by comparing the maximum slope of the solids achieved before avalanching against the horizontal. It is a dynamic measurement and could be considered a dynamic angle of repose. A sample size of 118 cm³ was loaded into a drum with a diameter of 11 cm and width of 3.5 cm. This drum was rotated at 0.3 rpm until 128 avalanches had occurred with an avalanche defined as a rearrangement of at least 0.65 vol% of the sample in the drum. Optical measurements with a resolution of 648 x 488 at 60 frames per second monitored the powder surface as the sample was rotated and software calculated the flowability indicators. Samples were measured in triplicate.

6.2.4 Supplemental experiments

A stainless steel sampling thief was used to withdraw samples at intervals during a trial that combined sugar spheres with 5 wt% MgSt. A sample was taken from the base of the V-blender directly below the sensor location identified in Figure 6.1. The samples were placed in weigh boats and photographs were taken to capture the progress of the lubricant coating.

The coefficient of restitution was measured for the plain and lubricated sugar spheres. Drop tests were performed onto the lid of the V-blender with the acoustic sensor attached in a similar setup to Muller et al. (25). The coefficient of restitution (COR) was determined by comparing the peak amplitude as the solids rebounded. The COR of three drop tests was averaged and the values are summarized in Table 6.3.

Table 6.3: Coefficient of restitution of sugar spheres

Lubricant Concentration	Coefficient of Restitution (COR)	
Plain spheres	0.76	
1wt%	0.63	
2.5wt%	0.61	
5wt%	0.58	

6.3 Results

6.3.1 Sugar spheres

Passive acoustics emissions were measured while solids tumbled in a V-blender. Using a sensor attached to the lid of the V-blender, three features were identified. These features were related to different phases of the particle motion within the V-blender: feature 1 was the result of fluctuations from the impact of particles on the lid and sliding down the side of the V-blender and across the lid, feature 2 was the result of particles sliding along the other side of the V-blender away from the sensor, and feature 3 was due to particles impacting the walls and bottom of the V-blender (16). These features were identified from acoustic emissions measured from sugar spheres tumbling in a V-blender (Figure 6.2a). The three features were very distinct and had large amplitudes. A lubricant, magnesium stearate, was then added to the spheres in the V-blender and the acoustic emissions were again measured. The effect of addition of 5wt% magnesium stearate was shown immediately after lubricant addition (Figure 6.2b) and then after mixing for 3 minutes (Figure 6.2c). The three features decreased in amplitude significantly after the lubricant addition and then decreased further with mixing. Feature 1 showed the largest change in amplitude.

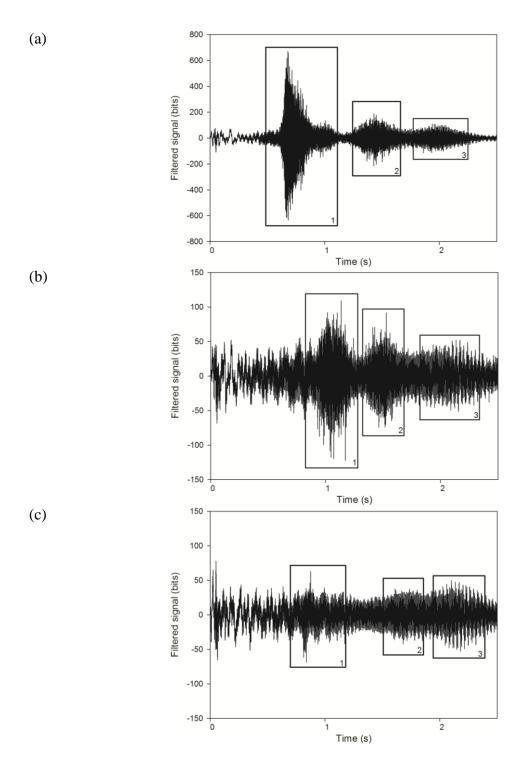


Figure 6.2: Filtered signal of sugar spheres (a) prior to and (b) immediately after lubricant addition, and (c) after dispersal for one rotation of the V-blender

The amplitude of feature 1 was determined over the entire mixing time (Figure 6.3). With the addition of 1wt% magnesium stearate (Figure 6.3a), the amplitude of feature 1

decreased immediately until approximately 8 revolutions and then the amplitude fluctuated around 100 bits. The addition of 2.5wt% (Figure 6.3b) and 5wt% (Figure 6.3c) magnesium stearate showed a similar trend. However as the amount of lubricant added increased, the initial measured amplitude decreased and the change in amplitude during the initial revolutions became more distinct. In addition, the amplitude measured after many revolutions decreased as the amount of added lubricant increased.

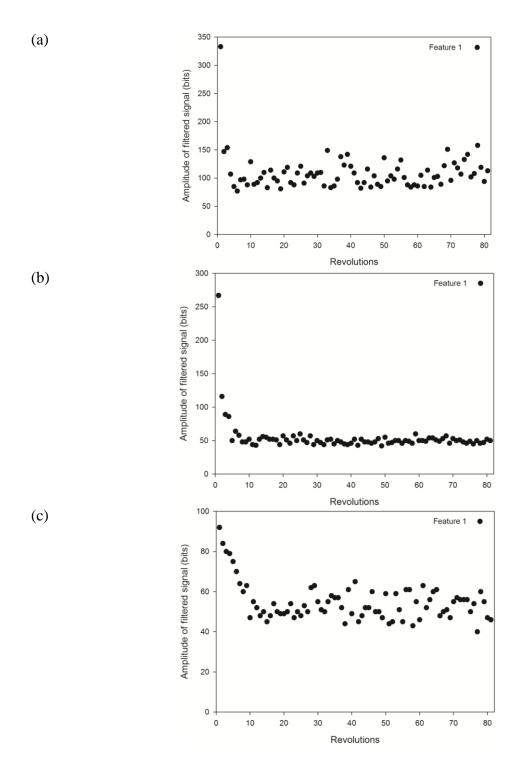


Figure 6.3: Maximum vibration amplitude for feature 1 of the sugar spheres for lubricant addition of (a) 1wt%, (b) 2.5wt%, and (c) 5wt% over the entire dispersal

The dynamic avalanche angle was measured to indicate the flowability of the solids. The angle was compared for the sugar spheres and the spheres combined with 1wt%, 2.5wt%

and 5wt% magnesium stearate (Figure 6.4). The avalanche angle increased for all levels of lubricant addition indicating a decrease in flowability. The increase in the avalanche angle also increased with lubricant concentration.

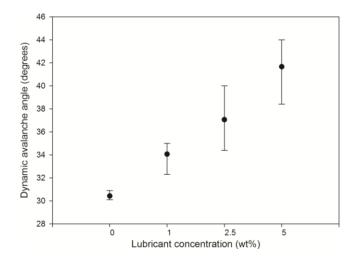


Figure 6.4: Avalanche angle for the sugar spheres before lubricant addition and after the addition of 1wt%, 2.5wt%, and 5wt%

A sampling trial was performed with sugar spheres and 5wt% magnesium stearate. Samples were removed at intervals to examine the lubricant dispersal. Photographs were taken of the samples at 1 revolution (Figure 6.5a), 10 revolutions (Figure 6.5b) and 30 revolutions (Figure 6.5c). After only 1 revolution, the lubricant was sitting on the surface of the sample and was not in contact with most of the spheres. By 10 revolutions, the lubricant had been dispersed into the sample but some lubricant was observed on the surface of the sample. At 30 revolutions, the lubricant was well dispersed with the sugar spheres.

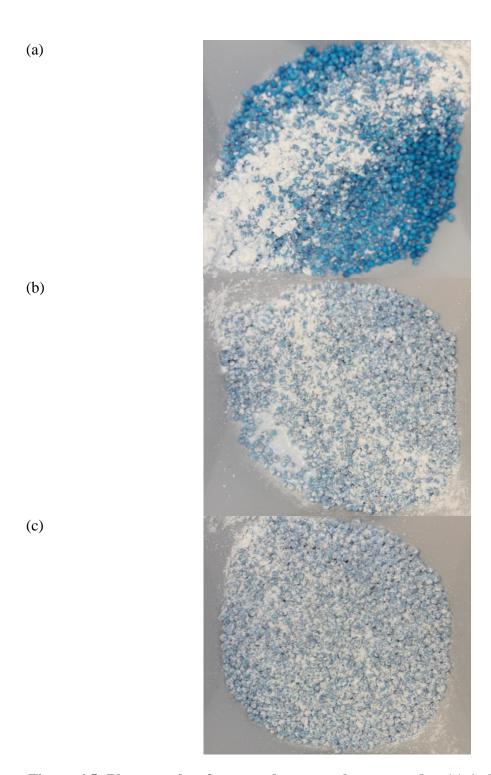


Figure 6.5: Photographs of sugar sphere samples removed at (a) 1, (b) 10, and (c) 30 revolutions after lubricant addition

Scanning electron micrographs of the sugar spheres were taken to compare the interactions between the sugar spheres and the magnesium stearate (Figure 6.6). The

sugar spheres had a smooth surface. The magnesium stearate flakes covered the surface of the spheres creating a rougher, less uniform surface.

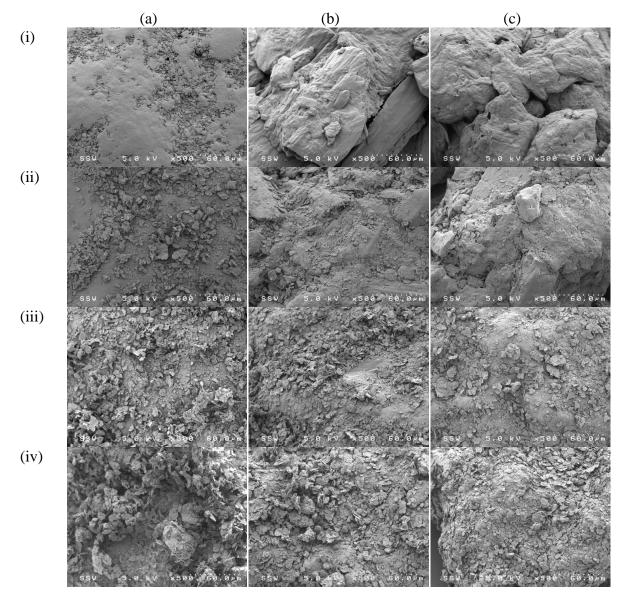


Figure 6.6: Scanning electron micrographs of (a) sugar spheres, (b) formulation A granules, and (c) formation B granules; (i) plain solids, (ii) 1wt%, (iii) 2.5wt%, and (iv) 5wt% lubricant dispersed

6.3.2 Formulation A

Comparing the passive acoustic emissions measured using formulation A granules (Figure 6.7a) to the sugar spheres (Figure 6.2a), the amplitudes were much smaller but the three identified features remained distinct. The effect of addition of 5wt% magnesium

stearate on the passive acoustic emissions is shown immediately after lubricant addition (Figure 6.7b) and then after 6 minutes of mixing (Figure 6.7c). Immediately following the addition of the magnesium stearate, the amplitudes of the features decreased. However with further mixing the amplitudes then increased and exceeded values for the unlubricated granules. Again, feature 1 showed the largest change in amplitude.

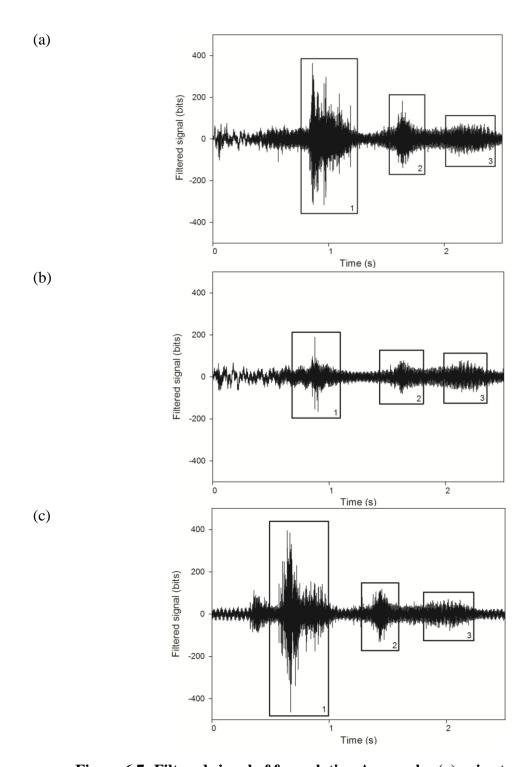


Figure 6.7: Filtered signal of formulation A granules (a) prior to and (b) immediately after lubricant addition, and (c) after dispersal for one rotation of the V-blender

To more closely monitor the dispersal of the lubricant with the granules, the amplitude of feature 1 was examined over the entire mixing time (Figure 6.8). With the addition of 1wt% magnesium stearate (Figure 6.8a), the amplitude increased beyond the range for the unlubricated granules but a trend with mixing time was difficult to identify. With the addition of 2.5wt% magnesium stearate (Figure 6.8b), a trend was easier to identify as the amplitude generally increased with time or number of revolutions. The addition of 5wt% magnesium stearate (Figure 6.8c) showed the clearest trend. The amplitude of feature 1 was initially small and increased until approximately 30 revolutions.

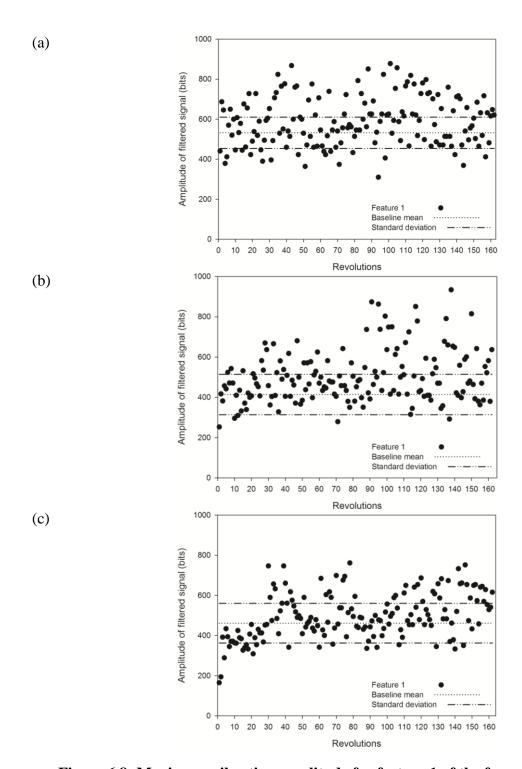


Figure 6.8: Maximum vibration amplitude for feature 1 of the formulation A granules for lubricant addition of (a) 1wt%, (b) 2.5wt%, and (c) 5wt% over the entire dispersal

The dynamic avalanche angle was measured for the formulation A granules to indicate flowability. The angle was compared for the granules and the granules combined with 1wt%, 2.5wt% and 5wt% magnesium stearate (Figure 6.9). The avalanche angle decreased with lubricant addition and as the lubricant concentration increased.

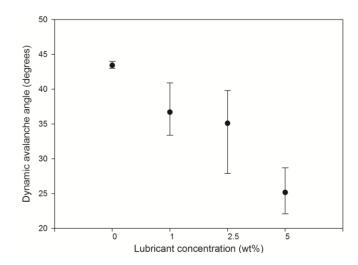


Figure 6.9: Avalanche angle for the formulation A granules before lubricant addition and after the addition of 1wt%, 2.5wt%, and 5wt%

Scanning electron micrographs were taken of the formulation A granules (Figure 6.6). The unlubricated granules were irregular in shape and surface morphology. The magnesium stearate primarily filled in the crevices of the granule surfaces.

6.3.3 Formulation B

Passive acoustic emissions were measured for a second granule formulation. The emissions measured from the formulation B granules (Figure 6.10a) were again smaller than the emissions from the sugar spheres (Figure 6.2a) and smaller than the formulation A granules (Figure 6.7a); the three features remained distinct. The effect of the addition of 5wt% magnesium stearate on the passive acoustic emissions is shown in Figure 6.10. As for formulation A (Figure 6.7), the addition of the magnesium stearate caused the amplitudes to immediately decrease followed by an increase with further mixing. Feature 1 showed the largest change in amplitude.

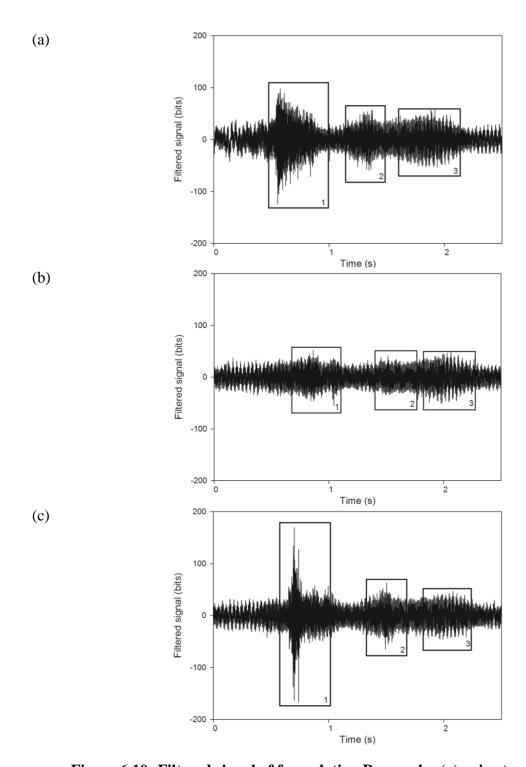


Figure 6.10: Filtered signal of formulation B granules (a) prior to and (b) immediately after lubricant addition, and (c) after dispersal for one rotation of the V-blender

The progress of the lubricant dispersal with the granules was monitored by determining the amplitude of feature 1 over time (Figure 6.11). The amplitude of feature 1 was initially very small and then showed a distinct increase with time or revolutions until an approximate steady state was reached. For the trial with 1wt% magnesium stearate, the steady state was reached quickly and remained near to or only slightly higher than amplitudes corresponding to unlubricated granules. The amount of time to reach this steady state and the amplitudes measured at steady state increased with magnesium stearate concentration.

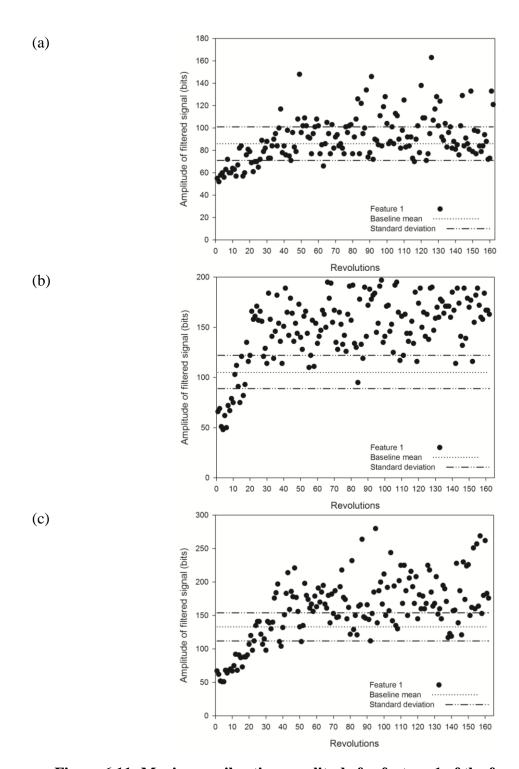


Figure 6.11: Maximum vibration amplitude for feature 1 of the formulation B granules for lubricant addition of (a) 1wt%, (b) 2.5wt%, and (c) 5wt% over the entire dispersal

The dynamic avalanche angle was measured for the formulation B granules to indicate flowability. The angle was compared for the granules and the granules combined with 1wt%, 2.5wt% and 5wt% magnesium stearate (Figure 6.12). Similar to the formulation A granules, the dynamic avalanche angle decreased with magnesium stearate addition.

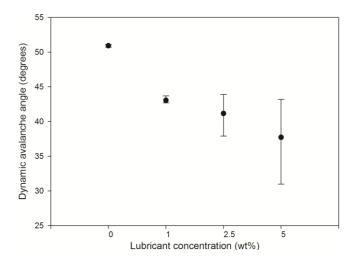


Figure 6.12: Avalanche angle for the formulation B granules before lubricant addition and after the addition of 1wt%, 2.5wt%, and 5wt%

Scanning electron micrographs were taken of the formulation B granules (Figure 6.6). Similar to the formulation A granules, the magnesium stearate primarily filled in the crevices of the irregular granule surfaces thereby forming more spherical shapes.

6.4 Discussion

To determine the feasibility of using passive acoustic emissions to monitor lubricant addition, sugar spheres were chosen as a model system. Figure 6.2a shows the filtered acoustic emissions produced from the sugar spheres from one rotation of the V-blender; the emissions were distinct and three features were clearly identifiable. These features were attributed to phases of the particle motion. As lubricants influence particle motion, it was expected that lubricant addition would have an effect on these features. The effect was identified immediately after lubricant addition (Figure 6.2b) and continued with further mixing (Figure 6.2c). The addition of the lubricant resulted in a decrease in the amplitude of the measured passive acoustic emissions.

Passive acoustic emissions measured in a V-blender have been shown to be affected by particle mass, coefficient of restitution and flowability (16, 17). The changes in mass of the solids due to magnesium stearate adhesion to the surfaces was considered negligible as only a small amount of magnesium stearate was added to the solids. The changes in the passive acoustic emissions were therefore attributed to the coefficient of restitution and flowability.

The coefficient of restitution is defined as the ratio of resultant velocities before and after the impact of two bodies (26). The COR was measured for the sugar spheres (Table 6.3). The COR decreased as the sugar spheres became coated with the magnesium stearate flakes. The collisions of the lubricant coated sugar spheres were therefore less elastic and more energy was dissipated during the collisions. This dissipated energy decreased the energy transmitted to the sensor resulting in a decrease in the amplitudes of the measured passive acoustic emissions.

The flowability was estimated through dynamic avalanche angle measurements. As shown in Figure 6.4, the avalanche angle increased with the addition of the lubricant indicating a decrease in flowability. The sugar spheres were approximately 1mm diameter smooth spheres that exhibited excellent flowability as indicated by a low avalanche angle of 30 degrees. The magnesium stearate flakes covered the surface of the spheres changing the surface morphology from smooth to rough. The inter-particle friction forces therefore increased resulting in a decrease in flowability. Stanford et al. (27) investigated particle morphology and stated that, particles that were irregular and angular in shape flowed poorly compared to smoother more rounded particles.

The amplitudes of the three features identified from the passive acoustic emissions decreased as lubricant was added to the sugar spheres with feature 1 showing the largest change (Figure 6.2). Feature 2 is primarily affected by the small collisions occurring during the sliding motion of the particles. Emissions contributing to this feature would have decreased due to the lower COR and hindered flowability which would have decreased the collision impact energy. Feature 2 amplitudes therefore decreased with lubricant addition, but the change was minimized by some dampening of the vibrations

due to the transmission distance to the sensor. Feature 3 is affected by the collisions of the particles on the walls and bottom of the V-blender. The measured emissions from these collisions decreased due to decreases in the COR with the lubricant. The changes due to lubricant addition, however, were minimized, again by dampening from both the bottom plate and transmission distance to the sensor. Feature 1 has the largest measured acoustic emissions due to particle collisions directly on the lid with the attached sensor. The measured emissions decreased with a decreased in the COR due to the lubricant addition. The change was significant as the energy from the collisions was transmitted easily to the nearby sensor.

The amplitude of feature 1 from the passive acoustic emissions showed the largest change with lubricant addition to the sugar spheres. The amplitudes of feature 1 were therefore examined as a function of mixing time (Figure 6.3). The initial measured amplitude decreased immediately and continued to decrease until approximately 10 revolutions at which time the amplitudes fluctuated around a steady state value at about 100 bits. After only 1 revolution of the V-blender, the magnesium stearate had only limited opportunity to be dispersed with the spheres. Most of the sugar spheres remained unaffected by the lubricant (Figure 6.5a). The spheres that were coated with lubricant had lower COR and flowability than uncoated spheres and made smaller contributions to the measured emissions resulting in a decrease in amplitudes. By 10 revolutions, the lubricant had covered the surfaces of most of the sugar spheres (Figure 6.5b). The lubricant covered spheres had low COR and flowability and therefore small contributions to acoustic emissions. As the lubricant was almost completely dispersed with the spheres, further mixing had minimal effect on the COR and flowability; the amplitudes of the measured acoustic emissions stabilized.

Trials were conducted mixing sugar spheres with 1wt% (Figure 6.3a), 2.5wt% (Figure 6.3b), and 5wt% (Figure 6.3c) magnesium stearate. The trend in acoustic emission amplitudes was similar for all trials. Larger amounts of magnesium stearate had larger effects on the acoustic emission amplitudes. The coverage and then thickness of the layer of magnesium stearate flakes on the sugar spheres increased (Figure 6.6). As a result, the COR (Table 6.3) and flowability decreased (Figure 6.4) which reduced energy emitted

and then transmitted to the sensor from particle collisions. As expected, the number of revolutions required to disperse the lubricant with the spheres increased with lubricant concentration from about 8 to 10 to 15 revolutions for 1wt%, 2.5wt% and 5wt% magnesium stearate respectively.

Acoustic emissions were also recorded from the V-blender during the mixing of two pharmaceutical placebo wet high shear granulated formulations (Table 6.1) with magnesium stearate. The filtered acoustic emissions for these granules before mixing with the lubricant are shown in Figure 6.7a and Figure 6.10a for formulations A and B, respectively. The three features associated with phases of particle motion within the Vblender could be clearly identified. The amplitudes of the acoustic emissions measured using the granules were smaller than those of the sugar spheres. The range of granule sizes and the mass of a granule was generally lower than that of the sugar spheres (Table 6.2) and the granules were not as spherical and exhibited poorer flowability as indicated by the dynamic avalanche angle (Figure 6.9 and Figure 6.12). As mass and flowability affect the vibrations produced from particle collisions, it was expected that the emission amplitudes of the granules would be smaller. The COR also affects the measured emission amplitudes. More energy is dissipated during a collision for particles with low COR resulting in less energy transmitted and then measured by a sensor. Due to their small size, it was not possible to reliably measure the COR of the granules. The COR of the granules, however, would be expected to be lower than that of the sugar spheres. Granules are multi-particle agglomerates with the particles joined through bridges. The bridges will allow the granules to partially deform upon collision. Energy from the collisions would be dissipated during the deformation, reflecting the low COR.

The emissions of both formulations were monitored as magnesium stearate was added. The features were identified immediately after lubricant addition (Figure 6.7b and Figure 6.10b) and then following mixing over 150 revolutions (Figure 6.7c and Figure 6.10c). Immediately after the addition of magnesium stearate, the amplitude of the features decreased but then, following more mixing, the amplitude increased beyond that measured with unlubricated granules. This trend was opposite to that observed with the sugar spheres. The overall effect of the magnesium stearate of increasing the emissions of

the granules was attributed to changes in the flowability and COR. The change in mass of the granules due to lubricant addition was very small and therefore the effects of mass changes were negligible.

The dynamic avalanche angle was measured for the granules to indicate the effect of the addition of the lubricant on flowability (Figure 6.9 and Figure 6.12). With the addition of magnesium stearate, the angle decreased which indicated an increase in flowability. The granules were not completely spherical (Table 6.2) and had an irregular, rough surface (Figure 6.6b and Figure 6.6c) due to the aggregation of the individual components. The magnesium stearate primarily filled in the crevices of the granules surfaces creating a more spherical particle. Spherical particles have improved flow due to a reduction in inter-particle friction. As the flowability improved, the velocity of a granule as it tumbled within the V-blender increased leading to a corresponding increase in collision energies and measured emissions. The effect of the magnesium stearate flakes filling the crevices on the granule surfaces on the COR was estimated to be small. The main contact surfaces during a collision would remain primarily a solid particle component of the granule and therefore the addition of the lubricant would have only slightly lowered the COR.

The amplitude of the three features increased overall as the granules were mixed with lubricant (Figure 6.7 and Figure 6.10). As with the sugar spheres, feature 1 showed the largest change. Although an improvement in flowability increased the amplitude of all 3 emission features, feature 1 reflects fluctuations due to collisions with the lid with the attached sensor and was therefore the most sensitive to any changes.

The amplitude of feature 1 was monitored as the lubricant was added and mixed with the granules (Figure 6.8 and Figure 6.11). The initial amplitude after addition was low and, as the lubricant mixed with the granules, the amplitude increased and then fluctuated above the range of the unlubricated granules. As established with the sugar spheres, this trend showed the progression of the lubricant dispersal.

The effect of lubricant concentration on the acoustic emissions was also investigated for the two granule formations. Trials were conducted mixing the granules with 1 wt% (Figure 6.8a and Figure 6.11a), 2.5wt% (Figure 6.8b and Figure 6.11b), and 5wt%

(Figure 6.8c and Figure 6.11c) magnesium stearate. The clarity of the trend varied between the two formulations, but improved as the lubricant concentration increased. As more lubricant was added, the crevices of the granules became filled with magnesium stearate flakes (Figure 6.6). This created a smoother and more spherical particle that exhibited better flowability as indicated by the dynamic avalanche angle (Figure 6.9 and Figure 6.12). The improved flowability allowed the granules to reach higher velocities before a collision leading to higher collision energies to be measured by the sensor.

There were differences in the acoustic emissions recorded for the two placebo granules. The amplitude of the emissions was smaller for granules of formulation B compared to formulation A granules. This was expected as the size and mass of an average granule was smaller for formulation B. Also, while the trend in the amplitude of feature 1 was the same for both formulations, as the lubricant was dispersed, the clarity of the trend varied. For the formulation A granules, it was very difficult to see a trend at 1 wt% magnesium stearate, but as the lubricant concentration increased, the clarity improved. For the formulation B granules, even at 1wt% magnesium stearate the trend was visible. The initial increase in the amplitude of feature 1 with mixing time could be identified and, from this, it was estimated that 30-40 revolutions of the V-blender were required to disperse the magnesium stearate with the formulation B granules. It was also observed that the steady state amplitude of feature 1 of the formulation B granules mixed with magnesium stearate increased with the lubricant concentration reflecting the positive effect of the lubricant on the flowability. Differences in the acoustic emissions of the two granule formulations were also partially attributed to their size distributions; formulation A granules had a wider size distribution which led to more variability in the measured acoustic emissions. The differences also reveal potential limitations of the method that need to be further examined; lubricant addition and dispersal will be more challenging to monitor as the granule size becomes smaller and the size distribution becomes wider.

It is important to add the proper amount of lubricant to granules prior to tabletting and critical to ensure they are mixed correctly so that the quality of the final tablet product is not affected. The results show that the addition of lubricant can be detected using passive acoustic emissions and monitoring these emissions could allow operators to determine

the progress of the operation. This not only provides more knowledge about the process, but allows for better process control thereby contributing to more efficient manufacturing while maintaining or even improving final product quality.

6.5 Conclusions

Passive acoustic emissions were measured from various solids mixed with a range of magnesium stearate lubricant concentrations in a V-blender. Three signal features related to particle motion were identified and feature 1, corresponding to emissions measured primarily from particle collisions with the lid, was found to be the most sensitive to the lubricant addition. Changes in the amplitude of feature 1 reflected changes in the particle flowability and COR due to the lubricant. The dispersal of the lubricant could be monitored especially with large granules with a narrow size distribution. This is important for lubricants as mixing past a critical point negatively impacts tablet quality. This feasibility study confirmed the potential for passive acoustic emissions to monitor lubricant dispersal during the mixing step with granules just prior to tabletting.

6.6 References

- 1. Fassihi AR, Kanfer I. Effect of compressibility and powder flow properties on tablet weight variation. Drug Dev Ind Pharm 1986; 12: 1947-1966.
- 2. Shi L, Feng Y, Sun CC. Initial moisture content in raw material can profoundly influence high shear wet granulation process. Int J Pharm 2011; 416: 43-48.
- 3. Torres MD, Moreira R, Chenlo F, Vazquez MJ. Water adsorption isotherms of carboxymethyl cellulose, gaur, locust bean, tragacanth and xanthan gums. Carbohydr Polym 2012; 89: 592-598.
- 4. Roblot-Treupel L, Puisieux F. Distribution of magnesium stearate on the surface of lubricated particles. Int J Pharm 1986; 31: 131-136.
- 5. Perrault M, Bertrand F, Chaouki J. An investigation of magnesium stearate mixing in a V-blender through gamma-ray detection. Powder Technol 2010; 200: 234-245.
- 6. Morin G, Briens L. The effect of lubricants on powder flowability for pharmaceutical application. AAPS PharmSciTech 2013; 14: 1158-1168.
- 7. Faqih AMN, Mehrotra A, Hammond SV, Muzzio FJ. Effect of moisture and magnesium stearate concentration on flow properties of cohesive granular materials. Int J Pharm 2007; 336: 338-345.
- 8. Liu LX, Marziano I, Bentham AC, Litster JD, White ET, Howes T. Effect of particle properties on the flowability of ibuprofen powders. Int J Pharm 2008; 362: 109-117.
- 9. Pingali KC, Saranteas K, Foroughi R, Muzzio FJ. Practical methods for improving flow properties of active pharmaceutical ingredients. Drug Dev Ind Pharm 2009; 35: 1460-1469.
- Jarosz PJ, Parrott EL. Effect of lubricants on tensile strengths of tablets. Drug Dev Ind Pharm 1984; 10: 259-273.
- 11. Johansson ME. Influence of the granulation technique and starting material properties on the lubricating effect of granular magnesium stearate. J Pharm Pharmacol 1985; 37: 681-685.
- 12. Kikuta JI, Kitamori N. Effect of mixing time on the lubricating properties of magnesium stearate and the final characteristics of the compressed tablets. Drug Dev Ind Pharm 1994; 20: 343-355.

- 13. Abe H, Otsuka M. Effects of lubricant-mixing time on prolongation of dissolution time and its prediction by measuring near infrared spectra from tablets. Drug Dev Ind Pharm 2012; 38: 412-419.
- 14. Bellamy L, Nordon A, Littlejohn D. Non-invasive monitoring of powder mixing with near infrared spectroscopy and acoustics. Spectrosc Eur 2004: 25-27.
- 15. Allan P, Bellamy L, Nordon A, Littlejohn D. Non-invasive monitoring of the mixing of pharmaceutical powders by broadband acoustic emission. Analyst 2010; 135: 518-524.
- 16. Crouter A, Briens L. Passive acoustic emissions from particulates in a V-blender. Drug Dev Ind Pharm 2015; 41: 1809-1818.
- 17. Crouter A, Briens L. The effect of granule moisture on passive acoustic emission in a V-blender. Powder Technol 2016; 299: 226-234.
- 18. Leach M, Rubin G, Williams J. Particle size determination from acoustics emissions. Powder Technol 1977; 16: 153-158.
- 19. Leach M, Rubin G, Williams J. Particle size distribution characterization from acoustic emissions. Powder Technol 1978; 19: 157-167.
- 20. Leach M, Rubin G, Williams J. Analysis of polydisperse systems of rigid particles from acoustic emissions. Powder Technol 1978; 19: 169-176.
- 21. Leach M, Rubin G, Williams J. Analysis of a Gaussian size distribution of rigid particles from their acoustic emissions. Powder Technol 1978; 19: 189-195.
- 22. Leach M, Rubin G. Size analysis of particles of irregular shape from their acoustic emissions. Powder Technol 1978; 21: 263-267.
- 23. Tily P, Porada S, Scruby C, Lidington S. Monitoring of mixing processes using acoustic emission. In: Harnby N, Benkreira H, Carpenter K, Mann R, eds. Fluid Mixing III. Rugby: The Institute of Chemical Engineers, 1988: 75-94.
- 24. Daubechies I. The wavelet transform, time-frequency localization and signal analysis. IEEE Trans Inf Theory 1990: 46: 961-1005.
- 25. Müller P, Trüe M, Böttcher R, Tomas J. Acoustic evaluation of the impact of moist spherical granules and glass beads. Powder Technol 2015; 278: 138-149.
- 26. Li LP, Sun SQ, Li SC, Zhang QQ, Hu C, Shi SS. Coefficient of restitution and kinetic energy loss of rockfall impacts. KSCE J Civ Eng 2015; 0: 1-11.

27. Stanford MK, DellaCorte C, Eylon D. Effect of particle morphology on flow characteristics of a composite plasma spray powder. J Therm Spray Technol 2004; 13: 586-592.

Chapter 7

7 General Discussion and Conclusion

Powder flow is critical during the manufacturing of pharmaceutical tablets. The tablet manufacturing process is a series of batch steps and the powders must be transferred between the different stages. During tabletting, the powder must flow easily and uniformly into the tablet dies to ensure tablet weight uniformity and the production of tablets with consistent and reproducible properties (1-3).

To help improve the flow, the active ingredient is granulated with various excipients. Then, during the final blending stage, additional excipients are added to further prepare the granules in preparation for tabletting. This blending is typically performed in a tumbling blender. The goal is to disperse the excipients among the granules without overmixing them as this can degrade the final tablet quality.

To ensure quality control of the final product, each step of the manufacturing process should be monitored and controlled. The development of process analytical technologies (PAT) can improve product monitoring with the aim of increasing efficiency, product quality and consistency and creating a better understanding of the manufacturing process. A variety of technologies have been investigated. However, many of these techniques require the use of invasive probes which disrupt the system or require extensive signal analysis.

The objective of this work was to develop passive acoustic emissions (PAE) as a PAT for solids tumbling in a V-blender. The ICH Q8 guideline for pharmaceutical development states the importance of developing technologies that improve process understanding and increase manufacturing flexibility with the goal of ensuring final product quality (4). As a result, capturing acoustic emissions from tumbling solids is only the first step in PAT development. It is also important to understand the factors that influence the acoustic signals during tumbling to gain better process knowledge. The research presented in this thesis demonstrates the robustness of PAE as a method for monitoring solids tumbling in a V-blender and blending processes by i) relating the PAE to critical quality attributes,

such as particle size and moisture content, ii) investigating the effect of process parameters, such as sensor location, fill level and scale and iii) monitoring lubricant addition and understanding how powder flow influences the acoustic signal.

Initially, there was a need to study particle properties and process parameters of tumbling solids (Chapter 3). The acoustic emission signals needed to be filtered to remove the oscillations due to the motion of the blender and focus on the emissions from the particle interactions. Then it was necessary to identify the ideal sensor location to obtain the most information about the process from the measurements. These initial trials were completed with sugar spheres tumbling in a Patterson-Kelley V-blender. Subsequent trials were completed with the sugar spheres varying the particle size, the fill level, and the scale of the V-shell. The effect of particle type was also investigated by comparing the acoustic emissions produced from the sugar spheres, microcrystalline cellulose (MCC) or lactose tumbling in the V-blender. A wavelet filter was applied to the acoustic emissions to remove the vibrations from the tumbling motion of the V-shell and the ideal sensor location was determined to be the lid of the V-shell due to the impact of the tumbling solids on the lid and transmission of the vibrations from other particle motion within the V-shell. The amplitude of the acoustic emissions was found to increase with the particle size due to the larger particle momentum. The fill level and the V-shell scale also influenced the measured vibrations as the particle motion was affected which in turn affected the momentum of the solids. By comparing the emissions from different particles, changes in particle flowability could be detected. The measured vibrations from passive acoustic emissions reflected particle motion and interactions within the Vblender.

Powder properties and behavior are critical to efficient and successful manufacturing of pharmaceutical tablets. As the powders must be transferred between the different manufacturing stages, the flowability of powders is critical. Work was done to investigate how changes in the moisture content of a powder affect its flowability (Chapter 4). The effect of moisture on the flowability of six pharmaceutical excipients (MCC, hydroxypropyl methylcellulose (HPMC), carboxymethyl cellulose (CMC), polyvinylpyrrolidone (PVP), corn starch, potato starch) was investigated. Powder

flowability was measured using established static techniques (angle of repose, Hausner ratio, and the Carr index) and dynamic avalanche measurements. Static techniques did not provide enough resolution to clearly identify changes in flowability due to the increasing moisture content. Avalanche time and its standard deviation showed that the flowability of MCC, CMC, PVP and potato starch decreased after a critical moisture content. The moisture decreased flowability by forming strong inter-particle liquid bridges. The flowability of corn starch increased as the moisture acted as a lubricant and the flowability of HPMC did not significantly change. Changes in the dynamic density of the powders were also found with the dynamic density generally decreasing as the moisture content increased. Changes in flowability and dynamic density can significantly impact tabletting and therefore the moisture content of solids should be monitored and controlled.

The feasibility of using PAE to monitor changes in solids moisture content was investigated while solids were tumbling in a V-blender (Chapter 5). Trials were conducted with wooden beads, sugar spheres and two placebo formulations of pharmaceutical granules in a V-blender. A wavelet filter was applied to the measured emissions to remove vibrations from the tumbling motion of the V-shell. Three signal features were identified in the acoustic emissions with each feature being attributed to phases of the particle motion within the V-shell. The maximum feature amplitude was found to vary with solids moisture content. Both particle mass and flowability had an impact on the acoustic emissions amplitude. Particle flowability changes were correlated to a critical moisture content obtained from solids drying profiles. The measured vibrations from passive acoustic emissions reflected changes in particle motion and interactions within the V-blender as the solids moisture content varied demonstrating the potential of PAE to obtain critical process information inline and in real-time.

Finally, as the flowability of solids has been shown to affect the acoustic signal, PAE were used to monitor lubricant addition (Chapter 6). Lubricants are typically added during the final blending stage in preparation for tabletting to reduce the friction and allow tablets to be cleanly ejected from the tablet press. Trials were conducted with sugar spheres and two placebo formulations of pharmaceutical granules in a V-blender. A

wavelet filter was applied to the measured emissions to remove vibrations from the tumbling motion of the V-shell. Three signal features were identified in the acoustic emissions with each feature being attributed to phases of the particle motion within the V-shell. The maximum feature amplitude was found to vary as the lubricant was dispersed into the granules with feature 1 showing the most significant change. The feature amplitude was found to be sensitive to the dispersal of the lubricant due to changes in the particle flowability. Differences in lubricant concentration were also detected. The results confirmed the potential for PAE to monitor lubricant dispersal and possibly other blending operations.

In summary, the findings provide support for the adoption of PAE as a PAT for blending processes. A relationship between PAE and particle interactions that reflected changes in particle properties and process parameters confirmed the information acquired is relevant to solids flow and blending. Therefore, PAE can be used with confidence to understand and accommodate process variability during product development and manufacturing. The results support the initiatives outlined in the ICH Q8 guidance to build process knowledge and increase manufacturing flexibility using PAT (4). With improved process knowledge, it would be possible to adjust operations in real-time to achieve the desired product quality, rather than relying on offline testing. In addition, PAE could be used to reduce development times for new products. Having real-time information would reduce the dependence on offline measurements, such that the process could be optimized in fewer iterations. It would also be easier to identify potential product issues; PAE were demonstrated to be sensitive to moisture content, so a secondary check would be in place before proceeding with any additional processing that would be impact by the presence of increased moisture. Overall, the work demonstrates PAE provide a robust measure of the complex interactions that occur during solids flow and blending and it is possible to extract relevant information to increase process understanding and assist in optimization and control.

Prior to this research, acoustic emissions had only been applied to monitor blending in fixed shell blenders, which are not typically used in industry during the final blending stage. Therefore, this work is the first application of passive acoustic emissions

monitoring on a tumbling blender. Also, while the previous studies using fixed shell blenders identified that the emissions were linked to particle size (5, 6); further investigation into the particle mechanics influencing the acoustic signal was not completed. This research establishes the fundamentals that impact the acoustic signal from a V-blender, which should allow the presented method to be applied to other tumbling blenders once the ideal sensor location has been identified. The most promising result from this research is the ability to monitor lubricant addition as this is directly applicable to industrial processes. With further improvements this method could be used in industry to monitor blending and identify an end-point.

This research focused on placebo granule formulations and model particle systems as it was a feasibility study to determine if PAE could be a PAT for solids flow and blending processes. The model systems were chosen as an approximation of granular systems as they were very similar in size but had a more uniform composition and shape. The acoustic measurements from the placebo granules had smaller amplitudes compared to the model systems due to differences in mass and flowability between the solids. Even though the acoustic emissions were smaller, it was still possible monitor changes in the process. Therefore, future work should include the analysis of commercial granule formulations that may involve more excipients and a broader size range.

This research has confirmed the feasibility of using PAE for monitoring solids tumbling in a V-blender. Additional work is required to translate the technique from a potential monitoring method to commercial implementation in pharmaceutical blending processes. Regulatory approval of new technologies into the pharmaceutical industry is slow and difficult. However, the potential impact of a new monitoring method is large: improved product quality and process efficiency, and reduced waste or the number of discarded batches.

7.1 References

- 1. Fassihi AR, Kanfer I. Effect of compressibility and powder flow properties on tablet weight variation. Drug Dev Ind Pharm 1986; 12: 1947-1966.
- 2. Shi L, Feng Y, Sun CC. Initial moisture content in raw material can profoundly influence high shear wet granulation process. Int J Pharm 2011; 416: 43-48.
- 3. Torres MD, Moreira R, Chenlo F, Vazquez MJ. Water adsorption isotherms of carboxymethyl cellulose, gaur, locust bean, tragacanth and xanthan gums. Carbohydr Polym 2012; 89: 592-598.
- 4. U.S. Department of Health and Human Services, Food and Drug Administration, Center for Drug Evaluation and Research (CDER), Center for Biologics Evaluation and Research (CBER) [Internet]. Silver Spring: Division of Drug Information; c2009 [revision 2 2009 Nov]. Guidance for Industry Q8 Pharmaceutical Development; [29 pages]. Available from: http://www.fda.gov/downloads/Drugs/GuidanceComplianceRegulatoryInformation/Guidances/ucm073507.pdf
- 5. Tily P, Porada S, Scruby C, Lidington S. Monitoring of mixing processes using acoustic emission. In: Harnby N, Benkreira H, Carpenter K, Mann R, eds. Fluid Mixing III. Rugby: The Institute of Chemical Engineers, 1988: 75-94.
- 6. Allan P, Bellamy L, Nordon A, Littlejohn D. Non-invasive monitoring of the mixing of pharmaceutical powders by broadband acoustic emission. Anal 2010; 135: 518-524.

Appendices

Appendix A: Sample matlab code for wavelet filter

Function[] = removeSin(filename,column)

% This function removes the low frequency, high amplitude sin wave from signal by
% performing a multilevel wavelet decomposition and subtracting the largest scale
% approximation (Level 12 was determined to be the best tradeoff between computation
% time and seems to remove frequencies below approximately 3Hz without affecting
% either the time or frequency encoded information

```
S = load(filename); % Load the signal S=S(:,column); % Column 1 or 2
```

% Perform 12-level wavelet decomposition

% Use 'wavedec' & 'wrcoef' matlab functions with a level 12 Daubechies 6 % approximation wavelet*

% Save file

```
[PATHSTR,NAME,EXT] = fileparts(filename);

name01 = cat(2,NAME,'_','filter',EXT);

file_01 = x;

Save(name01, 'file 01', '-ascii', '-tabs')
```

end

*Note: some of the code has been withheld

Curriculum Vitae

Allison Crouter

P	ost	Secon	ldarv	Edu	cation	and	De	gre	es:

Doctorate of Engineering Science

Chemical Engineering

2011 - 2016

The University of Western Ontario, London, Ontario, Canada

Thesis title: Passive Acoustic Emissions in a V-blender

Bachelor of Engineering Science

Chemical Engineering

2007 - 2011

The University of Western Ontario, London, Ontario, Canada

Awards and Accomplishments:

NSERC Doctoral Canadian Graduate Scholarship (CGS D)

2015-2016

The University of Western Ontario, London, Ontario, Canada

Ontario Graduate Scholarship (OGS)

2011-2015, 2015-2016 (declined)

The University of Western Ontario, London, Ontario, Canada

First Place, Oral Presentation

2013

Particle Technology Division, Research Bridges, Sarnia, Ontario, Canada

Related Work Experience:

Graduate Research Student, Chemical Engineering

2011-2016

The University of Western Ontario, London, Ontario, Canada

Teaching Assistant, Chemical Engineering

2011-2016

The University of Western Ontario, London, Ontario, Canada

Research Assistant, Chemical Engineering

2015

The University of Western Ontario, London, Ontario, Canada

Publications and Conference Proceedings:

Articles published in refereed journals

Crouter A, Briens L. Monitoring lubricant addition using Passive Acoustic Emissions in a V-blender. Powder Technology. Available online July 22, 2016.

Crouter A, Briens L. The effect of granule moisture on passive acoustic emissions in a V-blender. Powder Technology. 2016; 299: 226-234.

Crouter A, Briens L. Passive acoustic emissions from particulates in a V-blender. Drug Development and Industrial Pharmacy. 2015; 41: 1809-1818.

Crouter A, Briens L. The effect of moisture on the flowability of pharmaceutical excipients. AAPS PharmSciTech. 2014; 15: 65-74.

Non-refereed contributions

Crouter A. Passive Acoustic Emissions from Particulates in a V-blender. Institutional oral presentation at: Chemical and Biochemical Engineering Seminar, The University of Western Ontario; October 2014; London, ON. (PhD work).

Crouter A. The Use of Passive Acoustic Emissions to Monitor Particle Behaviour in a V-blender. Conference poster presentation at: Canadian Chemical Engineering Conference, The Canadian Society for Chemical Engineering; October 2014; Niagara Falls, ON. (PhD work).

Crouter A. Development of an inline method for monitoring the mixing of pharmaceutical powders. Institutional oral presentation at: Research Bridges, The University of Western Ontario; July 2013; Sarnia, ON. (PhD work).